STUDIES OF REACTION GEOMETRY IN OXIDATION AND REDUCTION OF THE ALKALINE SILVER ELECTRODE

FINAL REPORT

Eliot A. Butler

Angus U. Blackham

September 13, 1971

J. P. L. 952268

Brigham Young University

Provo, Utah

STUDIES OF REACTION GEOMETRY IN OXIDATION AND REDUCTION OF THE ALKALINE SILVER ELECTRODE

FINAL REPORT

Eliot A. Butler

Angus U. Blackham

September 13, 1971

J. P. L. 952268

This work was performed for the Jet Propulsion Laboratory, California Institute of Technology, as sponsored by the National Aeronautics and Space Administration under Contract NAS7-100

Brigham Young University

Provo, Utah

ABSTRACT

Two methods of surface area estimations of sintered silver electrodes have given roughness factors of 58 and 81 (Section VI). One method is based on constant current oxidation, the other is based on potentiostatic oxidation. More thorough examination of each of these oxidations seemed necessary for selecting optimum experimental conditions for surface area estimation.

Potentiostatic oxidations of silver electrodes as a function of temperature, hydroxide ion concentration, and applied potential have shown rather complex functional relationships (Section III). The appearance of a second current surge at potentials above 0.60 v (vs. Hg/HgO) results in an abrupt increase in charge acceptance. The current-time curves for the first stage of reaction have correlated best with a logarithmic growth law which suggested semiconductor properties for the growing layer of argentous oxide.

Constant current oxidations have been applied to various model-pore electrodes to provide information relative to the behavior of porous or sintered silver electrodes (Section II). A decrease in pore size was accompanied by a shorter penetration of oxide into the pore. Oscillations in the potential response have been correlated with dark and light bands on the surface of a strip electrode confined in a small glass tube in the electrolyte.

A variation of the constant current oxidation has given a possible approach to the determination of the kinetic parameters for the oxidation of silver in hydroxide solution (Section I). The cyclic current step method of Wijnen and Smit has given values of 0.7 - 1.4 ma/cm^2 for the exchange current density of a silver electrode along the first plateau. The acceptability of this method is based on the similarity in overpotential response of the silver-silver oxide system to that of the silver-ammonia and the ferrous-ferric systems. Results from the measurement of resistance along the second plateau have provided support for the interpretation that both ions and electrons are rate-determining charge carriers through this second plateau region.

Experiments with deposition, oxidation, and dissolution of radioactive silver have shown that the major ionic movement in the initial oxidation of silver is the transport of silver ions from succeedingly deeper regions in the electrode through the oxide to the outer electrolyte-oxide interface. (Section V).

Examination of both wire and sintered silver electrodes via scanning electron microscopy at various stages of oxidation have shown that important structural featuresare mounds of oxide (Section IV). In potentiostatic oxidations these appear to form on sites instantaneously nucleated while in constant current oxidations progressive nucleation is indicated.

TABLE OF CONTENTS

SECTION I

KINETIC STUDIES OF THE OXIDATION OF SILVER IN ALKALINE ELECTROLYTE

INTRODUCTION

The main parameters considered to be characteristic of the kinetics of an electrode process are the exchange current density, i_o; the rate constant, k^o, determined at the standard potential for the given process; and the transfer coefficient, α. Damaskin[1] has compared a number of approaches to the study of electrochemical kinetics. One of these is a method introduced by Wijnen and Smit[2] referred to as the cyclic current-step (c.c.s.) technique. Although they developed it for systems which are diffusion controlled with both the oxidized and reduced species as ions in solution we have examined the approach for systems in which one or both of the electroactive species are solids. Specifically, kinetic parameters have been determined for:

(1) the ferrous-ferric ion system in aqueous solution at a platinum electrode

(2) the $Ag\text{-}Ag(NH_3)_2^+$ electrode and

(3) the silver-silver oxide electrode.

With the c.c.s. technique the exchange current density (i_o) is determined from the potential response as a function of the frequency (f) of applied square wave currents in the 1-400 Hz range. The potential response generally follows the pattern indicated graphically as follows:

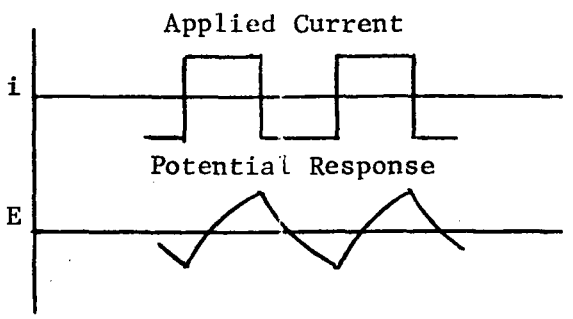

The relationship derived by Wijnen and Smit is

$$[\eta_{(\theta)'} - \eta_{(\theta)''}]_{\theta} = i_A \frac{RT}{nF} \left[\frac{1}{i_o} + \frac{4NL(\theta)}{(\pi F)^{\frac{1}{2}}}\right] \quad (1)$$

where θ, as the fraction of a cycle, has particular significance when its value is 0.5. For this value the quantity $[\eta_{(\theta)'} - \eta_{(\theta)''}]_{\theta} = 0.5$ is the peak to peak value of the potential response:

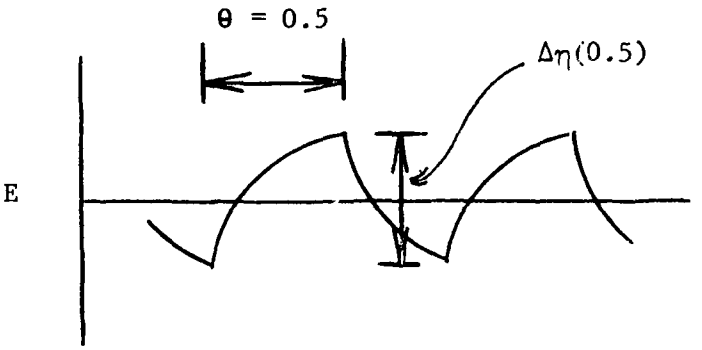

The function L(θ) appears in the derivation of Equation 1 as the cyclic conditions approach a steady state. For θ = 0.5, L(θ) = 0.27. N is given by

$$N = \frac{1}{nF}\left(\frac{1}{C^o_{ox}\sqrt{D_{ox}}} + \frac{1}{C^o_R\sqrt{D_R}}\right)$$

where C^o_{ox} and C^o_R are the concentrations of the oxidized and reduced species in the bulk solution of D_{ox} and D_R are the diffusion coefficients for the oxidized and reduced species. The applied current is i_A and n, F, R, T have their usual electrochemical significance.

Therefore if the peak to peak potential response is plotted as a function of the reciprocal of the square root of the frequency, the ordinate intercept is equal to $i_A RT/i_o nF$ providing for a direct calculation of i_o.

The transfer coefficient (α) is determined from the slope of a plot of log i_o versus log C^o_{ox} (C^o_R being kept constant), and the rate constant (k^o) from the intercept

$$i_o = nFk^o \quad (C_{ox}^o)^{1-\alpha} \; (C_R^o)^{\alpha}$$

$$\log i_o = (1-\alpha) \log C_{ox}^o + \log nFk^o \quad (C_R^o)^{\alpha}$$

For comparison, these kinetic parameters also have been determined for the ferrous-ferric system and the Ag - $Ag(NH_3)_2^+$ system from more conventional galvanostatic polarization data via Tafel plots. However, such an approach for the silver-silver oxide system is not possible because the build-up of oxide on the electrode surface during the time interval required causes changes in kinetics within that time interval.

EXPERIMENTAL

The experimental arrangement shown in Figure 1a is similar to that of Wijnen and Smit[2]. The square wave generator feeds the bridge circuit through resistance R_1, which governs the current passing through the cell. That part of the oscilloscopic trace due to iR drop may be eliminated from the trace by the adjustment of R_3, a compensating resistor. The value of R_3 is a measure of the resistance of the electrolyte plus the oxide film. Therefore, under conditions of low or negligible electrolyte resistance, this arrangement provides a direct method for measuring the resistance of oxide layers on the silver electrode.

The battery with a voltage divider adds to the output of the square wave generator so that the positive signal is equal and opposite in sign to the negative signal.

The c.c.s. measurements are made by observing the change in magnitude of the peak-to-peak voltage ($\Delta\eta_\theta$) on oscilloscope B when the cell operates as a two-electrode cell or on oscilloscope A when the cell operates as a three-electrode cell with a Luggin capillary connected to a suitable reference. These values of $\Delta\eta_\theta$ are plotted as a function of $1/\sqrt{f}$ for frequencies 4 - 100 Hz.

A diagram of the cell used for these experiments is shown in Figure 1b. The cell has a counter electrode of large surface area relative to the working electrode. Therefore, for some measurements, the platinum cylinder was considered to be non-polarized and used as the reference electrode. For other measurements, the cell operated as a three-electrode cell as indicated.

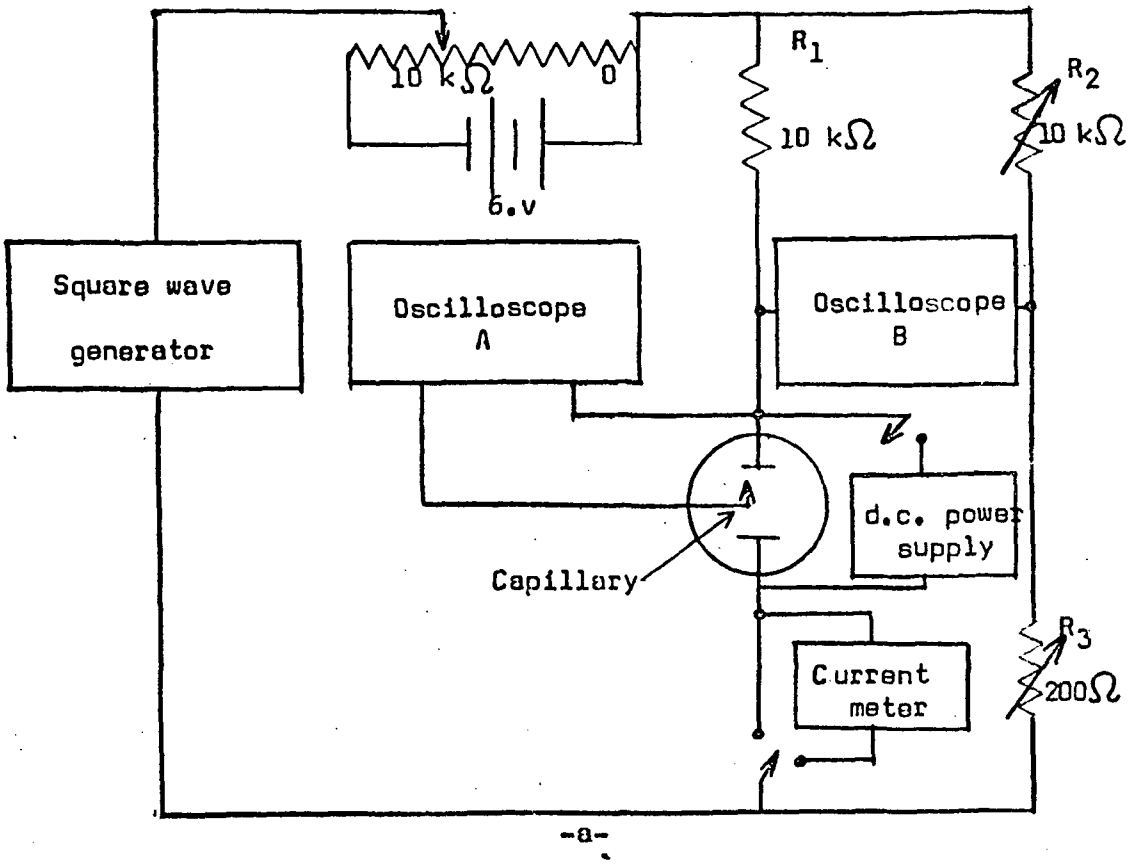

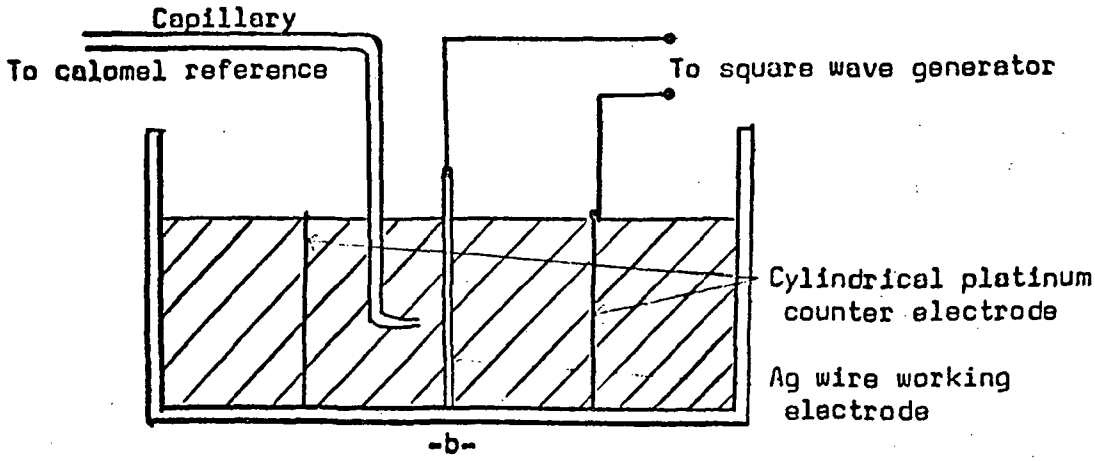

Fig. 1 .--Modified c.c.s. apparatus. a) circuit diagram
b) cell diagram.

RESULTS AND DISCUSSION

Ferrous-ferric system.--Wijnen and Smit[2] determined values of exchange current density from 2.1 to 5.2 ma/cm^2 as the concentration of the ferric ion changed from 1.0×10^{-3} to 1.0×10^{-2} M with the ferrous ion concentration held constant at 1.0×10^{-2}M in a solution 1 M in H_2SO_4. The values for α and k^o were 0.39 and 5.45×10^{-3} cm sec^{-1}, respectively. As a check on our experimental procedures, exchange current densities were determined for two different values of the square wave current density as shown in Figure 2. The solution was made 0.010 F each in ferrous sulfate and ferric sulfate and 1.0 F in H_2SO_4. Our values of 2.1 and 2.2 ma/cm^2 for i_o compare favorably. The linear part of the curves extend over a frequency range of from 4 to 25 Hz.

Silver - $Ag(NH_3)_2^+$ system.--This system represents an intermediate stage in the transition from systems in which both electroactive species are in solution to one such as the silver-silver oxide system where neither electroactive species is in solution. The results of a series of determinations at various concentrations of the oxidized species--$Ag(NH_3)_2^+$--are presented in Figure 3. From the intercepts, the calculated exchange current densities are 0.34, 0.63, 0.73, and 1.17 ma/cm^{-2} as the concentration of $Ag(NH_3)_2^+$ changes from 2.5×10^{-4} to 2.5×10^{-1} M in powers of ten. The graph of log i_o versus log C_{ox}^o is given in Figure 4. From the slope the transfer coefficient, α, is 0.82 and the rate constant, k^o, is 1.6×10^{-2} cm/sec.

The Tafel plot of galvanstatic polarization data for this system is shown in Figure 5. The values for i_o and α are 1.07 ma/cm^2 and 0.67 respectively; the values reported by Vielstich and Gerischer[3] are 0.66 ma/cm^2 and 0.5.

The results of a set of runs in which the applied square-wave current was varied are given in Figure 6. For a four-fold increase in applied current, there is a two-fold increase in exchange current. Wijnen and Smit recommended that determinations be made in the $\Delta\eta_\theta$ range of 10 mv. Our data were taken at higher $\Delta\eta_\theta$ values (up to 50 mv). This may account for the dependence of exchange current on applied current.

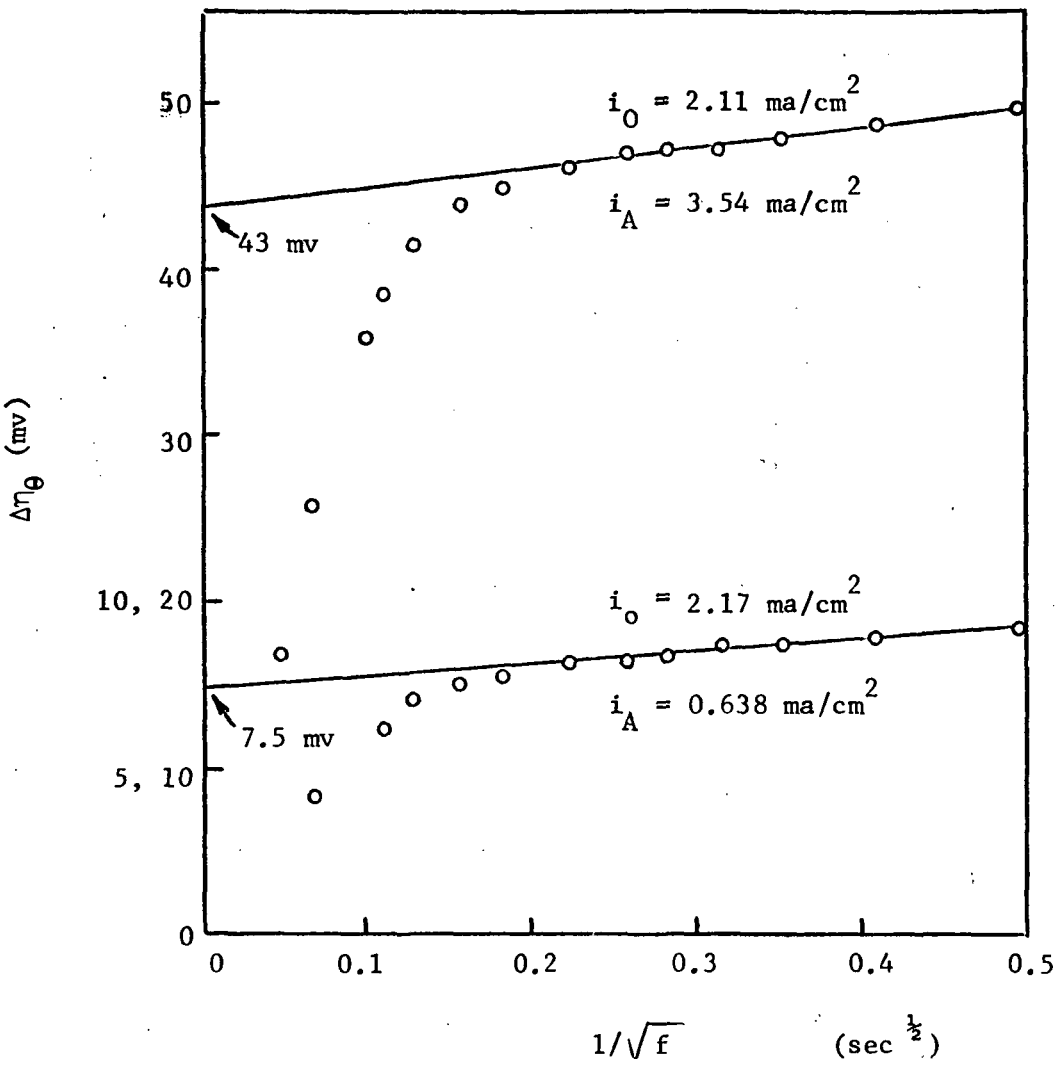

Fig. 2--C.C.S. Measurements of the Ferrous-Ferric System

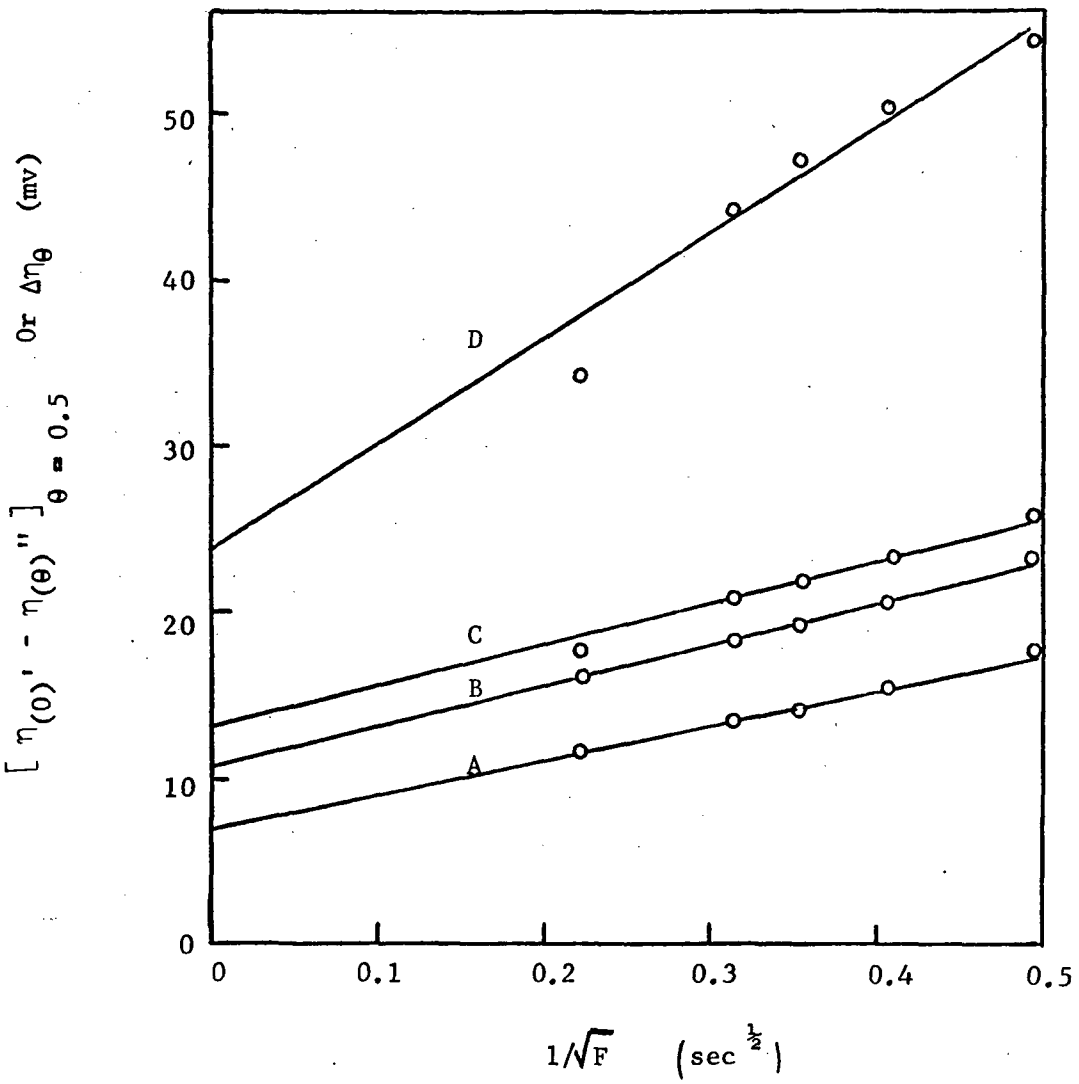

Fig. 3--Determination of i_o at $\theta = 0.5$ for the Ag-$Ag(NH_3)_2^+$ System. Concentration of ammonia: 14.7 M. Current density i_A = 3.14×10^{-4} amp/cm^2. Concentration of $Ag(NH_3)_2^+$ (C_{ox}^o) A- 2.5×10^{-1} M; B- 2.5×10^{-2} M; C- 2.5×10^{-3} M; D- 2.5×10^{-4} M. Calculated i_o values: A- 1.17 ma/cm^2; B- 0.73; C- 0.63; D- 0.34.

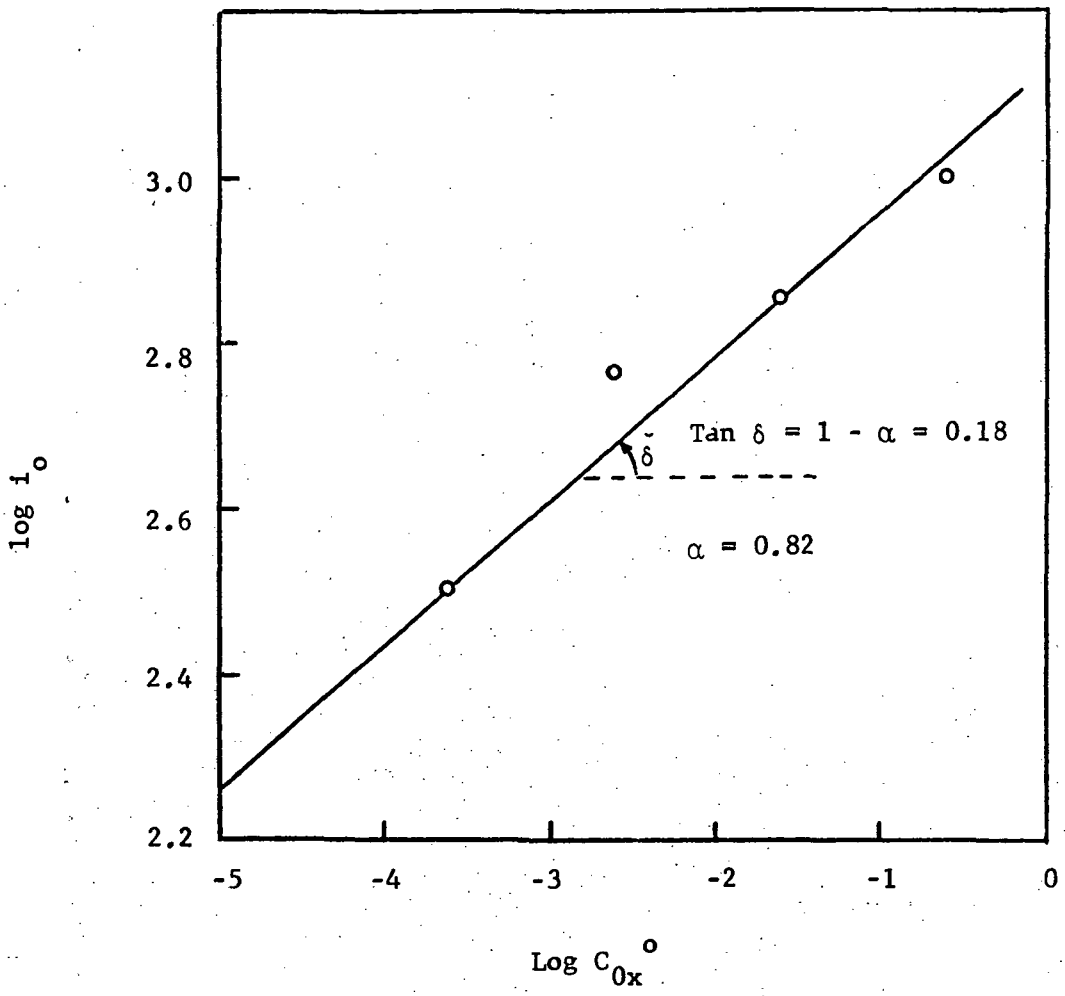

Fig. 4. --Determination of α from a plot of log i_o versus log C_{0x}^{o}.

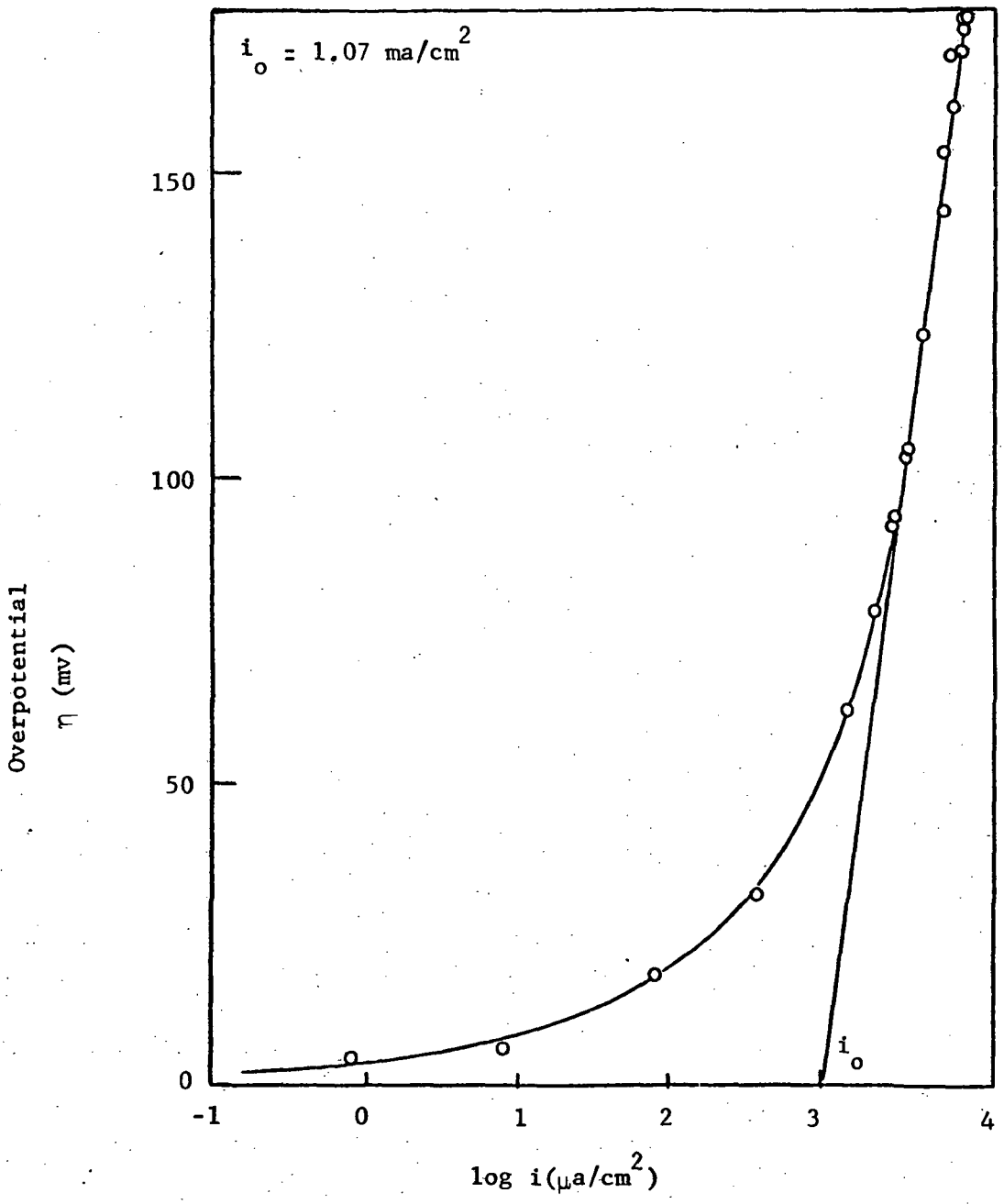

Fig. 5 --Tafel plot of galvanosatic polarization data for determination of i_o.

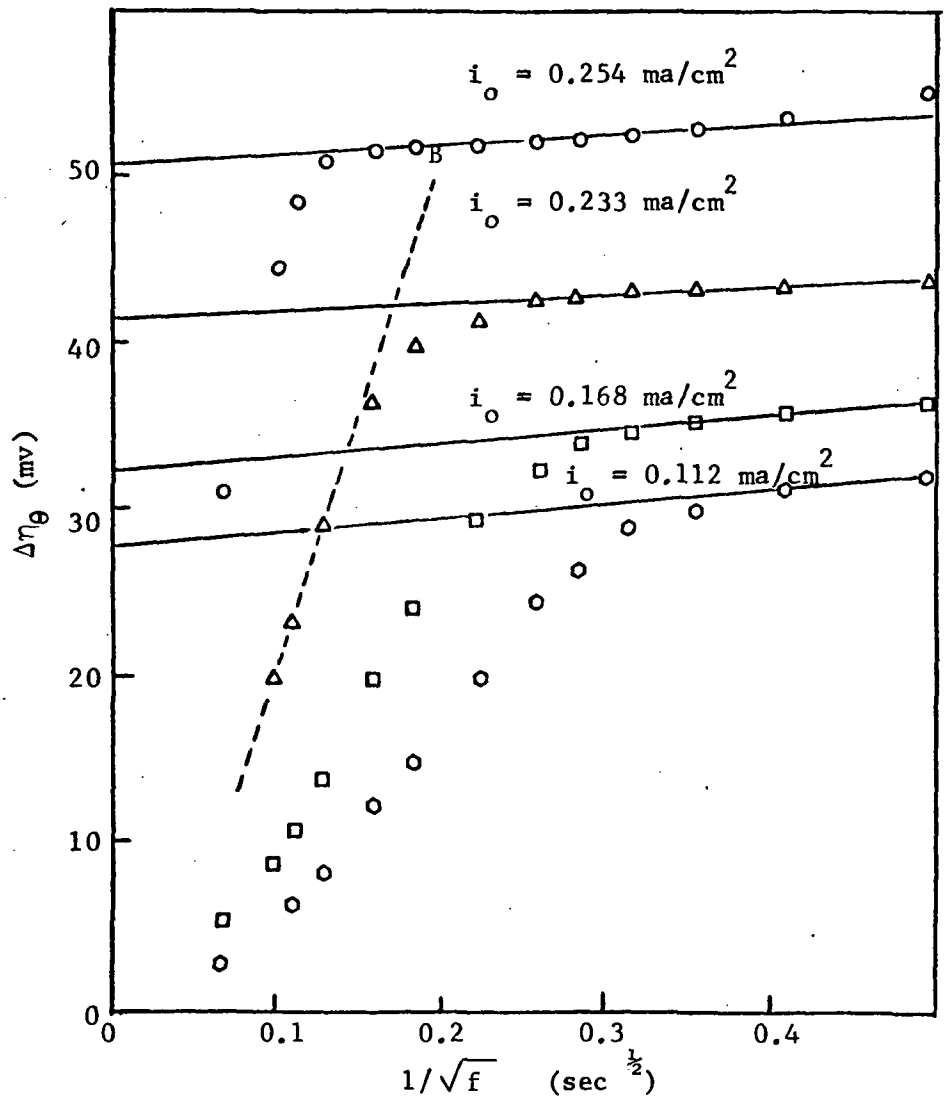

Fig. 6--C.C.S. Measurements of the Ag-Ag$(NH_3)_2^+$ System

○ $-i_A$ = 0.510 ma/cm^2
△ $-i_A$ = 0.382 ma/cm^2
□ $-i_A$ = 0.215 ma/cm^2
⬡ $-i_A$ = 0.124 ma/cm^2

At higher frequencies, it is possible to draw a straight line through some of the data points as shown by line AB in Figure 6. This line gives a negative intercept and therefore is not related to the exchange current density.

Silver-silver oxide system.--A graph of $\Delta\eta_\theta$ versus $f^{-\frac{1}{2}}$ for the silver electrode in KOH solution is given in Figure 7. The data points were taken at the initial part of the Ag - Ag_2O oxidation (before any Ag_2O had formed). This curve does not have a relatively small slope in the low frequency range as did the ferrous-ferric, and Ag - $Ag(NH_3)_2^+$ systems. This curve is followed closely by data obtained when the cell is replaced by a capacitor (750 mfd) and a resistor (170 ohms) connected in parallel. Therefore, a large double layer capacitance is indicated for a silver electrode as it is oxidized in KOH. This high capacitance does not permit a linear region with a positive intercept such as is necessary for calculation of exchange currents.

However, as the oxide film forms and increases in thickness the double layer capacitance markedly decreases.[4,5] Therefore, suitable c.c.s. measurements can be made along the first plateau of the Ag - Ag_2O oxidation. Typical of these measurements are the data of Figure 8. The calculated exchange-current densities from these data are given in Figure 9 (1.4-0.7 ma/cm^2) along with the corresponding position along the Ag - Ag_2O plateau. The experimental procedure used in obtaining these data involved repeated interruptions of the constant current oxidation (3.1 ma/cm^2) along the first plateau when the individual c.c.s. measurements were made. Repeated interruptions were later shown to lengthen the first plateau.

Therefore, a similar set of determinations (Figure 10) was made, but where each point involved only the interruption for obtaining that point. A clean unused silver wire was required for each c.c.s. measurement. Because a new electrode was used for each oxidation, the question of reproducibility of the first oxidation plateau had to be considered. Satisfactory reproducibility was observed with a careful cleaning procedure as indicated in Table I.

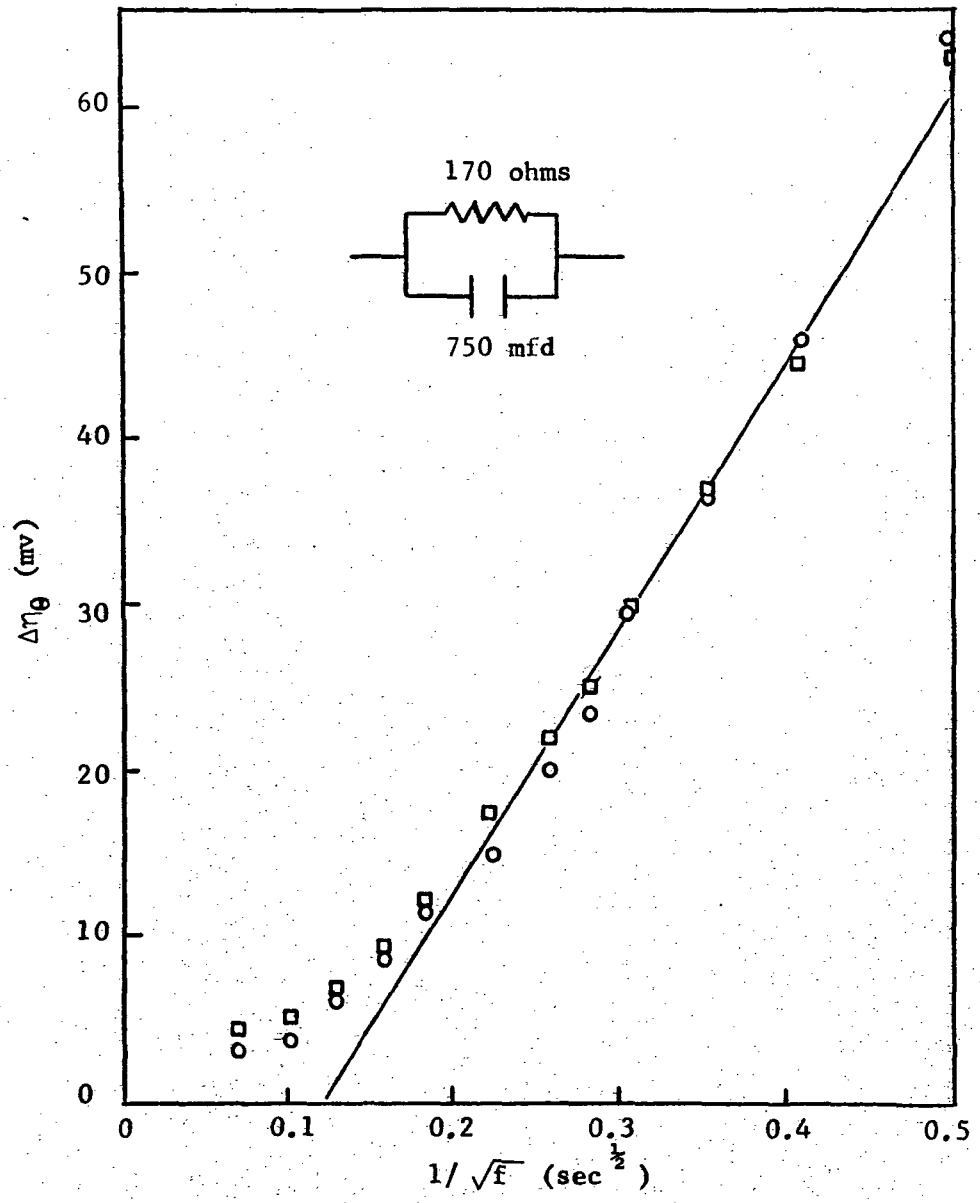

Fig. 7--A comparison of c.c.s. data of the Ag-Ag_2O System with c.c.s. data of an equivalent circuit.

□ - Data for the Ag-Ag_2O
○ - Data for the Equivalent Circuit

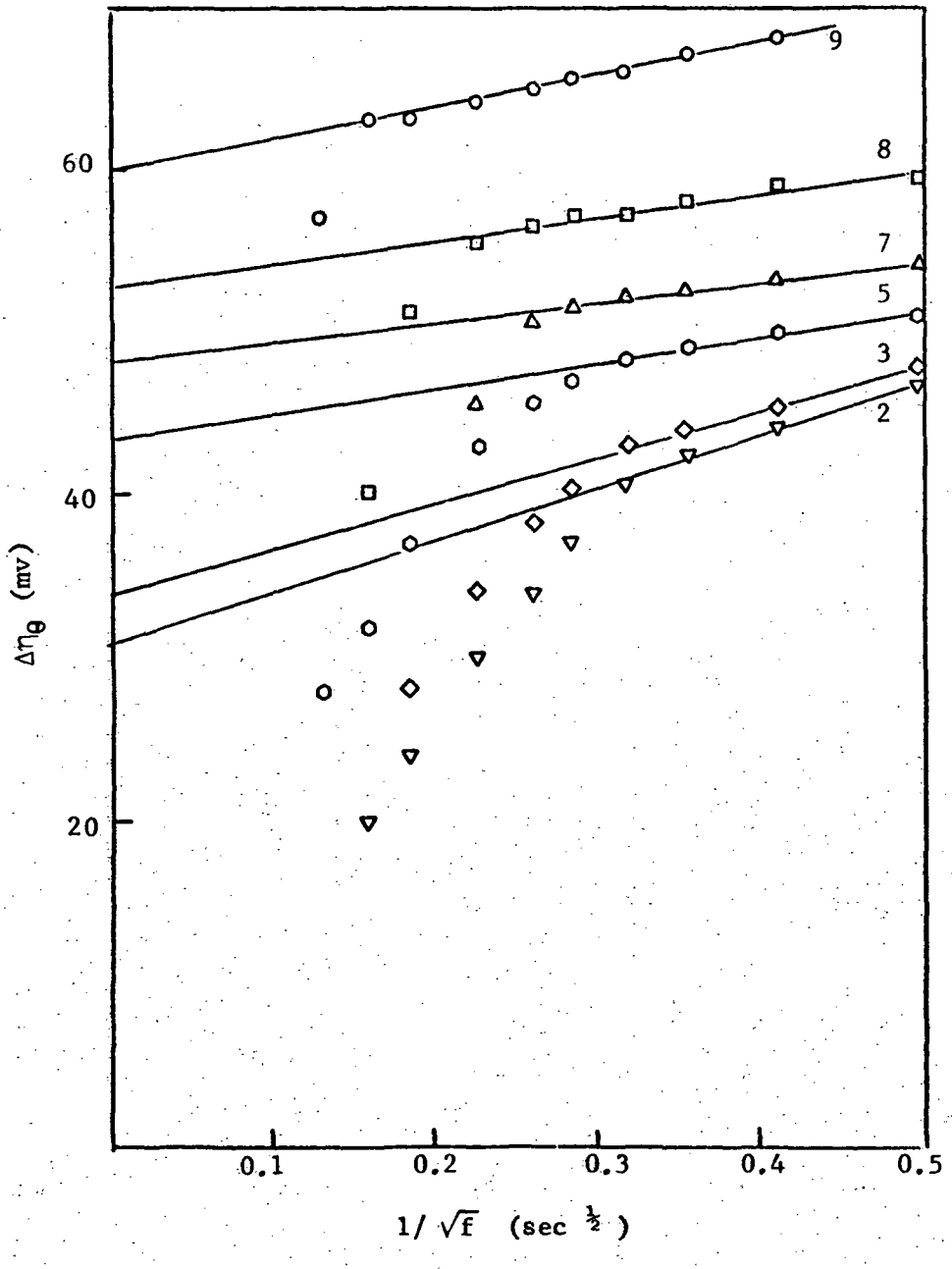

Fig. 8--Typical plots of c.c.s. measurements on the Ag-Ag_2O system. The run numbers correspond to numbers given in Figure 9.

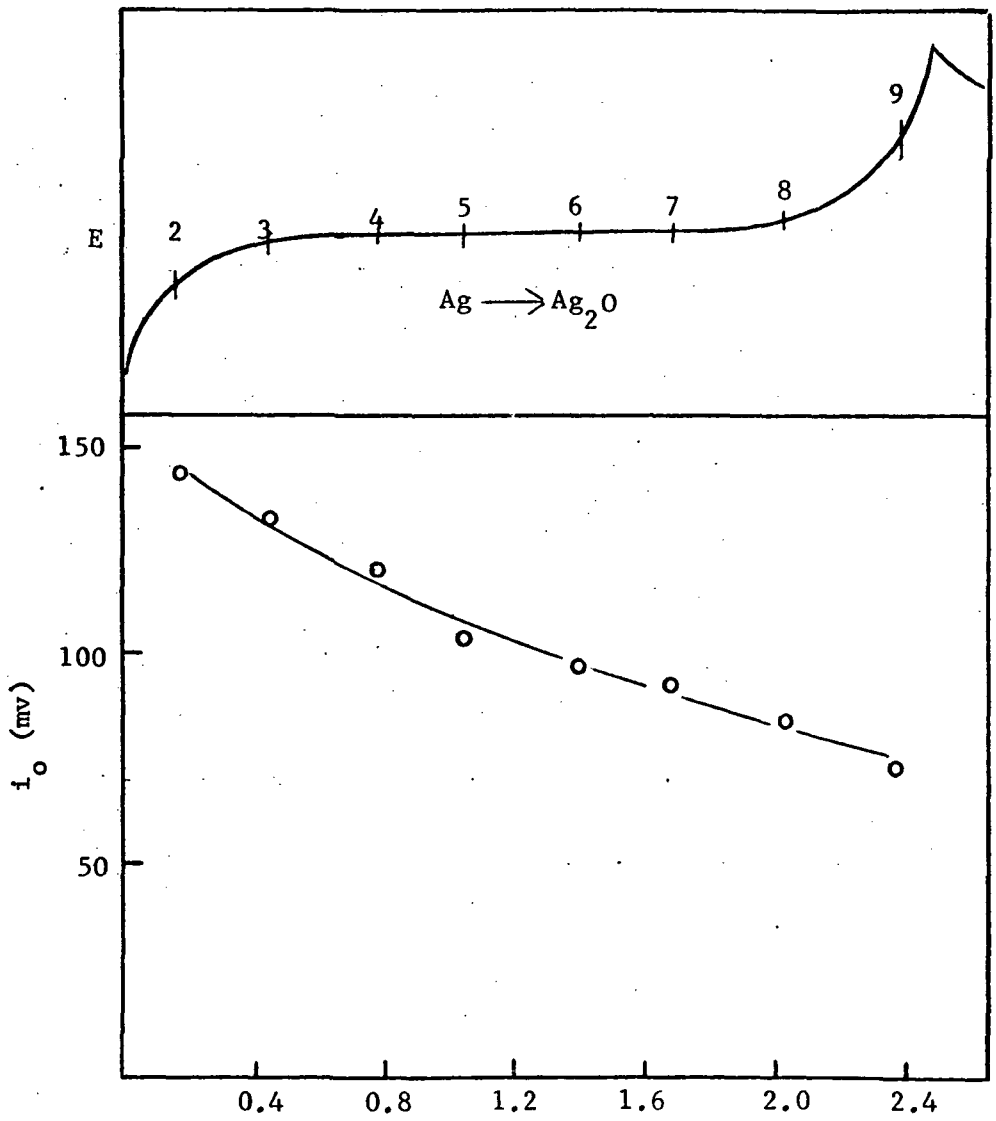

Fig. 9--Plot of i_o versus time along first oxidation plateau, with corresponding points marked on the potential-time curve. The numbers correspond to interruptions in the d.c. charging when the i_o measurements were made.

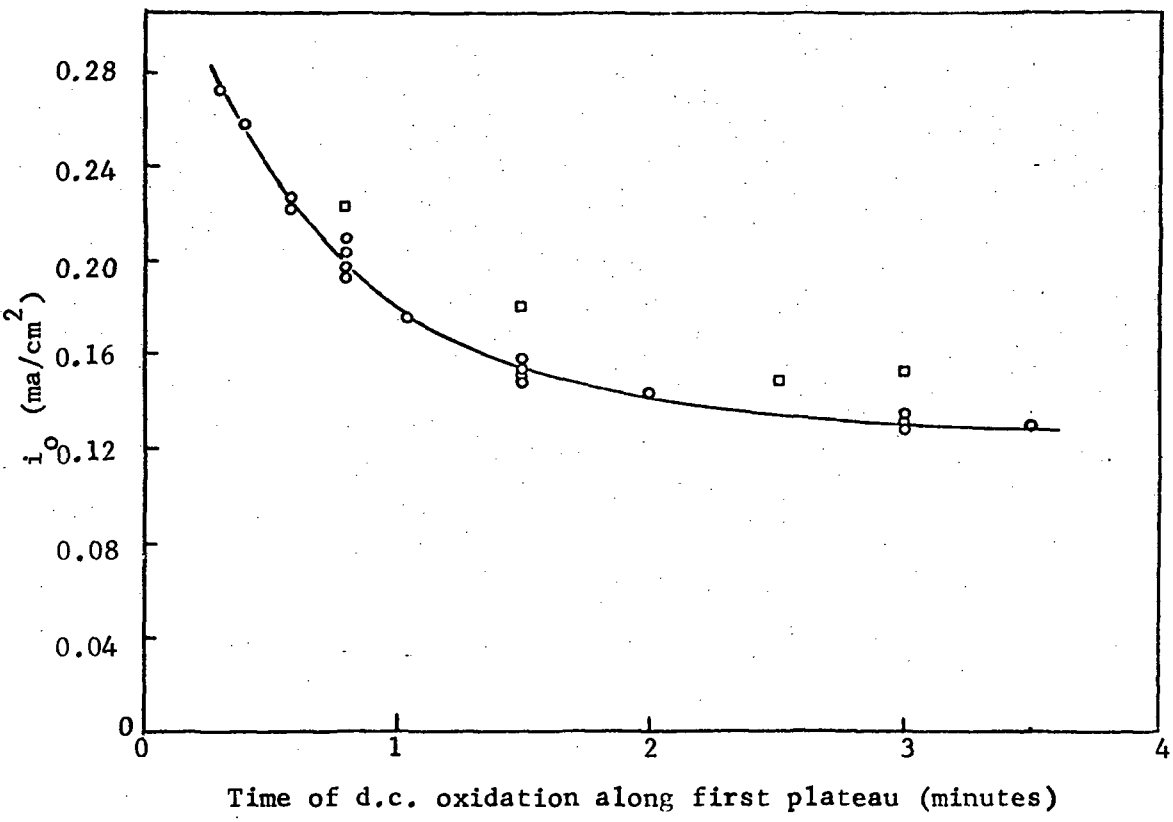

Fig. 10--Plot of i_o versus time of oxidation along first plateau. Square wave current density 0.412 ma/cm^2. Total first plateau length 4.0 minutes. □ = points calculated from c.c.s. measurements taken before oscilloscope trace had stabilized. ○ = points calculated after stablization.

TABLE I

REPRODUCIBILITY OF FIRST OXIDATION PLATEAU DURING FIRST, SECOND AND THIRD OXIDATIONS AFTER PREPARATION OF THE ELECTRODES AS INDICATED IN THIS PROCEDURE

Cleaning Procedure:

Silver wire was cut, wiped with absorbent paper and dipped in alcoholic KOH. The electrode was then rinsed thoroughly in distilled water and anodized in ammonia solution for four minutes at 0.4 ma/cm^2. The electrode was rinsed and stored in distilled water until it was used.

Conditions:

Oxidizing current density . . . . . 0.74 ma/cm^2
Temperature . . . . . 25°C

Run Number	Plateau Length (min)	% Deviation from Mean
	First Oxidation	
1	2.65	0.0 %
2	2.69	1.50%
3	2.64	.38%
4	2.62	1.13%
5	2.67	.75%
	Second Oxidation	
1	2.68	0.0 %
2	2.76	3.5 %
3	2.92	2.1 %
4	2.92	2.1 %
5	2.86	0.0 %
	Third Oxidation	
1	2.62	6.8 %
2	2.70	3.9 %
3	2.78	1.1 %
4	2.86	1.8 %
5	3.10	13.8 %

Under these conditions, i_o values in the range 0.28 to 0.12 ma/cm^2 were obtained as shown in Figure 10. These are lower by a factor of about five from the values in Figure 9. The reasons for this difference are: (1) the roughness factors for the second set of determinations is lower because of the cleaning procedure and the single interruption; and (2) the i_o values are dependent on the applied current density as shown in Figure 11. In region III of this figure the voltage response is 60-80 mv, considerably higher than the 10 mv response recommended by Wijnen and Smit.[2] This high voltage response of the Ag - Ag_2O electrode is necessary since the square-wave current must be sufficient to charge the double layer of the Ag - Ag_2O electrode in alkaline solution in order to give a meaningful voltage response.

Another consideration is the effect of the square-wave current on the structure and surface properties of the oxide film. It has been reported by Wales[6] that the charging capacity of the alkaline silver electrode can be increased 40-50% by superimposing an a.c. signal on the d.c. oxidizing current. Although in our case the square wave current and the d.c. current are not running simultaneously, the instability of the voltage response after application of a square-wave current at a particular frequency indicates surface or structural changes in the oxide. Figure 12 shows plots of voltage response versus time since interruption of the d.c. oxidation for five different frequencies and at 3 different points in the oxidation plateau. Significant features of this plot are: (1) the instability of the voltage response during the first few minutes after the interruption, (2) the relatively parallel lines of stable voltage response at later times, and (3) the fact that the plot made at 3 minutes into the d.c. oxidation took several minutes more to stabilize than was needed at 0.8 minutes or 1.5 minutes into the oxidation. These features lend support to the argument that the electrode is being physically changed by the pulsed current, since according to Wijnen and Smit[2], only about 100 cycles at any frequency should be needed to give a stable voltage response. The curve in Figure 10 was obtained from data in the stable regions of Figure 11.

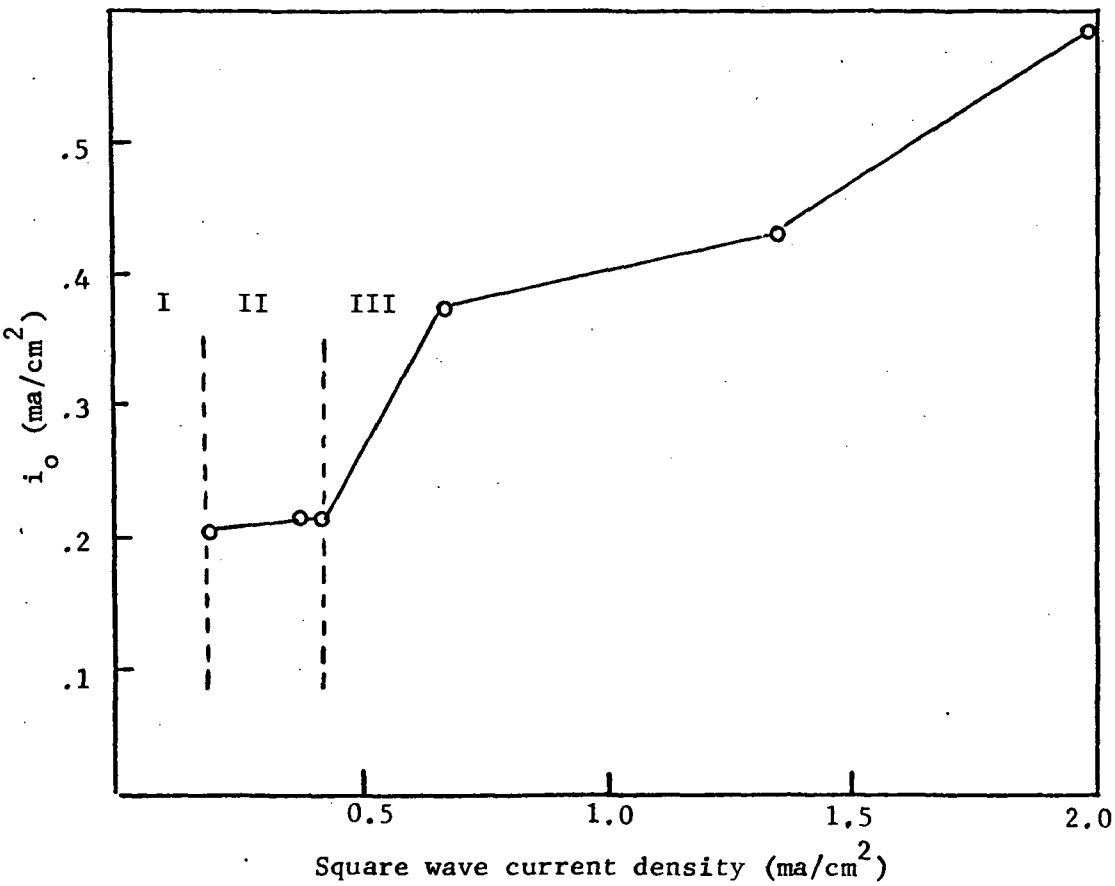

Fig. 11--Plot of i_o versus square wave current density at 1 minute into d.c. oxidation. I-region where plots of $\Delta\eta_\theta$ versus $1/\sqrt{f}$ give no linear portion. II-region where i_o is constant with increasing square wave current density. III-region where voltage response is distorted at low frequencies, and i_o increases with increasing current density.

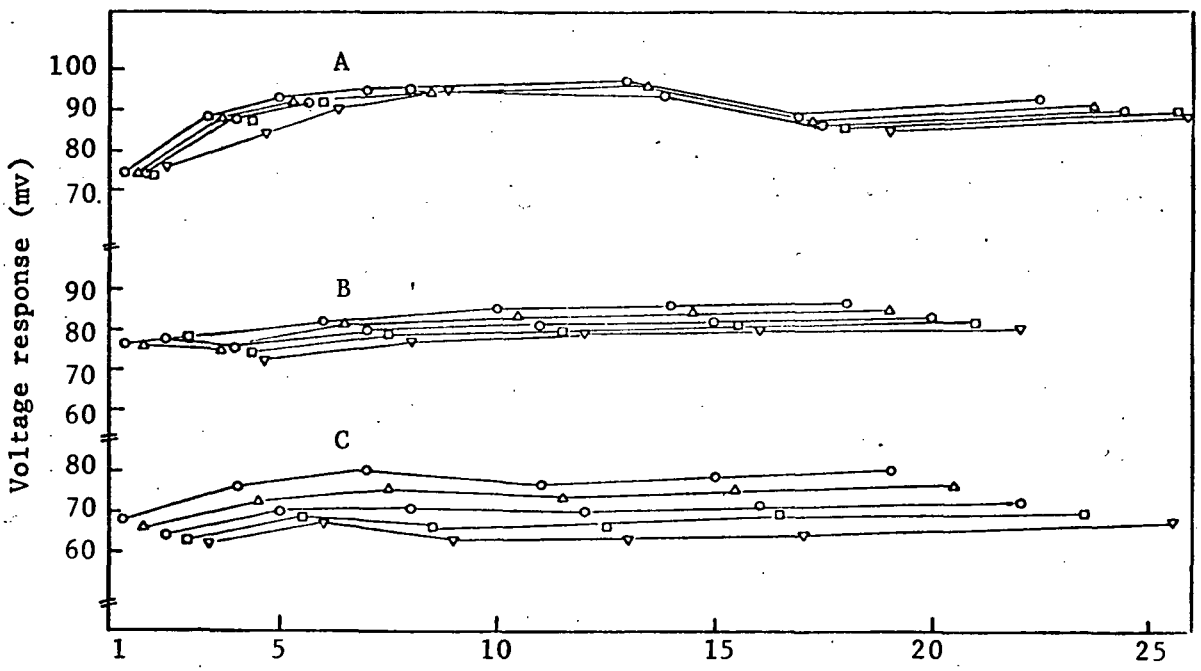

Fig. 12--Plot of electrode voltage response versus time since interruption of d.c. oxidation for five different frequencies. O- 3Hz, Δ -4 Hz, O- 6 Hz, □ - 8 Hz, ∇ - 10 Hz. Square wave current density = .412 ma/cm^2. First plateau length 4.0 minutes.

A Interruption at 3 minutes into d.c. oxidation
B Interruption at 1.5 minutes into d.c. oxidation
C Interruption at 0.8 minutes into d.c. oxidation

RESISTANCE OF THE SILVER OXIDE FILM

The bridge circuit used for the c.c.s. measurements provided a means for the determination of the resistance of the layer of oxide on an electrode. The proper adjustment of R_3 noted in Figure 2a would change the potential response as follows:

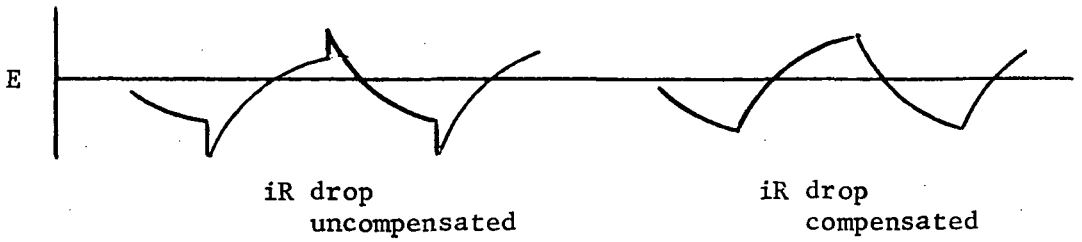

EXPERIMENTAL

The reading on the precision helipot, R_3, gave the total cell resistance from which the initial resistance caused by the solution iR drop was substracted to give the oxide film resistance. The resistance was measured as a function, the amount of charge accepted by the electrode, the concentration of the electrolyte, and the extent of cycling.

The trends in the values of the resistance prompted some measurements of charge acceptance at various stages of oxidation through the second plateau. At each stage the ratio Q_H/Q_T was determined. This ratio is the fractional part of the total charge accepted to the point in question along the second plateau which has produced AgO or adsorbed atomic oxygen. The apparatus used for these determinations is diagrammed in Figure 13.

Determination of Q_H/Q_T.--The ratio Q_H/Q_T was obtained in the following way:

1. A silver foil electrode was oxidized for a particular time t_2 along the second plateau. An average time t_a is determined for the complete oxidation along the second plateau to oxygen evolution. The extent of oxidation along the second plateau is then expressed as the percentage, $100\ t_2/t_a\%$.
2. The total charge accepted, Q_T, during the time t_2 was determined by

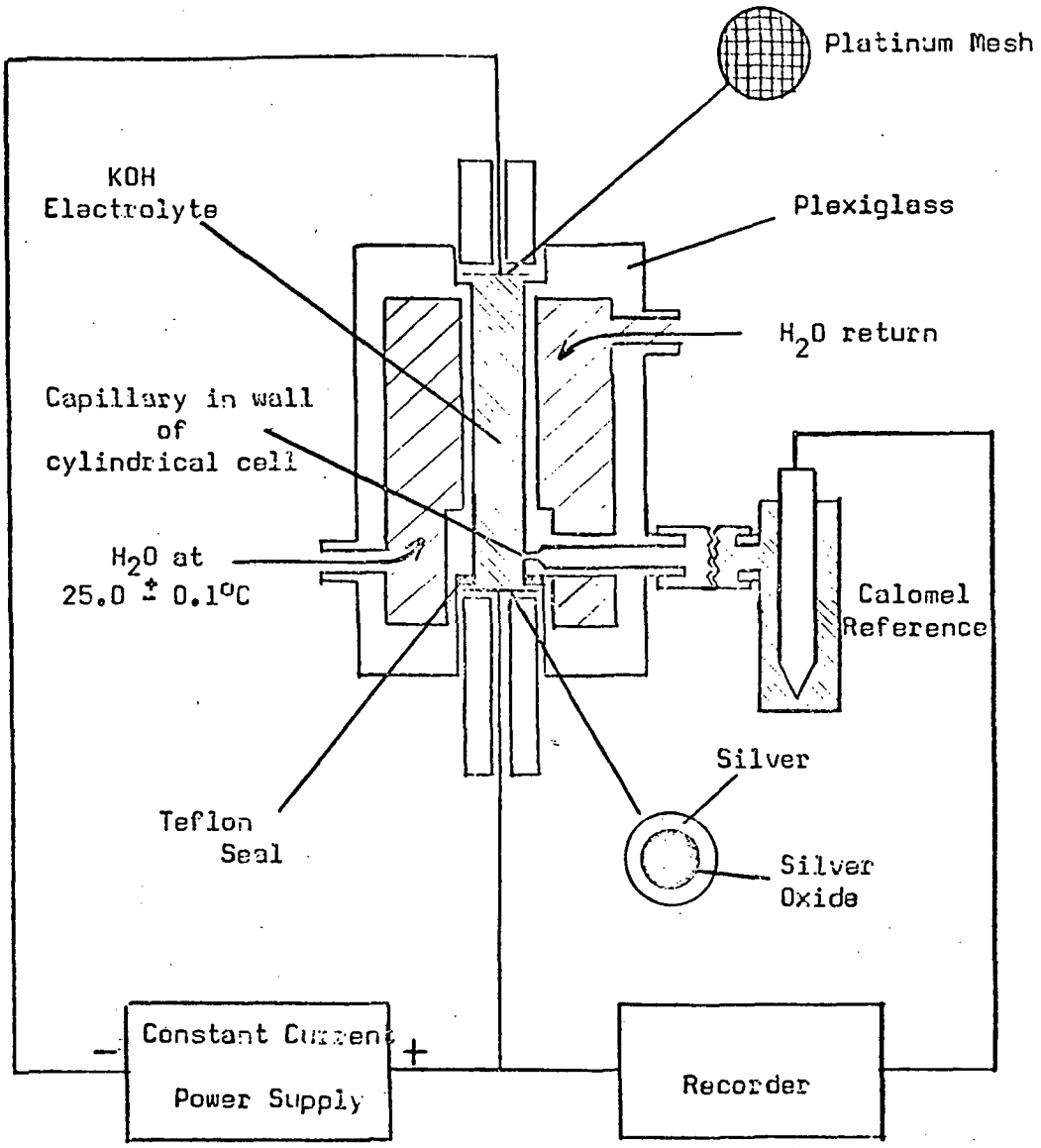

Fig. 13.--Apparatus for charge acceptance data from which the values of the ratio, $r = Q_H/Q_{total}$, were determined.

$$Q_T = i\ t_2$$

where i is the constant current used for the oxidation.

3. The charge, Q_H, responsible for the formation of AgO or adsorbed atomic oxygen was determined by dissolving the silver oxides from the electrode in 0.5 F NH_3, analyzing for silver by atomic absorption spectrophotometry and applying the equation

$$Q_H = i\ (t_1 + t_2) - \frac{y}{W} F$$

where y is the weight of silver in the dissolved oxide, W is the equivalent weight of silver, F is the faraday and t_1 is the time of the first plateau.

4. The ratio Q_H/Q_T was plotted as a function of the extent of oxidation along the second plateau.

RESULTS AND DISCUSSION

The results of resistance measurements (via the c.c.s. technique) made on a silver electrode during the second and fifth successive oxidation-reduction cycles are given in Figure 14. The cycling did not change the shape of the resistance curve, but the magnitude of the resistance of the oxide layer did change. This increase in resistance parallels an increase in charge acceptance with cycling as noted in this table:

Cycle	Relative Charge Acceptance Time of Oxidation (minutes)	Maximum Resistance during 2nd Plateau (ohm-cm^2)
1	2.34	0.35
2	3.29	0.97
3	3.96	1.51
4	4.32	2.09
5	4.58	2.14

Data taken in 1.09 KOH

The influence of the concentration of the KOH electrolyte on the resistance is shown in Figure 15 for five different concentrations. The resistance-time curves are normalized to an arbitrary potential-time curve.

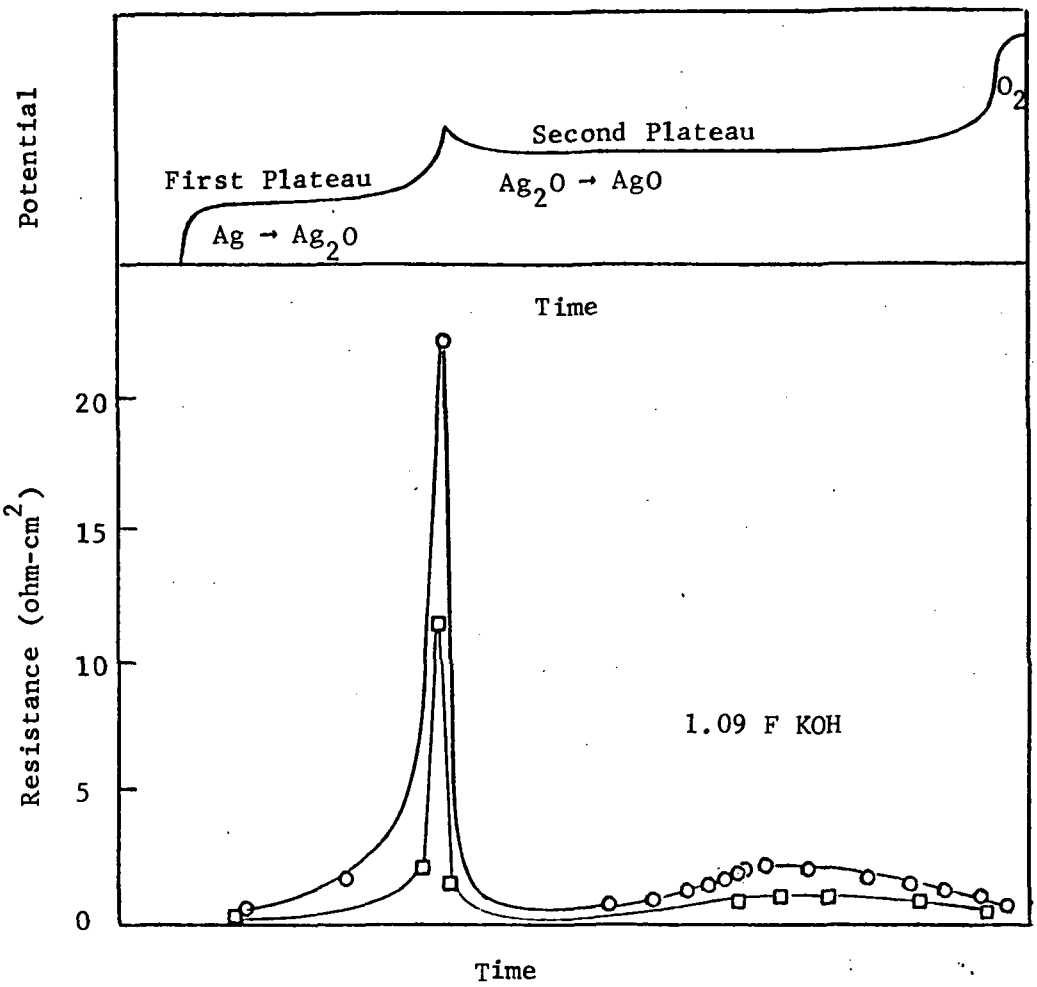

Fig. 14--The resistance of the oxide film on a silver electrode during the oxidation part of the second and fifth cycles normalized on the time coordinate to the generalized potential-time curve at the top.

□ 2nd cycle - time of oxidation - 3.29 min.

○ 5th cycle - time of oxidation - 4.58 min.

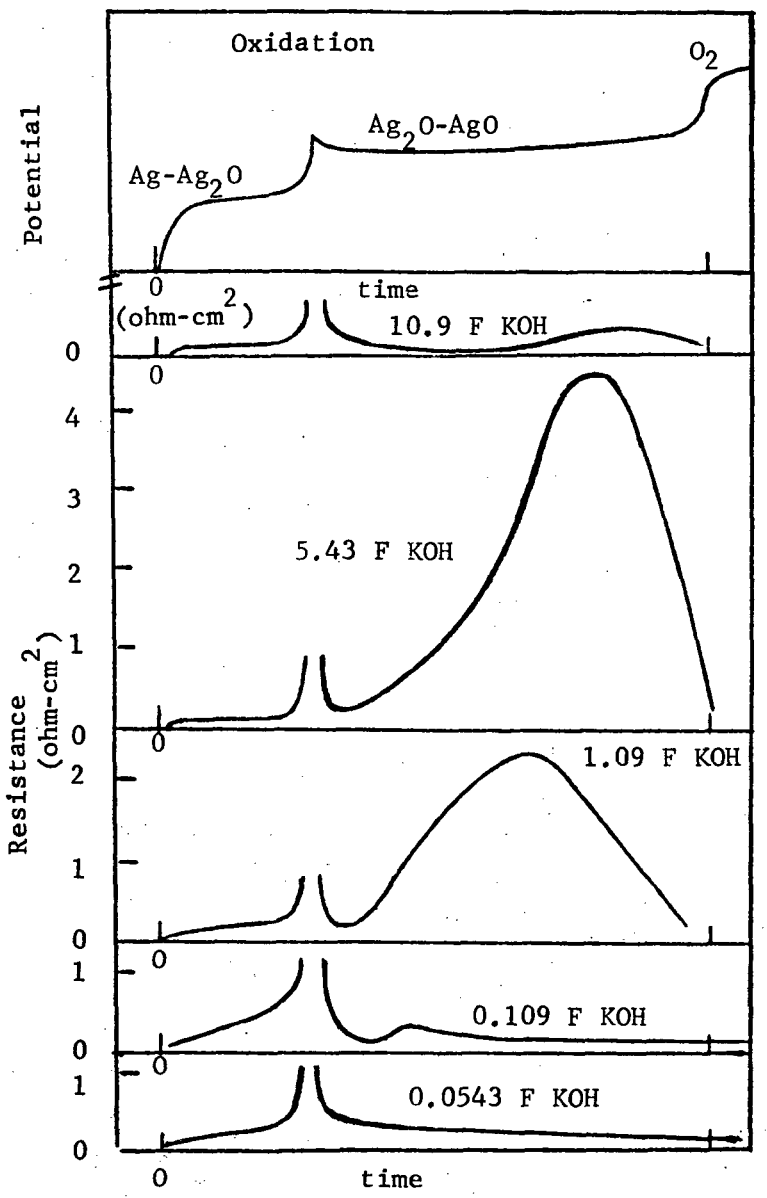

Fig. 15--The resistance versus time curves for the oxidation of silver in KOH solutions. All of these data were obtained at constant current charging of 3.57 ma/cm^2 and then normalized on the time coordinate to the generalized curve at the top.

The charging times (to oxygen evolution) at a constant current of 3.57 ma/cm^2 varies from 1.48 to 9.47 minutes. The maximum resistance of 5.15 $ohm\text{-}cm^2$ during the second plateau occurs in the 5 F KOH solution where the charge acceptance is also the largest.

If one assumes that complete coverage of the electrode occurs early in the first plateau as the results of Briggs, Fleischman, Lax and Thirsk[7] suggest, then an interpretation of resistance based upon factors other than a suddenly completed coverage[5] of the silver surface by the oxide film is required. A possible interpretation involves the consideration of charge carriers (Ag^+, OH^-, $O^=$, or e^-) through a primary Ag_2O layer 50-100 Å in thickness and consisting of small randomly oriented crystals.[7] This interpretation is based on the principle that the resistance of the oxide film to the passage of ions is greater than the resistance to the passage of electrons.[8]

During the first plateau, ions must pass through an Ag_2O layer of increasing thickness. The resistance and potential must rise. When the potential is high enough, nucleation of AgO can occur and the Ag_2O - AgO reaction begins at the electrolyte-Ag_2O interface.[9] At this point most of the current flow through the Ag_2O film is carried by electrons released by the surface reaction

$$Ag_2O + 2OH^- = 2AgO + H_2O + 2\ e^-$$

and a decrease in ohmic resistance results. The $Ag_2O \rightarrow AgO$ reaction soon ceases to be a surface reaction and the resistance increases as the AgO deposit builds up. This is because ions ($O^=$ or OH^-) are the charge carriers through the increasing thickness of AgO. About 60% of the way along the AgO plateau (in 1.09 F KOH) the resistance begins to decrease and a slow rise in electrode potential is noted.

At this stage of oxidation (60% along second plateau) the resistance of the oxide layer in 1.09 F KOH is about nine times that in 0.10 F KOH. If the resistance were due to the actual amounts of AgO per unit surface in the oxide layer one would expect about nine times as much AgO in the layer formed in 1.09 F KOH as in 0.10 F KOH. From Figure 15 the oxide layer formed in 1.09 F KOH is about four times (7.65/2.02) as thick as

that formed in 0.10 F KOH. That there is more AgO per unit surface formed in 1.09 F KOH is shown in Figure 16 where the ratio Q_H/Q_T is plotted as a function of percentage oxidation through the second plateau region. Although the precision is poor, there is probably two to three times more AgO per unit weight of surface oxide in the 1.09 F KOH oxidation as in the 0.10 F KOH oxidation. Therefore, the actual amount of AgO in 1.09 F KOH is eight to twelve times that in 0.10 F KOH which correlates well with the observed difference in resistance.

The ratio Q_H/Q_T is the fractional part of the total charge accepted during the second plateau which forms AgO or adsorbed atomic oxygen. This ratio emphasizes the fact that although the second plateau is usually associated with the reaction $Ag_2O \rightarrow AgO$ there is still a significant quantity of Ag being oxidized to Ag_2O during the second plateau. In fact, the data of Figure 16 show $Ag \rightarrow Ag_2O$ to be the main reaction.

Figure 16 also shows the ratio Q_H/Q_T doubling as the reaction proceeds from 60% to 90% completion along the second plateau. These results suggest the beginning of another reaction at the electrolyte-electrode interface such as

$$2OH^- \rightarrow O_{adsorbed} + H_2O + 2e^-$$

where a gradually decreasing fraction of the current through the underlying oxide is carried by ions. As more of the current is carried by electrons the resistance gradually decreases. This is consistent with the observation that the oxide-film resistance is low at oxygen evolution where the current through the underlying oxide is carried by electrons from the reaction

$$OH^- \rightarrow O_2 + 2H_2O + 4e^-.$$

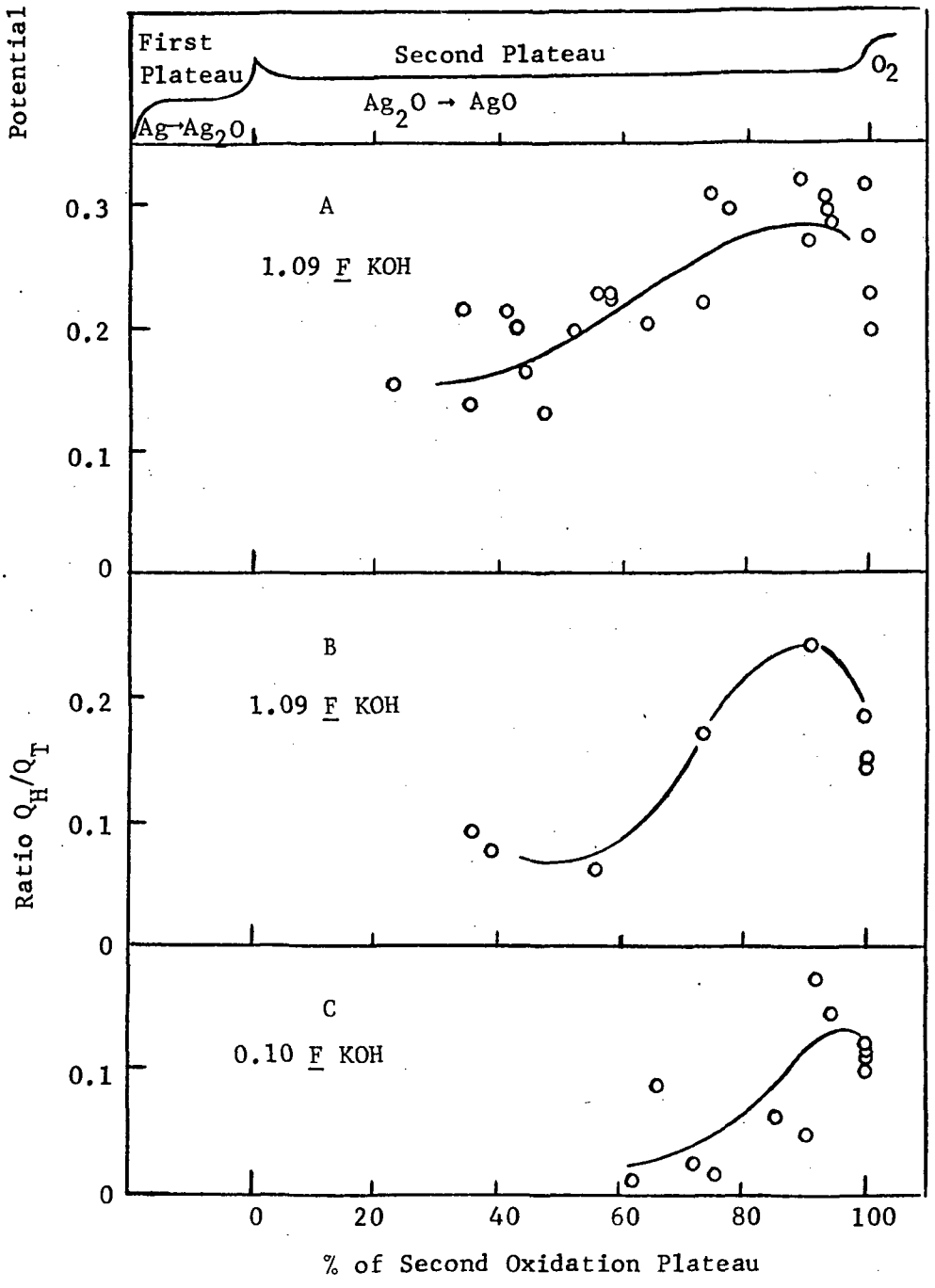

Fig. 16-- The ratio, Q_H/Q_T, plotted against percent of the second plateau. The 1.09 F KOH in A was reused in successive determinations and in B it was replaced after each run.

SECTION II

OXIDATION OF MODEL-PORE ELECTRODES

INTRODUCTION

This section describes an investigation of the oxidation of model-pore electrodes. The mechanism of oxidation in a pore is of concern because a very large fraction of the surface area of a sintered silver electrode is contributed by the walls of the pores which comprise the substructure of the electrode. Numerous types of model-pore electrodes are discussed in the literature.[10-15] Two types were used during this investigation. The type of electrode used in most of the experiments consisted of a hexagonal close-packed array of silver wires. The other model-pore electrode consisted of an 18 mm wide strip of silver tightly fitted into an 18 mm diameter glass tube.

EXPERIMENTAL

During the course of the investigation, two configurations of the wire electrode and two configurations of the strip electrode were used. These are illustrated in Figures 17 and 18.

The two configurations of the wire model pore electrodes were:

A. Glass or acrylic plastic body with a circular hole, and

B. Two piece acrylic body with a hexagonal hole.

The second configuration (b) was constructed to hold electrodes consisting of nineteen or more wires. The circular hole in configuration A will hold that many wires, but the array is random, and the resulting pores are non-uniform. In both configurations electrolyte flowed slowly into the stem located near the top of the holder, through the electrode, and into the reservoir. The electrode wires were fused at the top to a larger diameter wire that led to the current source. Uniform wire lengths were obtained by abrading the ends of the wires with 600 mesh silicon carbide paper. Each wire in the electrode was washed with cleanser and rinsed. In some

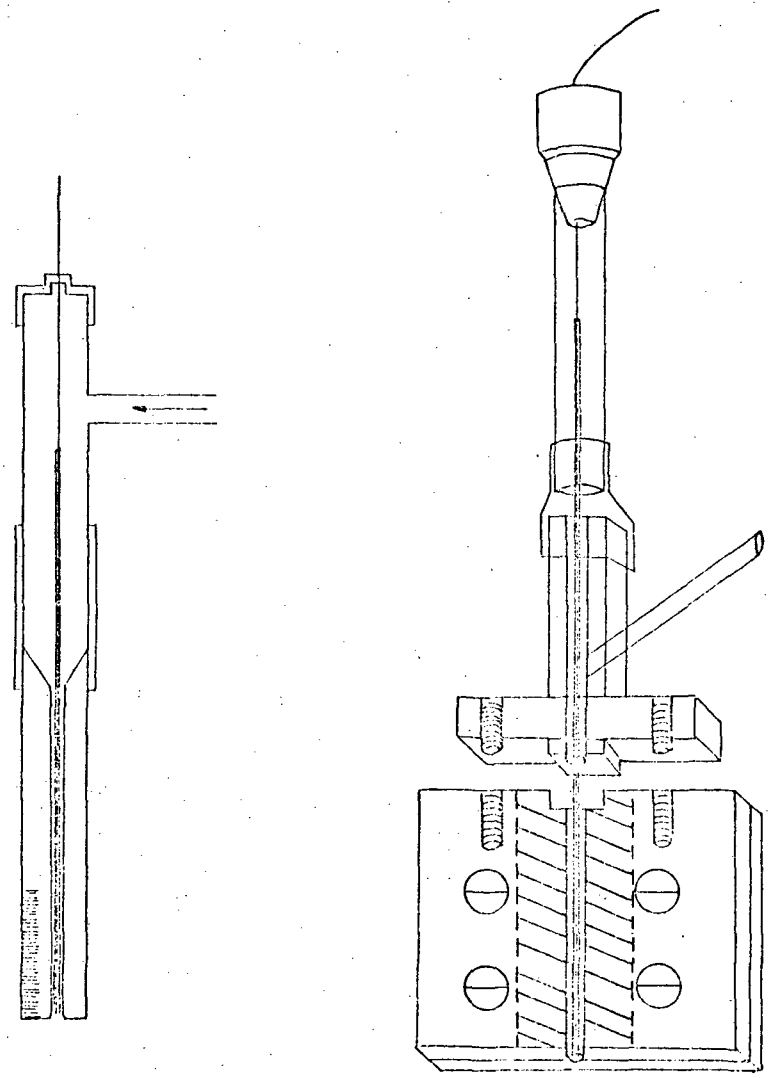

(a) (b)

Figure 17. Model-pore electrodes

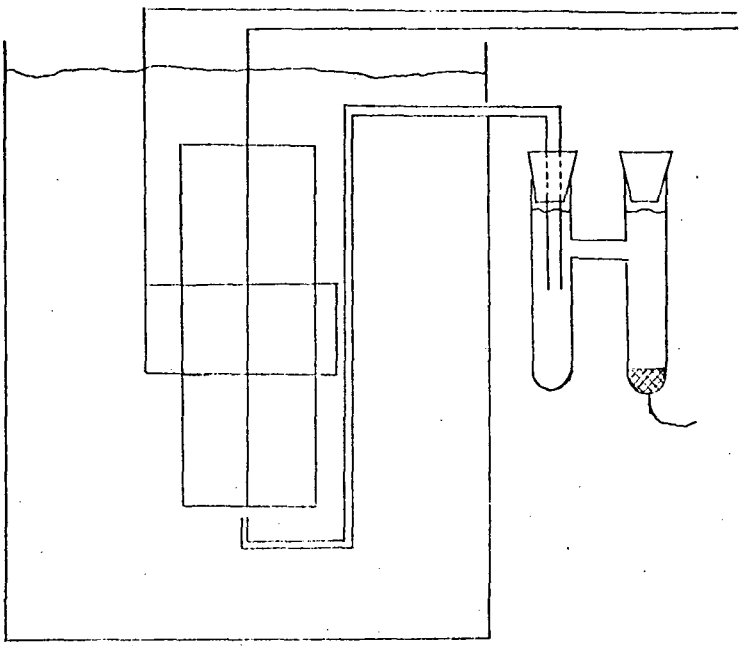

(a)

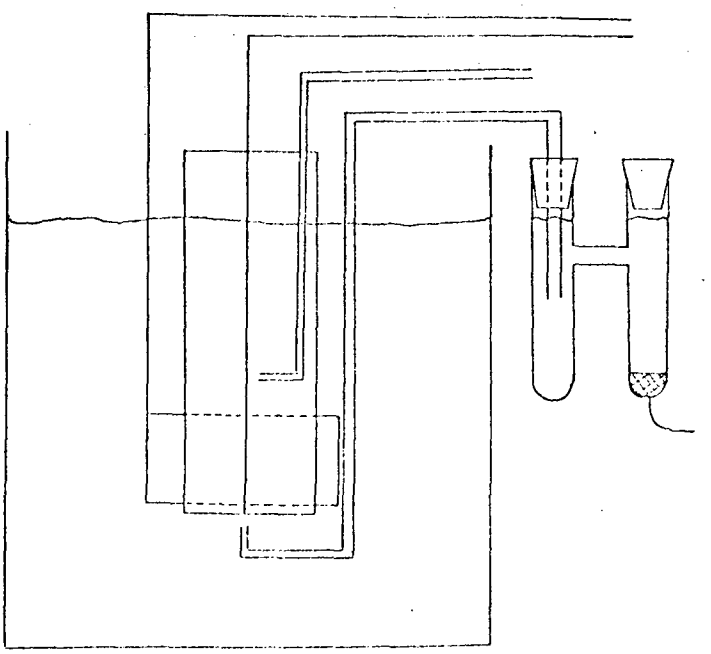

(b)

Figure 18. Strip model-pore electrode.

experiments the polished ends were masked with expoxy cement. Several dimensions of five wire model-pore electrodes are contained in Table II. The counter electrodes were platinum and the reference electrodes were calomel.

In each of the wire electrode configurations the small diameters of the wires made it very difficult to follow the oxide penetration into a pore during the course of an oxidation. This difficulty was overcome by constructing a strip electrode. As shown in Figure 18, the configurations of the strip electrode were:

1. Electrode completely submerged, with the reference electrode located some distance from it, and
2. Electrode partially submerged, with two luggin capillaries coming from the reference electrodes to the mouth of the pore and to a point midway up the pore.

The counter electrodes were of platinum and the reference electrodes were Hg/HgO.

The various concentrations of KOH electrolyte were prepared from a 45% KOH solution marketed by Baker Chemical Company and analyzed by them to contain only 0.01% K_2CO_3.

The constant current was supplied by an Electronics Measurements power supply, Model C633.

RESULTS AND DISCUSSION

Figure 19 is a representative potential-time curve for the oxidation of a model-pore electrode. When the current is first applied the potential rapidly rises (Region A) and a translucent brown film is observed to cover the surface of the silver wires to a depth into the pore of at least 2 cm. In Region B the current increases linearly with time while a dark brown oxide (Ag_2O) progresses into the pore. The linear increase in potential is probably caused by the increase in electrolyte resistance as the reaction proceeds deeper into the pore. There is no observable change on the electrode in Region C. The next linear increase in potential (Region D) is characterized by a further growth of the Ag_2O into the pore and the appearance of a black oxide (AgO) near the mouth of the pore. The potential

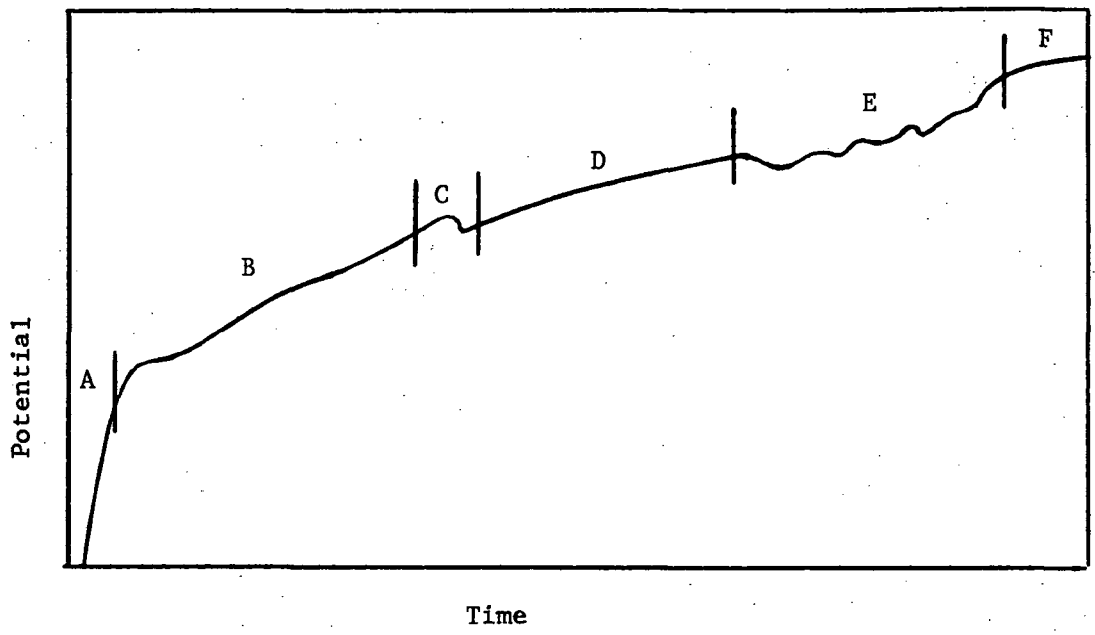

Fig. 19--Representative potential-time curve for the oxidation of a model pore electrode at 0.822 $\mu A/mn^2$ in 0.1 F KOH. The letters correspond to conditions described in text of the report.

TABLE II

DIMENSIONS OF REPRESENTATIVE WIRE MODEL PORE ELECTRODES

Description		Electrodes				
		1	2	3	4	5
Wires	Number	7	7	7	7	7
	Size (mil)	51	40	25	20	10
	Radius (mm)	0.646	0.512	0.322	0.254	0.127
Cross Sectional Area (mm^2)	Electrode	11.77	7.42	2.93	1.82	0.457
	Wires	9.17	5.77	2.33	1.41	0.355
	Pores	2.60	1.65	0.60	0.41	0.102
Surface area per mm into the pore	Wires	28.3	22.5	14.1	11.2	5.59
Ratio of wire cross sectional area (mm^2) to total wire surface area (including the tip) in a 21 mm electrode (the average length).		0.0154	0.0136	0.00784	0.00598	0.00302
Ratio of wire cross sectional area (mm^2) to surface area per mm into the pore		0.324	0.256	0.165	0.126	0.0672

oscillations shown in Region E were obtained using both wire and strip model-pore electrodes, but only at certain current densities and electrolyte concentrations. Only on the strip electrodes was it possible to observe a physical change of the electrode surface that corresponded to the potential oscillations. It consisted of the alternate appearance of dark grey and light grey horizontal bands as the oxide moved up the pore. The growth of the dark band occurred at the same time that the potential was rising to the oscillation peak, while the light band formed as the potential descended to the oscillation minimum. The greater the amplitude of oscillation, the more pronounced was the band; the longer the period of oscillation, the wider the band.

During the oxidation of wire model-pore electrodes at high currents, and where there are no potential oscillations, the upper edge of the advancing AgO is preceded by a thin dark band. It has the same appearance as the dark grey band observed during potential oscillations, but differs from it in that it is constantly present and moving during oxidation. By the beginning of oxygen evolution (noted at the tip of the electrode) the Ag_2O and AgO had penetrated to average depths of about 10 mm and 4 mm. In Region F the evolution of oxygen is clearly evident.

At low current densities (8 $\mu a/cm^2$) in dilute electrolyte and at most currents in concentrated (11.5F) electrolyte the potential-time curve had the shape usually obtained in the oxidation of exposed wires and strips. The first plateau had a negligible slope, and there were very few, if any, potential oscillations in the second plateau. These curves were probably obtained because at low current densities, or with high concentrations of electrolyte, the iR drop up the pore is negligible.

The results of wire model-pore electrode oxidations show that the extent of penetration into the pores by both Ag_2O and AgO decreases as pore diameter decreases. The resistance of the electrolyte per mm into a pore increases as the pore diameter decreases. The resulting larger iR drop per mm into the pore allows the oxides to penetrate a small diameter pore a relatively short distance before the potential at the mouth of the pore rises to that of oxygen evolution.

Table III contains the lengths (in seconds) of the first plateau at various currents for wire electrodes of three sizes (A, B, and C). Notice that the order of pore diameter is A>B>C. The order of surface area exposed to electrolyte is C>A>B. Electrodes A and B each have 7 parallel wires while C has 19 parallel wires.

TABLE III

First Plateau Lengths (sec) for Three Model-Pore Wire Electrodes

Electrode	Pore Cross-Sectional Area (mm^2)	Exposed Surface Area (cm^2)	Length (sec) at 250μa	500μa	1100μa	1600μa	2000μa
A	1.50	.86		492	90	45	33
A				486	96	45	33
B	.95	.67	750	132	22		
B			742	168	26		
C	.93	1.13	1200	270	36	15	
C			1200	258	36	17	

It can be seen that, at 500μa, the plateau length is longer for electrode A than for electrode B. This would be expected if the amount of charge accepted by this electrode were only a function of surface area exposed to electrolyte. Comparison of plateau lengths for electrodes A and C, however, shows a substantial decrease even though electrode C has 30% more exposed surface area than does electrode A. This anomaly can be explained by the relationship between depth of oxide penetration into a pore and the diameter of that pore. The much smaller diameter of the pores in electrode C have a much larger iR drop per mm into the pore than do the pores of electrode A. This larger iR drop prevents the potential on much of electrode C's exposed surface area from rising to that of Ag - Ag_2O before the potential at the mouth of the electrode rises to that of Ag_2O-AgO.

What follows next is a more detailed discussion of electrode phenomena in Regions A, B and E.

Region A. The thin brown film that spreads quickly into the pore in the first few seconds of oxidation has been shown, by scanning electron

microscopy, to be a fairly compact aggregate of small oxide mounds. These are believed to be the nucleation sites for the larger (10x) but less populous mounds that are observed in later stages of oxidation. Our SEM work has also shown that nucleation is a function of potential. The spread of the brown film from the mouth of the pore up into the pore would seem to confirm this. During a constant current oxidation the potential would gradually increase at a given point in the pore until nucleation was accomplished, and oxide growth begun. The first few sites nucleated would not be sufficient to handle the oxide growth required by the fixed current and the potential would rise at the nucleation sites. With a rise in potential at the nucleation sites there would be a corresponding rise in potential all along the pore. In the unoxidized area immediately above the sites the potential would rise to that of nucleation and a new aggregation of mounds would be formed. The nucleation-potential rise cycle occurs on such a short time scale and in such small dimensions that the macroscopic appearance would be that of continuous growth of the film into the pore. The cycle would stop when sufficient sites had been formed to accommodate the oxide growth required by the current.

Region B. A few electrodes had wires on which there were long, shallow scratches along the length of the wire. When the electrode was oxidized, Ag_2O was observed to grow inside these grooves to a distance of some 17 mm into the pore. The usual depth of penetration into a pore is only 3-8 mm. It appears that the scratch is a site of preferential oxidation of either its geometry or its strained surface. The geometry of the scratch would have the effect of creating a pore of larger diameter and one, therefore, which would have a smaller iR drop per mm into the pore. Considering the other possibility, some authors have observed that silver and other metals will undergo corrosion at lower potentials when the metal is subjected to stress or strain.[16-19] Smit has discussed the change in the shape of the Fermi surface at points of strain as a possible source of these potential differences.[20]

As shown in Figure 18a the strip electrode was positioned such that the distance between the top of the electrode and the electrolyte level was equal to the distance between the bottom of the electrode and the

bottom of the container. This was done to provide equivalent current paths to both ends of the electrode. When this condition of equivalent current paths is not met, preferential growth is observed at the end of the electrode having the shortest current path to the counter electrode. However, there still appears to be preferential growth from the bottom of the electrode even when the current paths are equidistant. This phenomenon can be explained in terms of the dissolution-precipitation mechanism of Ag_2O growth discussed by Miller.[21] The precipitation part of this mechanism includes a super-saturated solution of complexed silver (I), near the electrode surface, from which the Ag_2O precipitates on the nucleated sites discussed earlier. The preferential oxidation is probably caused by convection currents carrying the more dense, super-saturated layer of complexed silver (I) towards the mouth of the pore. The effect of convection currents on the super-saturated solution has been used by Brieter to explain the preferential film formation on horizontal zinc electrodes as opposed to vertical electrodes.[22]

In the potential-time curves of all the oxidations, except those at the highest currents, a plateau could be detected in the $Ag\text{-}Ag_2O$ potential region. In Figure 20, the potential of this plateau is plotted against the applied current for each of eight different electrolyte concentrations. The slopes of the lines decrease with increasing electrolyte concentration. On each electrolyte curve the potential of the first plateau increases with increasing current. At low currents the plateau potential is not nearly so sensitive to electrolyte concentration as it is at higher currents. This would suggest that the differences in plateau potential are a result of varying degrees of electrolyte depletion near the electrode surface. Calculation shows that in 0.1 F KOH the hydroxide ions required to form an oxide film of thickness X Å are contained in an electrolyte layer of 1000X Å thickness. When the electrolyte near the electrode surface is gently stirred, the first plateau potential drops approximately 20 mv.

Region E. Figures 37E and 37F in the SEM section of this report are micrographs of a surface which was light grey with dark grey spots. It can be seen that the light grey surface has a number of large oxide mounds on it while the dark grey surface has a close array of much smaller

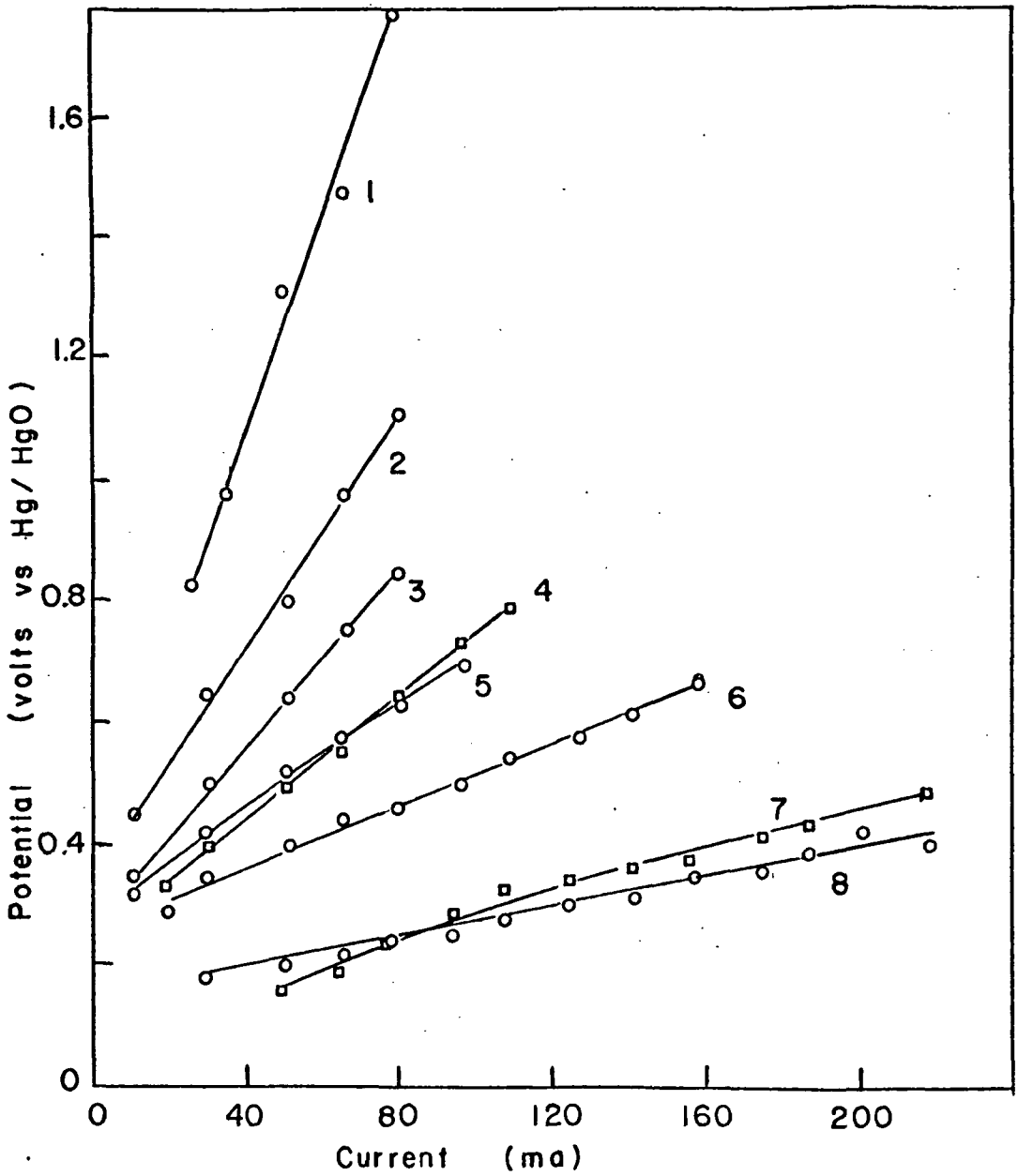

Fig. 20--Potential of first plateau as a function of current and electrolyte concentration.

KOH concentration

1	0.10 N	5	0.49 N
2	0.24 N	6	1.0 N
3	0.35 N	7	11.5 N
4	0.57 N	8	4.9 N

mounds. It would appear, therefore, that the potential oscillations are caused not by Ag_2O-AgO oxidation alone, but also by phenomena associated with the additional formation of Ag_2O. In SEM studies of wires oxidized at various constant currents it was found that large mounds similar to those in Figure 37F occurred at low current densities while the smaller mounds in Figure 37F occurred at high current densities. The light and grey bands, therefore, must reflect the different current densities in the pore.

At the beginning of a series of oxidation-reduction cycles on a model-pore electrode the potential oscillations were small in number and magnitude. They quickly increased in size and number during the first 10-15 cycles and gradually thereafter. After about 30 continuous cycles a maximum of 7-12 oscillations were observed. Through a series of from 2 to 5 cycles an oscillation appeared first as an inflection (I), then a plateau (P), and finally a full oscillation (F). These are shown below.

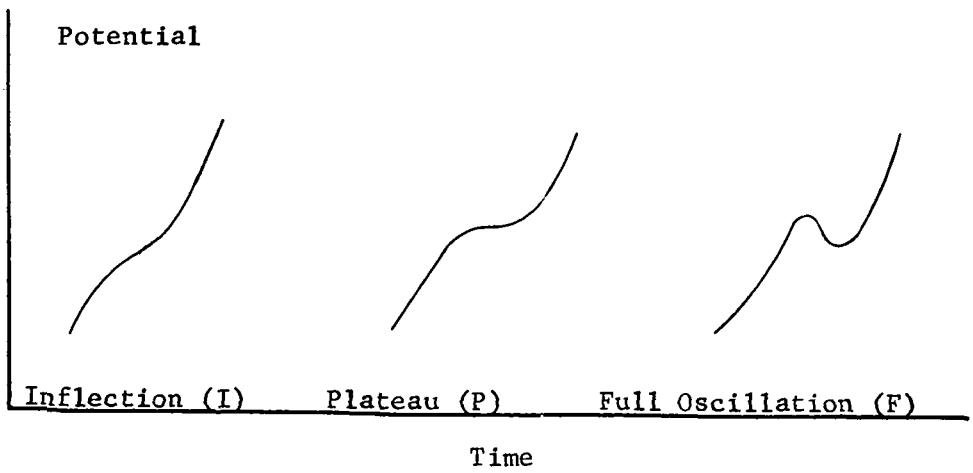

Table IV shows the effect of cycling on the number and shape of potential oscillations.

The previously mentioned growth pattern of an oscillation, and the increase in the number of peaks during cycling, occurred not only with fresh electrodes, but also with a cycled electrode that had been inactive for three or more hours. It may be that a freshly reduced electrode has some highly reactive silver on its surface much like that observed by Krebs and Roe when they electro-deposited thin films of silver on a single

TABLE IV

OSCILLATIONS ON A CYCLED ELECTRODE

Determinations	i (ma)	F KOH	1				2				3				4			
			I	P	F	Total	I	P	F	Total	I	P	F	Total	I	P	F	Total
55 - 58	50	0.3	1	8	2	11	1	5	5	11	1	6	5	12	1	5	6	12
69 - 71	50	0.4	0	3	4	7	1	2	5	8	1	2	6	9				
73, 75, 87	50	0.4	1	1	5	7	1	2	5	8	0	2	7	9				
79 - 82	65	0.4	1	8	0	9	1	7	4	12	1	6	5	12	1	7	4	12

I = Inflection

P = Partial oscillation

F = Full oscillation

silver crystal.[23] Mamantov, et al have also reported the existence of this highly reactive silver.[24] Deposition did not proceed in a layer-like fashion, but rather gave rise to hemispherically shaped deposits. Our SEM studies have shown that reduced silver wire also has hemispheres of silver on its surface.

In Table IV, we showed that the number and shape of the potential oscillations were affected by cycling. Table V gives descriptions of oscillations produced during oxidations at various currents and electrolyte concentrations. For most electrolyte concentrations, the total number of oscillations (7-12) increases with increasing current to a maximum, past which the number decreases with increasing current. Another observed trend is in the effect of electrolyte concentration on oxidations made at the same current. At low concentrations, the oscillations are primarily inflections and plateaus. As the concentration is increased, they develop into full oscillations. Another maximum in the total number of oscillations is observed in going across a current row.

Table V

Description of Oscillations Occurring in Oxidation Runs
at Various Currents and Electrolyte Concentrations

i	$[OH^-]$																											
	0.1				0.2				0.3				0.4				0.5				0.6				0.7			
(ma)	I	P	F	T	I	P	F	T	I	P	F	T	I	P	F	T	I	P	F	T	I	P	F	T	I	P	F	T
10					0	0	2	2	0	0	2	2	0	0	2	2												
20	2	0	0	2	0	1	4	5	0	0	3	3	0	0	2	2	0	0	2	2	0	1	1	2				
30	2	0	0	2	1	3	4	8	1	2	3	6	0	1	3	4	0	0	2	2	0	1	2	3	0	2	6	8
50	2	0	0	2	3	4	0	7	1	5	6	12	0	2	7	9	0	2	4	6	0	1	2	3	0	1	2	3
65	2	0	0	2	6	5	1	12	1	9	4	14	1	4	6	11	1	1	6	8	0	1	3	4	0	0	2	2
80	2	0	0	2	7	0	0	7	3	7	0	10	2	11	0	13	2	2	7	11	0	2	3	5	0	0	3	3
95													3	0	0	3	3	10	0	13	0	2	4	6	0	2	1	3
110																	2	2	0	4	1	1	5	7	0	2	2	4
125																					1	1	6	8	0	2	2	4
140																					1	3	5	9	0	2	2	4
155																					6	6	0	12	1	1	2	4
170																									1	0	3	4
185																									1	1	2	4
200																									1	0	3	4
215																									0	2	2	4
230																									1	3	0	4
245																									1	4	0	5

SECTION III

CHARGE ACCEPTANCE OF SILVER ELECTRODES UNDER POTENTIOSTATIC CONDITIONS

INTRODUCTION

This section gives the results of a study of potentiostatic oxidations of silver in alkaline solution over a range of hydroxide ion concentrations, temperatures, and potentials. The effects these variables have on the charge acceptance of the silver electrode have been investigated. Also, the applicability of various growth rate laws has been explored. Conclusions as to the controlling factors of the reaction are drawn. Inferences are also made from the effects of the above variables on the terms of the growth rate equations.

EXPERIMENTAL

The data in this section were obtained under two different experimental conditions. All data, except those involved in initially determining the applicability of various growth rate laws, were taken from oxidations made on the same silver electrode in a Haring cell.[25] The area of the silver electrode was 4.0 cm^2. After each oxidation, the oxide was removed at a potential of 0.00 volts vs. Hg/HgO. A McKee-Pederson Potentiostat MP-1026 was used to make these potentiostatic oxidations and reductions. Platinum was used for the counter electrode. Hg/HgO was the reference electrode. Data were taken at $0^{\circ}C$, $25^{\circ}C$, and $50^{\circ}C$. At each temperature, runs in 0.1 N, 1.0 N, 5.0 N, and 11.1 N KOH were made under potentiostatic conditions with potentials ranging from 0.40 v to 0.75 v vs. Hg/HgO. The cell was maintained at $0^{\circ}C$ by placing it in an ice bath. For the runs at $50^{\circ}C$, the cell was placed in a water bath which was thermostated at $50^{\circ}C \pm 0.1^{\circ}$. All other runs were done at room temperature ($\sim 25^{\circ}C$).

The current as a function of time was recorded by a Sargent strip-chart recorder that measured the iR drop across a resistance wire. Charge acceptance

was obtained from these plots by measuring the area under the curve with a Keuffel and Esser planimeter and by the use of Simpson's rule of numerical integration.

Those data involved in initially determining the applicability of the various growth rate laws were obtained by oxidizing 0.10 inch silver wire potentiostatically in 0.100 N KOH at room temperature. The cell used is shown in Figure 21. The equipment used for the oxidation of the electrode and the measurement of the current is shown in Figure 22. The potentiostat is an Analog Devices Model 119A 20ma operational amplifier. The current through the cell is measured by amplifying the voltage across a 10 ohm precision resistor by a factor of 100 and recording the resulting signal on a Varian multi-range strip-chart recorder. An Analog Devices Model 231J chopper-stabilized operational amplifier is used in a gain-of-100 amplifier configuration in order to accurately record signals as small as 0.1 microvolt using a 10 mv recorder.

The electrodes were cleaned with an abrasive cleanser before they were placed in the cell. They were then oxidized and reduced for 15 to 20 cycles to stabilize the surface characteristics and to establish a uniform history. Data were obtained by oxidizing an electrode at a selected potential until the current became very small (10-50 $\mu a/cm^2$). The electrode was then rapidly reduced (400 ma/cm^2) and held at the potential of reduction of water for several seconds. The current as a function of time was recorded during oxidation on the strip chart recorder. Charge acceptance was calculated by Simpson's rule of numerical integration using data from these current-time functions.

In both experiments the electrolyte was prepared from 45% KOH reagent obtained from the J. T. Baker Chemical Company. This reagent contained 0.01% K_2CO_3. It was diluted to the proper concentration with distilled H_2O through which N_2 had been bubbled to expel CO_2. The electrolyte was changed daily to minimize CO_2 contamination.

RESULTS AND DISCUSSION

The same general shape of the current vs. time curve was observed at all temperatures, potentials and hydroxide ion concentrations. At lower

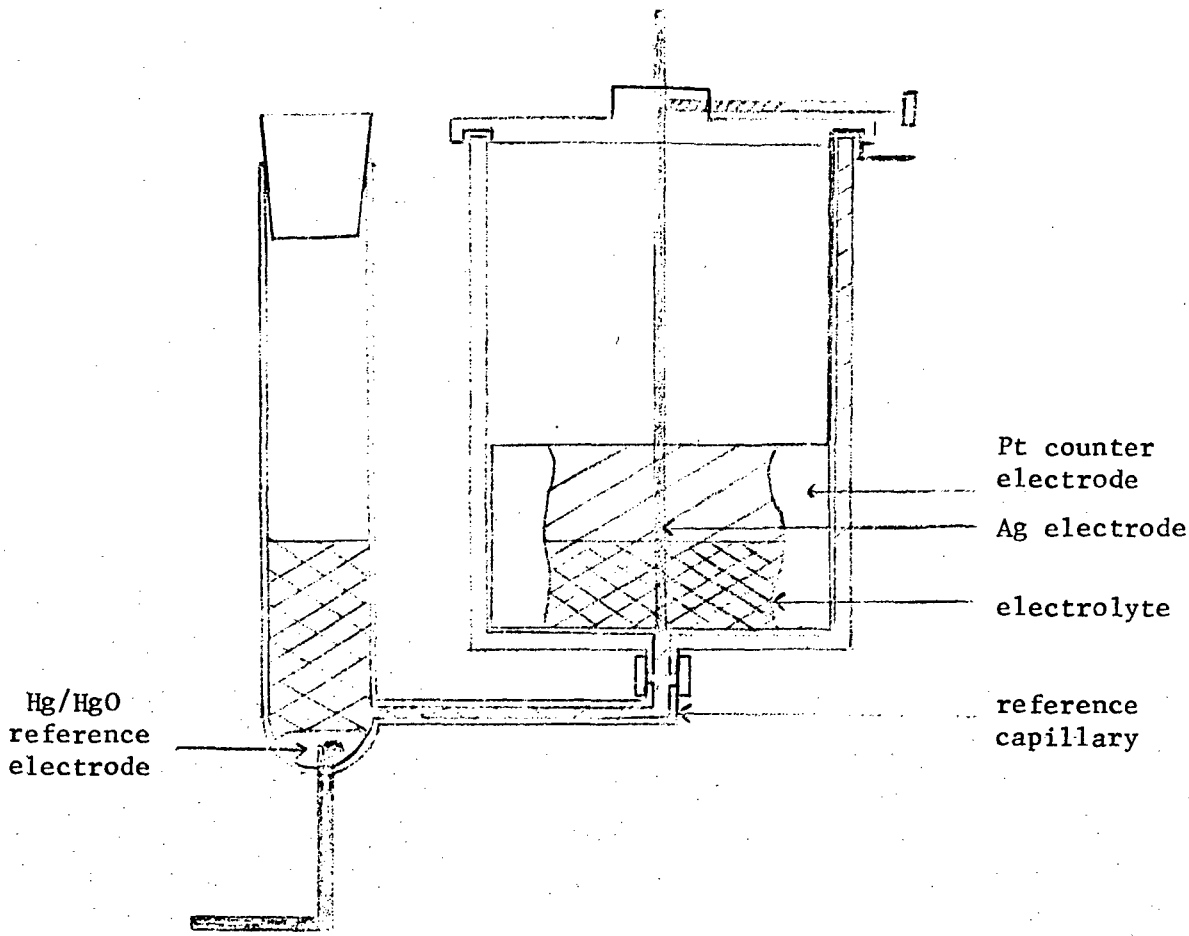

Figure 21. Cross sectional view of cell used in study of potentiostatic oxidation of silver.

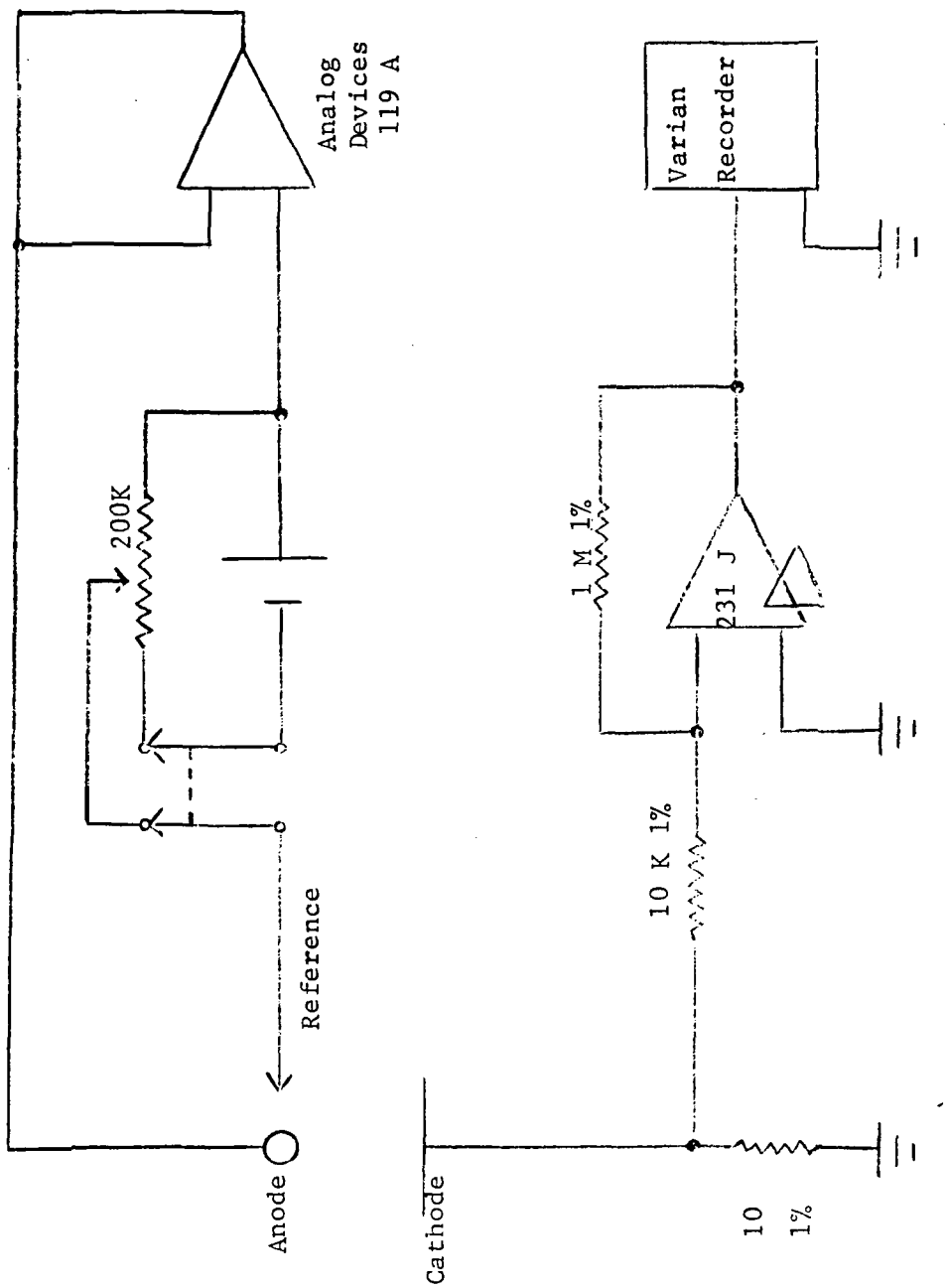

Figure 22. Potentiostat used in potentiostatic oxidations of silver. The gain of 100 current measuring circuit is included.

potentials there was a single current surge which "tailed off" to the background current (Figure 23a). At higher potentials there was a second current surge which was usually first observed at 0.60 v vs. Hg/HgO. When this second current surge first appeared as a function of increasing potential, it was very broad and low (Figure 23b). At higher potentials, the second surge became narrower and the peak value became larger (Figure 23c). Also, at these higher potentials, the time required to reach the maximum of the second surge became progressively smaller, until it almost blended in with the first surge (Figure 23d).

The behavior observed at $0^{o}C$ was somewhat anomalous. Here the second current surge seemed to be "repressed." It appeared at the normal potentials but never reached the peak values observed at other temperatures. This effect became more pronounced as the concentration of the electrolyte was increased. Also, the second surge "died out" as potentials above 0.65 v were applied at this temperature.

Charge Acceptance. Figure 24 shows the variation of charge acceptance with the potential at which the oxidation was run in the various concentrations of KOH at $0^{o}C$. Figures 25 and 26 show the results at $25^{o}C$ and at $50^{o}C$. A summary of the general trends and important observations taken from these three figures is indicated in tabular form as follows:

CONDITIONS	TRENDS IN CHARGE ACCEPTANCE
From 0.40 v to 0.60 v at 0^{o} and $25^{o}C$ for all concentrations	Values range from 25 to 150 mcoul/cm^2 with no linear function of hydroxide ion concentration. There is some slight decrease with increasing potential.
From 0.40 v to 0.60 v at $50^{o}C$ for all concentrations	Values range from 100 to 250 mcoul/cm^2 which is a significant increase over charge acceptance at the lower temperatures.
At 0.60 v for 5.0 N and 11.1 N KOH at all temperatures	A two- or three-fold increase in charge acceptance corresponding to the first appearance of the second current surge.
From 0.60 v - 0.75 v for 0.10 N and 1.0 N KOH at all temperatures (except 1.0 KOH at $0^{o}C$)	A gradual increase in charge acceptance with increasing potential after appearance of the second current surge.
From 0.60 v - 0.75 v for 5.0 N and 11.1 N KOH at all temperatures	A decrease in charge acceptance with increasing potential after abrupt increase at 0.60 v.

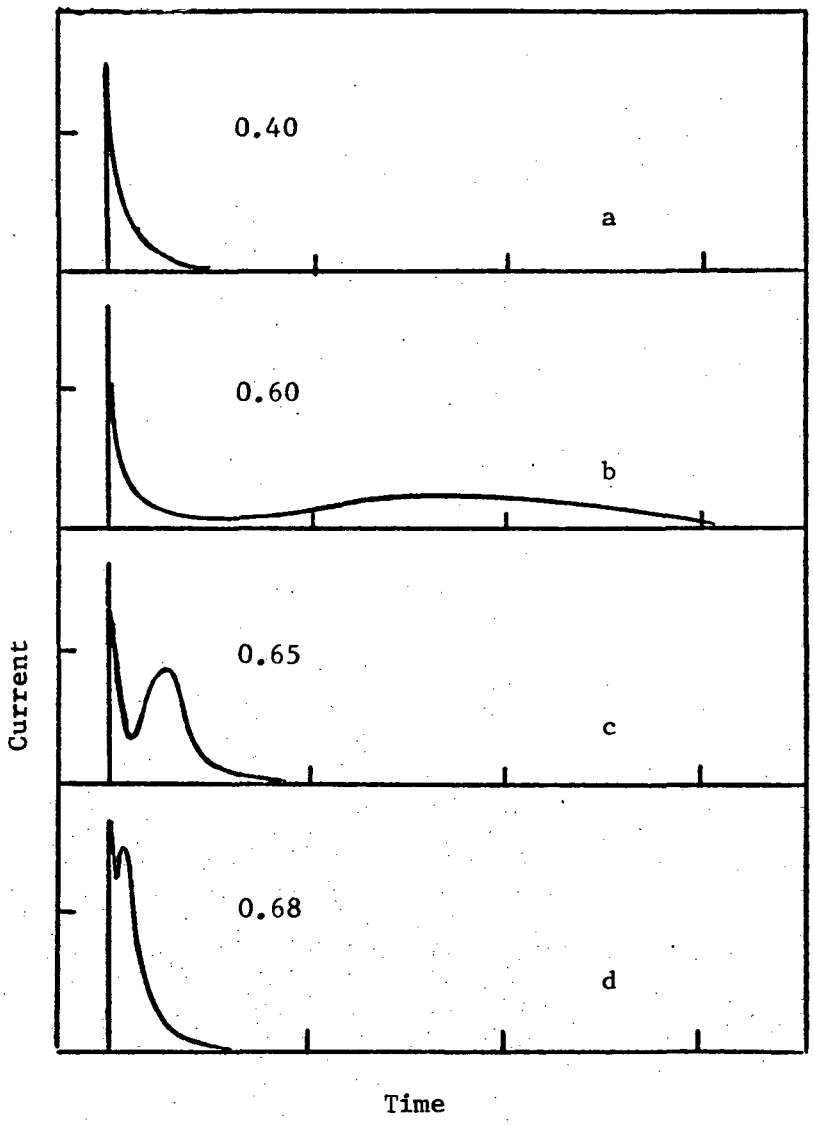

Fig. 23--Family of current-time curves showing potentiostatic oxidation of a silver electrode in a Haring cell. The numbers indicate the applied potential. (volts vs. Hg/HgO)

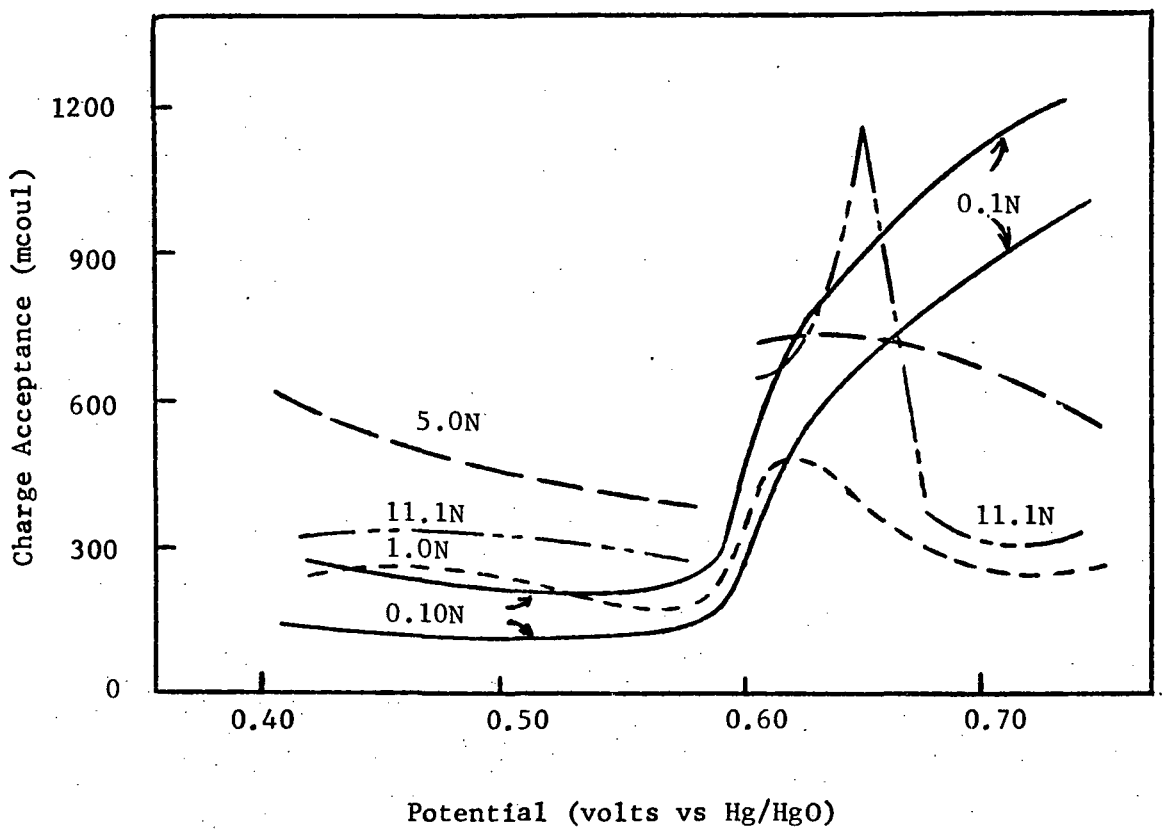

Fig. 24--Charge acceptance vs applied potential for potentiostatic oxidations at 0° C.

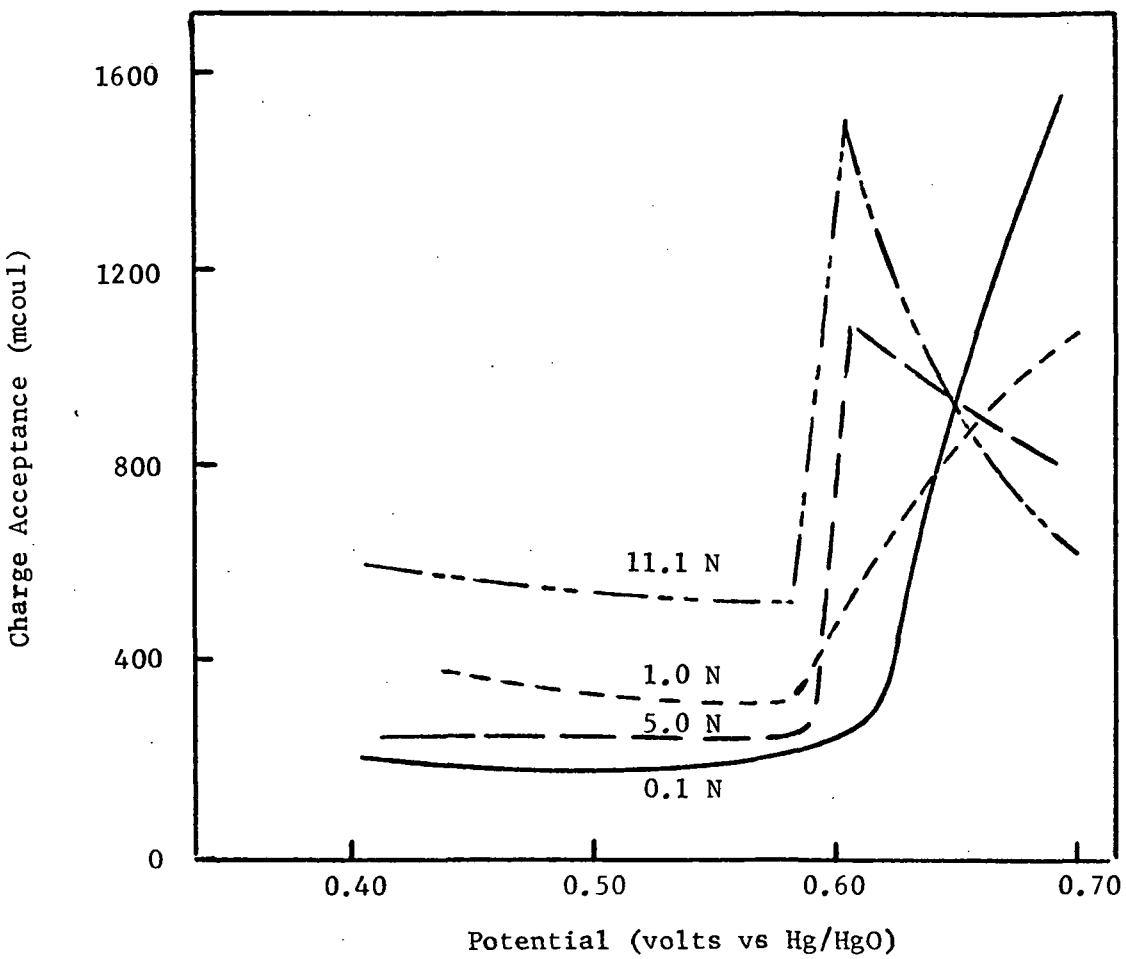

Fig. 25--Charge acceptance vs applied potential for potentiostatic oxidations at 25°C.

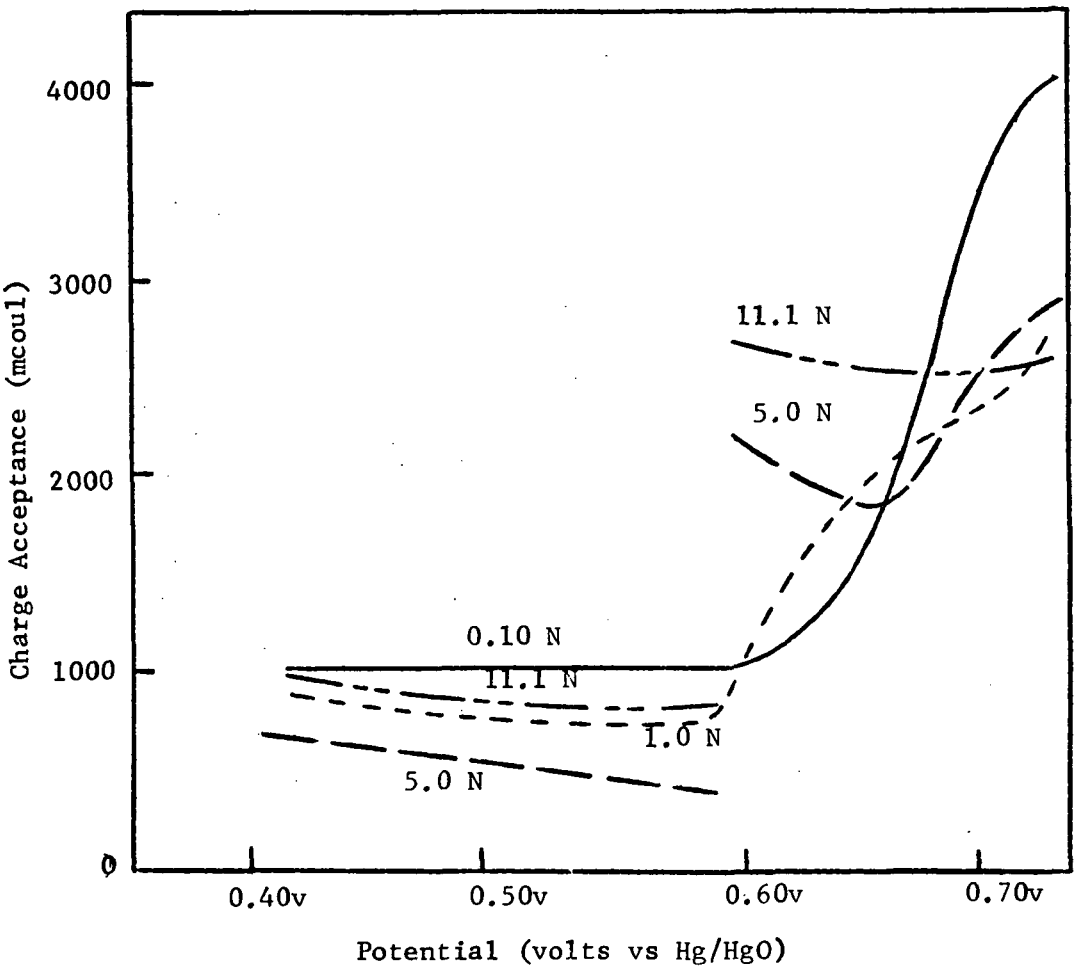

Fig. 26--Charge acceptance vs applied potential for potentiostatic oxidations at 50°C.

The most striking observations from these data are the abrupt increase observed in the charge acceptance at 0.60 v vs. Hg/HgO (corresponding to the appearance of the second current surge) and the increase in charge acceptance obtained at 50°C. The second current surge accounts for most of the charge acceptance in those oxidations where it occurs. The charge acceptance resulting from this second current surge is observed to decrease at higher applied potentials even though the peak value of the current increases.

In 0.1 N KOH we obtained two different types of current vs. time curves. The more frequent shape has been described above and was the shape obtained in all other electrolyte concentrations. Figure 27a shows an oxidation curve of the other type. Comparing this with Figure 23d shows that both the 1st and 2nd current surges were wider and that the peak value of the second current surge was smaller than those normally observed. Another significant change was observed in the shape of the reduction curve. Figure 27b shows a reduction curve usually observed; Figure 27c shows an anomalous reduction curve. The reduction curve was much broader and had a region in which the reduction current remained almost constant. The anomalous oxidations gave higher charge acceptances. In Figure 24 there are two curves corresponding to the charge acceptance obtained in two different series of runs in 0.1 N KOH at 0°C. The series with the higher charge acceptance gave the anomalous current vs. time transients while the series with the lower charge acceptance gave the more conventional current vs. time curves. The reason for this behavior is not known as the experimental conditions in both cases were the same.

History Effects. The history of an electrode has a profound effect upon its properties. Several interesting effects have been observed. A dramatic departure from the above-described shape of the current vs. time curve was observed after the electrode had been cycled 200-300 times. When the potential was applied, the current rose to a constant value and remained there for a time before dropping off to background. Applying different potentials seemed not to have any effect on this abnormal behavior. The electrode was then removed and cleaned with an abrasive cleanser. The more conventional behavior was again observed. After cleaning there was

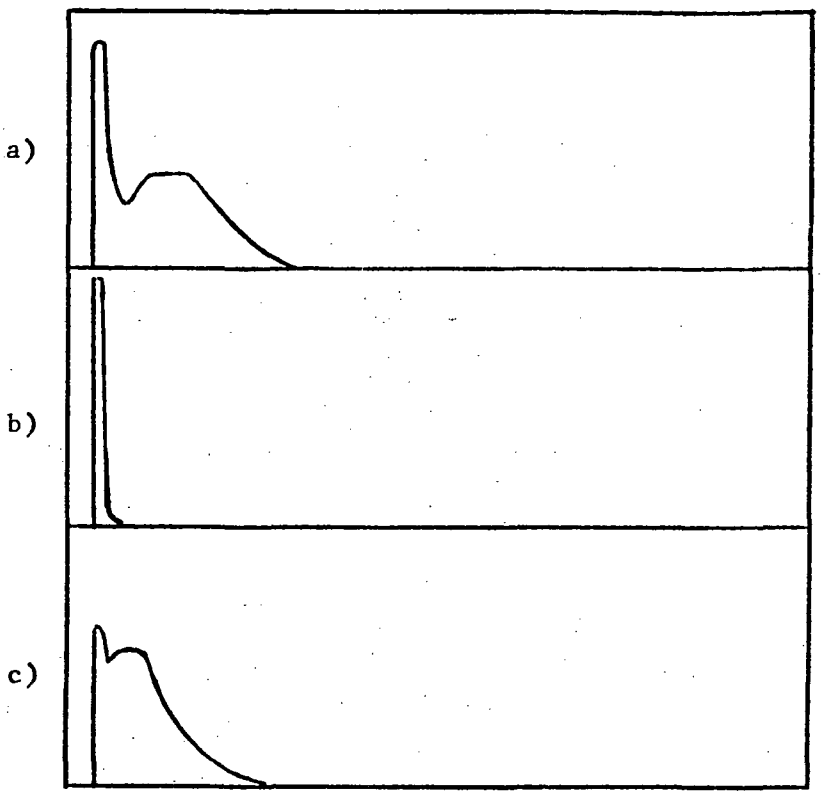

Fig. 27-- a) Current-time curve of potentiostatic oxidation at 0.68 v in 0.1 N KOH at 25°C.
b) Current-time curve of potentiostatic reduction at 0.00 v vs Hg/HgO.
c) Current-time curve of potentiostatic reduction at 0.00 v vs Hg/HgO in 0.1 N KOH at 25°C.

a significant decrease in charge acceptance which gradually increased with continued cycling.

Because of the above observations we adopted the following experimental procedure. The silver electrode was removed from the cell and scoured with an abrasive cleanser after each series of runs. A series of runs consisted of a set of potentiostatic oxidations and reductions using potentials ranging from 0.40 v to 0.75 v vs. Hg/HgO. During a series of runs the temperature was held constant and all oxidations and reductions of that series were done in the same electrolyte. At the beginning of each series the electrode was cycled ten times at 0.40 v vs. Hg/HgO. Following this cycling, the potential was increased for each oxidation in 0.05 v intervals--0.45 v, 0.50 v, etc.--until 0.60 v was reached. Three successive oxidations were performed at 0.60 v followed by an oxidation at 0.61 v and another at 0.62 v. Then another oxidation was done at 0.60 v. Following this oxidation, the potential was increased for each successive oxidation in 0.01 v intervals--0.61 v, 0.62 v, 0.63 v, etc.--until 0.70 v was reached. An oxidation was then run at 0.75 v. Following this basic sequence various oxidations were done to substantiate previously observed phenomena or to study history effects on the electrode.

An interesting history effect was noted at all temperatures and concentrations. To illustrate, the values of charge acceptance at a single potential in 0.1 N KOH at 0°C were:

	Potential	Charge Acceptance
Cycle 14	0.60	200 mcoul
Cycle 15	0.60	190 mcoul
Cycle 16	0.60	190 mcoul
Cycle 17 and 18 (2 runs - one at 0.61 v and one at 0.62 v)		
Cycle 18	0.60	300 mcoul

There is a significant increase in charge acceptance at 0.60 v after the electrode had been cycled twice at potentials higher than 0.60 v.

This effect was even more dramatically shown in a series at 25°C in 0.1 N KOH. The charge acceptance obtained at 0.62 v was 300 mcoul. However, after the cycling from 0.63 to 0.75 v was completed, another run at 0.62 v was made. This run gave a charge acceptance of 1600 mcoul. Thus the charge acceptance was increased 5-fold following cycling at

potentials ranging from 0.63 v to 0.75 v.

Also, the higher the potentials used in previous cycling, the higher the charge acceptance observed. For example, the charge acceptance obtained at 0.63 v following an oxidation at 0.58 v was only 60% as large as the charge acceptance obtained at 0.63 v after the electrode was first cycled at 0.60 v and 0.61 v.

Applicability of Growth Rate Laws. In an effort to understand the oxidation mechanism, we have plotted the data that we obtained from the potentiostatic oxidation of silver wire in alkaline solution according to equations that have been derived to study growth rates of other metal oxides. Göhr and Lange note that the decrease in oxidation rate with time is not linear as would be expected if the reaction rate were controlled by an Ohm's law potential drop across the oxide.[26] They note an exponential decrease of reaction rate. Cabrera and Mott believe that this results from a weakening of the electric field across the oxide.[27]

The data obtained from potentiostatic oxidation of the silver wire electrodes were plotted according to four different relationships which have been proposed to describe several oxidation mechanisms:

1. Lingane's equation for diffusion controlled reactions relates the log of current to time.[28]
2. Parabolic expressions of charge acceptance as a function of the square root of time have been derived, (a) for reactions controlled by diffusion of ions through the oxide layer and (b) for nonconducting oxides in a low field.[29]
3. The charge acceptance at constant time for nonconducting oxides in high fields has been related directly to the oxidizing voltage.[29]
4. The fourth equation expresses oxide thickness as a function of the log of time. This is an empirical relationship found to hold for many semiconducting oxides. Uhlig has derived this relationship from basic theoretical considerations.[30]

The first of these growth rate laws failed to describe our experimental data. Thus we may conclude that diffusion of hydroxide ion through the electrolyte to the electrode surface is not the limiting process in the reaction. The third of these equations also failed to describe our data

as was expected since high fields were not achieved. For the majority of our data, the parabolic growth rate law did not apply. However in a few cases, the data agreed well with this equation (Figure 28). This leaves the results unclear. In some cases the rate of the reaction may be controlled by diffusion or migration of ions through the oxide layer.

The last of these laws, which relates oxide thickness to the log of time, gave reasonable agreement with our data. Because dry Ag_2O has been characterized as a p-type semiconductor of high resistivity, one might expect silver oxide to obey this equation.[31]

Uhlig in his theoretical derivation of this empirical equation states that a small difference in distribution of excess charge in the space charge layer of the oxide determines whether the equation results in a simple one-stage logarithmic, a two-stage logarithmic, or a cubic expression.[30] If the excess charge is uniformly distributed in the space charge layer a one-stage logarithmic expression results: If we assume charge acceptance to be proportional to oxide thickness then

$$Q = k_o \log \left(\frac{t}{\tau} + 1\right)$$

where k_o and τ are constants. If τ is much less than t then

$$Q = k_o \log t - k_o \log \tau$$

and a linear plot of charge acceptance vs. the log of time is obtained.

If the oxide is allowed to grow until a layer appears which has a non-uniform distribution of the excess charge, a second stage of growth occurs. The equation which Uhlig derives for this diffuse charge density layer is also logarithmic but the values of k_o and τ are different. This type of growth results in a linear plot of charge acceptance vs. log t with a break at the time corresponding to the change from uniform to nonuniform charge density in the oxide.

If the charge distribution is such that an assumption made in the derivation of the logarithmic equations is not valid, a second assumption can be made which results in a cubic expression of the form

$$(Q + a)^3 = bt + c$$

where a, b, and c are constants.

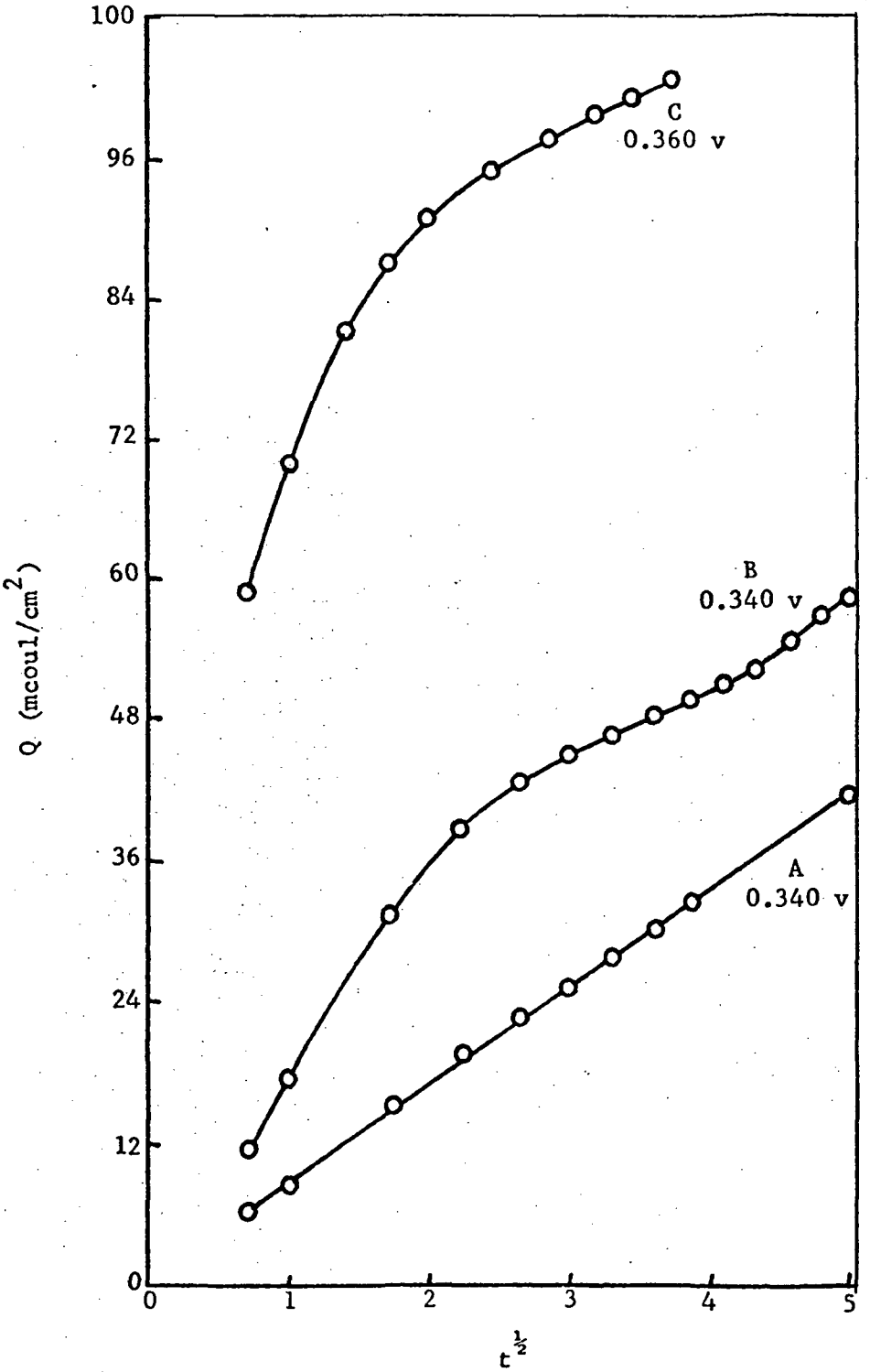

Figure 28. Charge acceptance as a function of the square root of time. The linearity of curve A supports a parabolic growth law but the deviation from linearity found in curves B and C places the results in doubt.

Figure 29 represents several of the oxidations which resulted in linear relationships of the charge acceptance vs. the log of time. Plots which were linear within the limits of error in measurement were obtained at potentials of 0.280 v (where oxidation is first observed) to 0.440 v (which is the highest potential plotted.) A definite break can be seen in some of the curves, indicating a two-stage logarithmic growth rate.

The linearity of much of the data supports the view that silver oxide is a semiconductor and that its semiconductor properties control the oxidation mechanism. The nonlinearity of some of the data is seen in Figure 30. These curves may indicate the influence of Uhlig's cubic equation. If a semiconductor growth equation is the controlling law under the conditions of our oxidations it is apparent from the diversity of curves obtained that the critical space charge distribution in the semiconductor oxide has not been reproducible.

Logarithmic Growth Rate Law. Data at different temperatures, potentials, and concentrations were plotted to see how well they obeyed this equation. Oxidations performed at 0.40 v, 0.55 v, and 0.60 v in 0.1 N, 1.0 N, 5.0 N, and 11.1 N KOH at $0^{o}C$, $25^{o}C$, and $50^{o}C$ were examined. In all cases, except at $50^{o}C$ in 0.1 N KOH, the plots of charge acceptance vs. the log of time gave a straight line or else two straight lines similar to those obtained previously and shown in Figure 29. The oxidations in 0.1 N KOH at $50^{o}C$ gave an "S" shaped curve.

The best straight line or lines described by the data was obtained by means of a least squares method. A summary of the results is presented in Table VI. Several trends are to be noted. First, there is in general a decrease in the value of the slope as the applied potential is increased (Figure 31). Second, there is a great decrease in the slope in 5.0 N KOH relative to the slope at the same potentials and temperatures in the higher and lower concentrations (Figure 31). Third, at $50^{o}C$ the value of the slope is substantially larger than at $0^{o}C$ and $25^{o}C$ under similar conditions.

According to Uhlig's derivation of this logarithmic growth rate law, the slope of the initial line of charge acceptance plotted vs. the log of time should be given as follows:

$$k_o = \frac{\varepsilon kT}{4\pi\rho e^2 L}$$

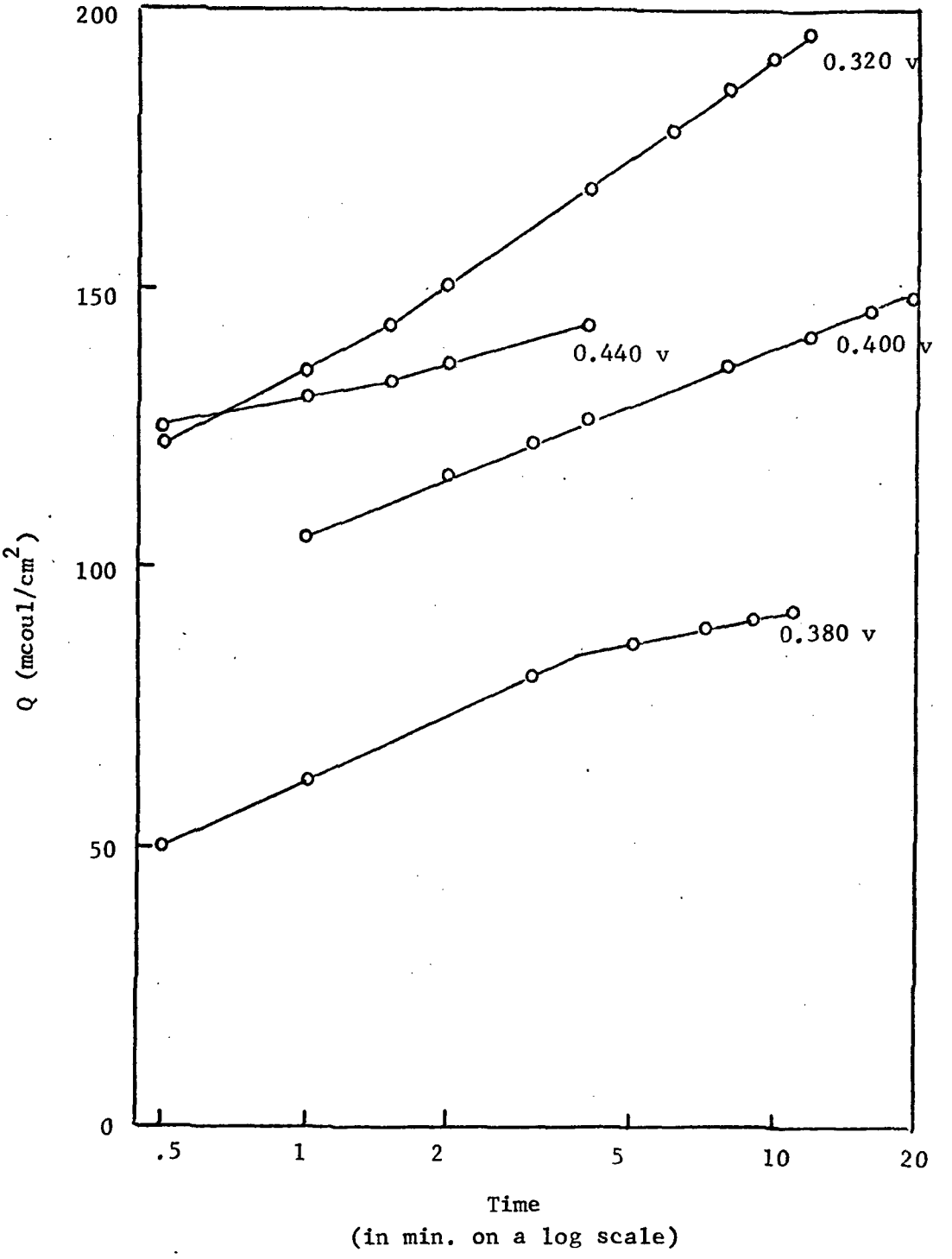

Fig. 29--Charge acceptance as a function of the log of time as derived for semiconductor oxides. The data are from potentiostatic oxidations at four potentials in 0.100 N KOH.

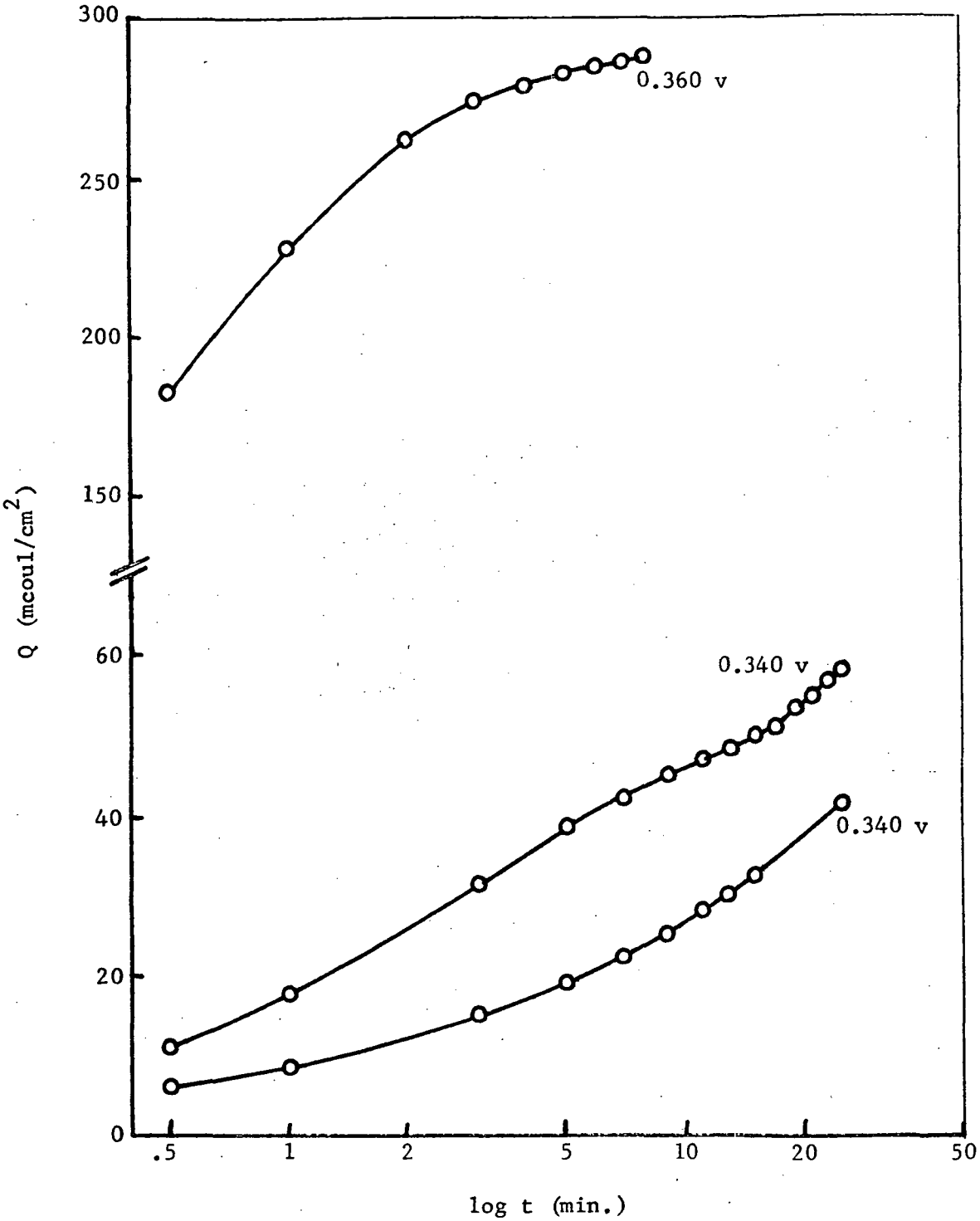

Figure 30. Charge acceptance as a function of the log of time as derived for semiconductor oxides. The nonlinearity of some data is represented.

TABLE VI

SLOPES OF CHARGE ACCEPTANCE VS. LOG OF TIME PLOTS

k_o is the slope of the first line (in coulombs); k_o', the slope of the second line (if it occurs); and t (in seconds) is the time at which the change from the first to the second line occurs (change from uniform to diffuse space charge).

		0.40 v			0.55 v			0.60 v		
		k_o	k_o'	t	k_o	k_o'	t	k_o	k_o'	t
0.1N	0°	0.0376	0.0275	5	0.0159	0.0288	6	0.0160	0.0259	5
	25°	0.0714	0.0203	3.6	0.0361	0.0177	1.7	0.0498	0.0277	1.9
	50°	Doesn't follow			Doesn't follow			Doesn't follow		
1.0N	0°	0.0582	--	--	0.0342	--	--	0.0295	0.0221	5
	25°	0.0853	0.0576	7.6	0.0389	0.0599	6	0.0343	0.0533	3
	50°	0.251	0.0710	3.9	0.0420	0.0509	7	0.0176	0.0155	2.7
5.0N	0°	0.124	0.0851	6	0.0600	0.0338	2	0.0412	0.0338	3
	25°	0.0288	0.0184	2	0.0231	0.0174	2	0.0221	0.0538	3.8
	50°	0.0841	0.0325	2.1	0.0247	0.0338	2	0.0380	0.0939	3.7
11.1N	0°	0.0928	0.0554	2.8	0.0293	--	--	0.0266	--	--
	25°	0.0794	0.0489	5.9	0.0503	0.0431	3	0.0455	--	--
	50°	0.223	0.114	5.8	0.149	0.0700	9	0.156	--	--

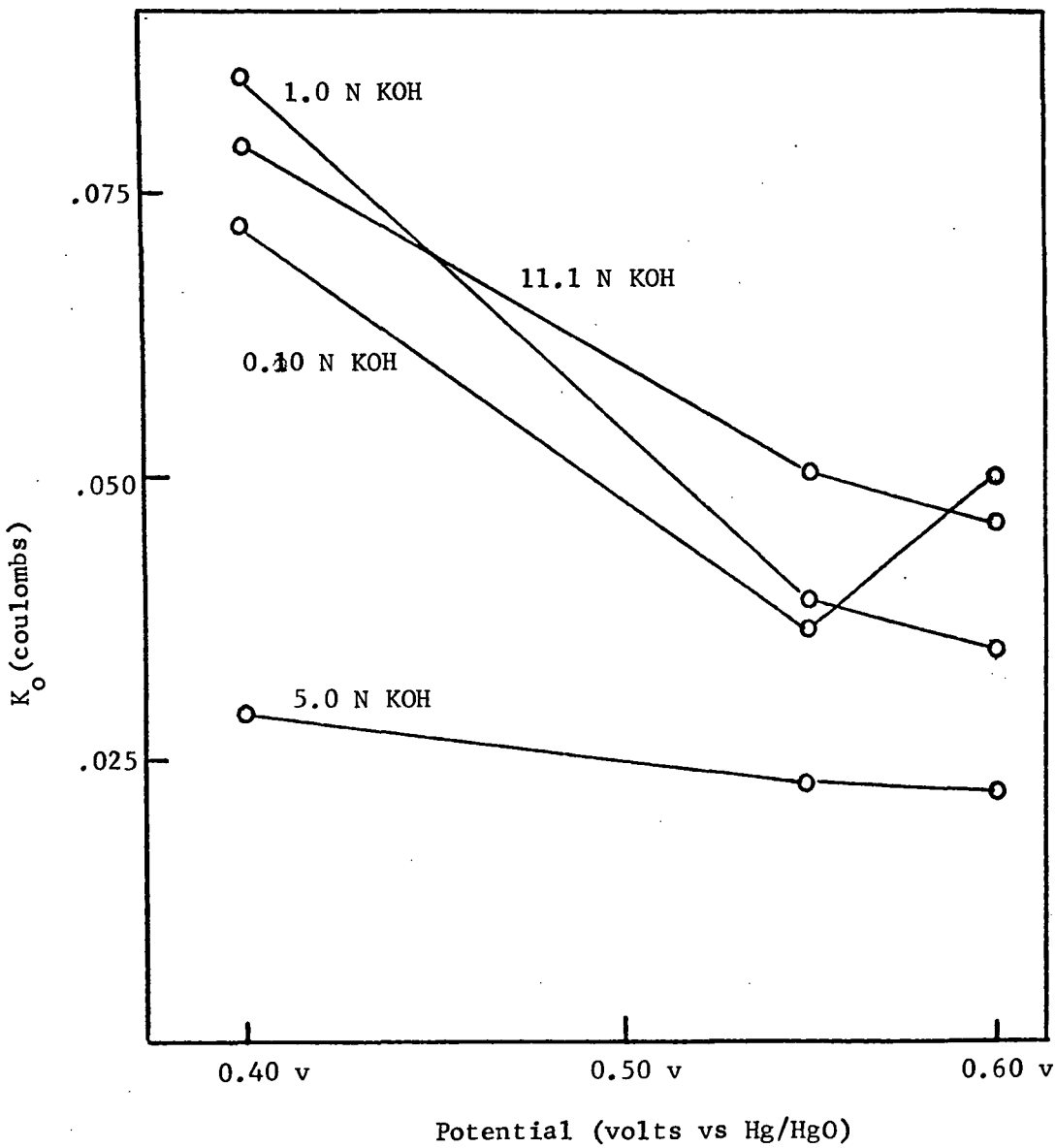

Fig. 31-- Plot of K_o vs applied potential for oxidations in various hydroxide ion concentrations at 25°C.

where ϵ is the dielectric constant of the oxide, ρ is the density of the trapped electrons (or holes) in the oxide, e is the charge on the electron, and L is the maximum thickness of the uniform charge layer.[30,32] Although Uhlig's derivation applies to the high-temperature oxidation of metals with molecular oxygen, we have examined it for possible application to an electrochemical oxidation. The decrease in k_o with an increase in the applied potential indicates that the product ρL must increase with increasing potential. Whether ρ, L or both exhibit this potential dependence has yet to be determined. The direct relationship between slope and temperature is not immediately obvious. This may be the result of a dependence of ρ, the density of the trapped electrons in the oxide, upon the temperature.

Uhlig, in his derivation, focused his attention exclusively to the metal-oxide interface as the location of the rate-limiting process. It appears that this is inadequate for our electrochemical situation, as we have noted a marked effect of the electrolyte concentration on the slope. This indicates that there is a rate-limiting process occurring at the oxide-electrolyte interface. It may be possible to incorporate these observations into Uhlig's equations by relating electrolyte concentration, in some not-yet-apparent way, to ρ, the density of trapped electrons, and/or to L, the thickness of the space charge.

SECTION IV

SURFACE STUDIES WITH SCANNING ELECTRON MICROSCOPY

INTRODUCTION

Most of the proposed mechanisms for oxide growth on a silver electrode in alkaline solution have been derived from kinetic data.[33-37] Wales and Burbank supplemented their kinetic data with X-ray diffraction data on a working silver electrode.[38] They concluded that oxidation of the Ag to Ag_2O and AgO occurred by formation of distinct crystals rather than expansion of the preexisting lattices. Wales and Simon have recently examined cross-sections of sintered silver electrodes using optical microscopy.[39] With transmission electron microscopy Briggs et al. observed structural features on silver electrodes which aided their interpretation of the kinetics of oxidation of silver electrodes.[7] The scanning electron microscope (SEM) was used in the work reported here to aid our interpretation of the charge accepted by silver electrodes in alkaline solution under both potentiostatic and galvanostatic conditions.

EXPERIMENTAL

The scanning electron microscope employed in our study is the Stereoscan Mk II, made by the Cambridge Instrument Company. A good discussion, by Kimoto and Russ, of SEM theory, techniques, and applications is available.[40] The samples examined were sections of 10 and 20 mil silver wires and 3½ x 4 cm sintered silver plates. The wires and plates were oxidized at constant current and constant potential in various concentrations of KOH electrolyte. The electrolyte was prepared from a commercial 45% KOH solution marketed by the Baker Chemical Company and analyzed by them as containing less than 0.01% K_2CO_3. The apparatus used in the oxidation of the wires is illustrated in Figure 32a. The stirrer was used in only a few oxidations, and they will be identified later in the discussion. The counter electrode was platinum, and the reference electrode was Hg/HgO. Figure 32b illustrates the apparatus employed in the oxidation of the

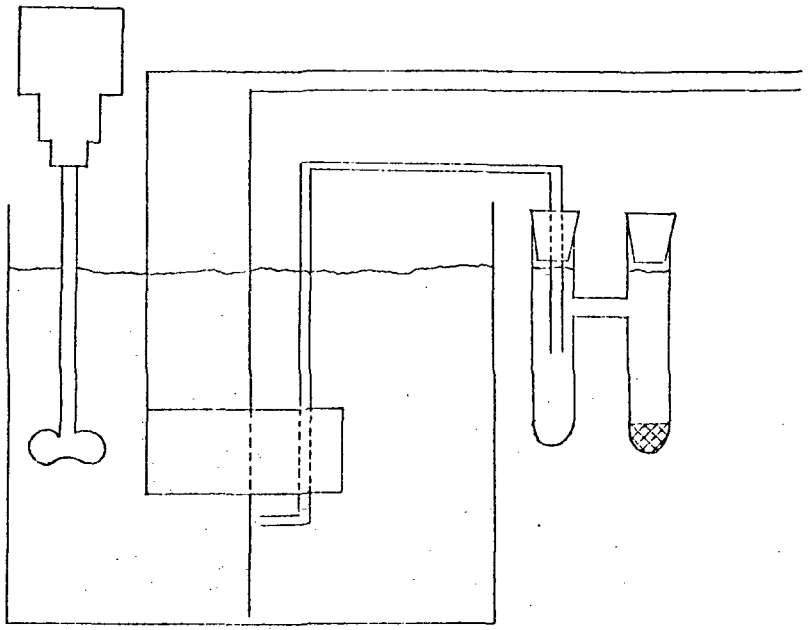

Wire Electrodes
(a)

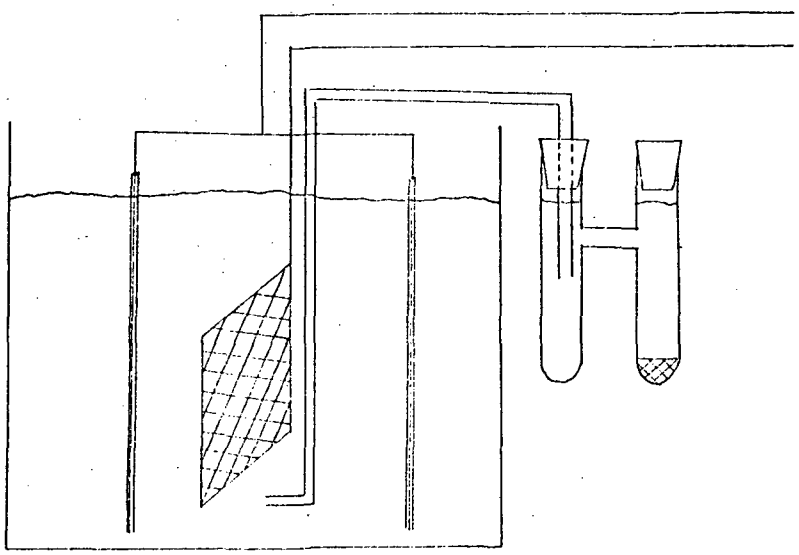

Sintered Electrodes
(b)

Figure 32. Oxidation Apparatus

sintered silver plates. The counter electrodes were 1.2 mm thick silver sheets 4 cm x 8 cm; the reference electrode was Hg/HgO. The constant current was supplied by an Electronics Measurements power supply, Model C633. The constant potential was obtained from the circuit described in JPL 951911 Final Report.[41]

RESULTS AND DISCUSSION

In the first portion of this section the effect of potential on the size and number of oxide mounds is discussed. In the second portion of the section the effect of current density on mound size and number is discussed. The third portion contains a discussion of the microscopic appearance of the surfaces of unoxidized, oxidized, and cycled silver electrodes. The last portion contains descriptions of some electrode phenomena.

Potentiostatic Oxidations

Figure 33 shows the surfaces of potentiostatically oxidized wires as a function of potential and charge. The wires were oxidized in 5 F KOH at 0.260 v, 0.420 v, and 0.620 v until they had accepted 0.005, 0.010, 0.030, and 0.040 μeq of charge. In these micrographs one cm on the micrograph is equivalent to 13,000 Å on the electrode surface.

Nucleation.--The uniform size of the mounds early in the oxidations indicates that there is almost instantaneous nucleation of sites in potentiostatic oxidations. There is a trend in Figures 33 A, E, and I of an increasing number of mounds with increasing potential. This same trend was observed by Fleischman, et al., in their investigation of the oxidation of single crystal silver.[7]

Oxide Mounds.--The existence of oxide as mounds rather than as a homogeneous, uniformly thick layer can be explained by a mechanism of dissolution followed by precipitation. This mechanism consists of three steps; the ionization of the elemental silver, the formation of a complex silver (I) species ($Ag(OH)_2^-$ according to Dignam, et al.), and the precipitation of Ag_2O from a super-saturated layer of this complexed silver (I).[21] According to the theory the formation of mounds is a result of selective precipitation on nucleated sites. Hemispherical mounds have also been observed on silver

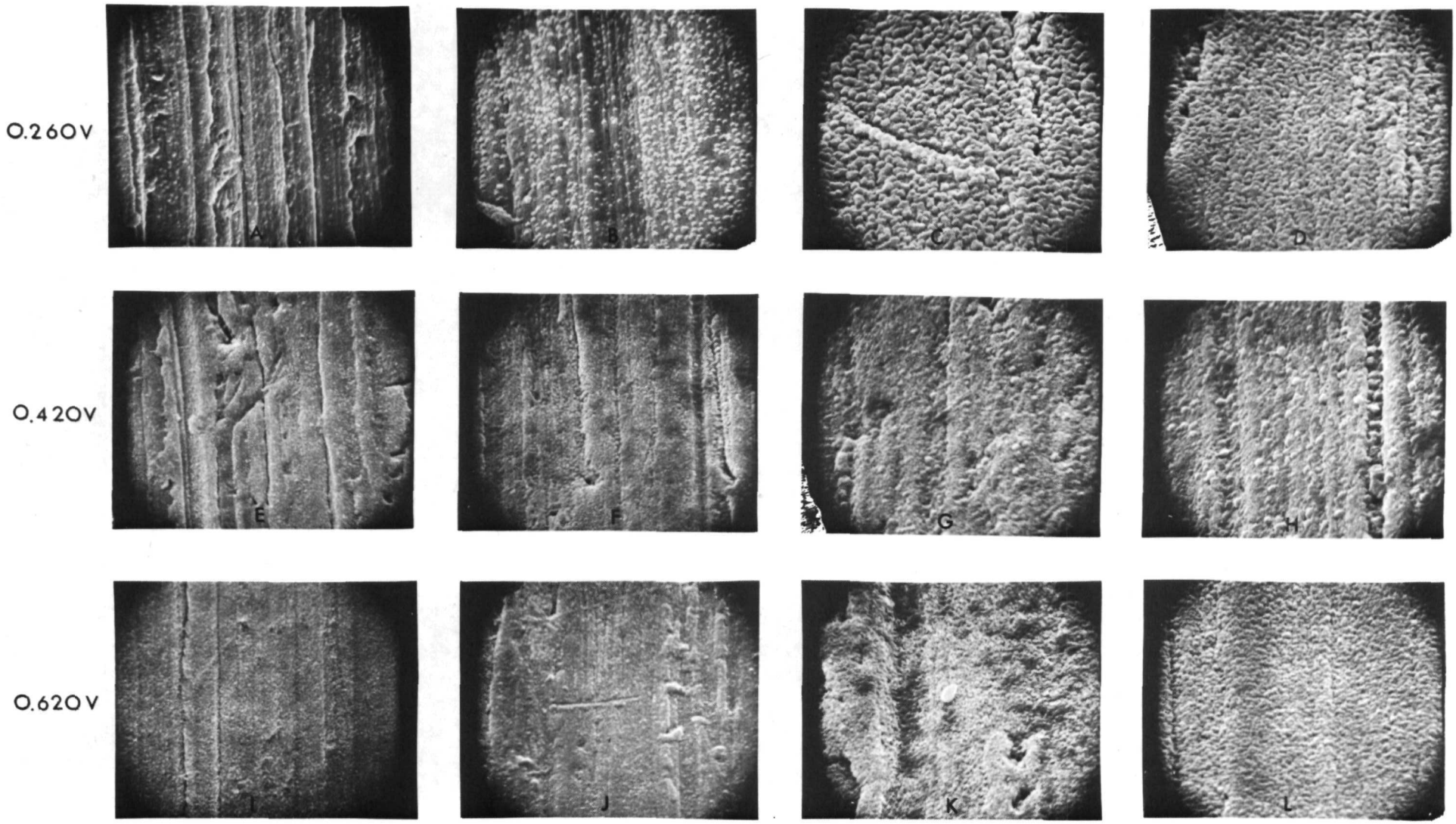
0.260V
0.420V
0.620V
A
B
C
D
E
F
G
H
I
J
K
L
0.005 μeq
0.010 μeq
0.030 μeq
0.040 μeq

FIGURE 33

surfaces during two other precipitation processes, the precipitation of vaporized AgBr on silver and the electrodeposition of silver on a single silver crystal.[42,43]

Basal Layer.--The amount of charge represented in the mounds on the surfaces prepared at 0.260 v was subtracted from the total charge the electrodes had accepted. The difference between these two figures was assumed to be the amount of charge located in the compact, or basal layer. The points at which the micrographs were taken and the calculations made are shown below:

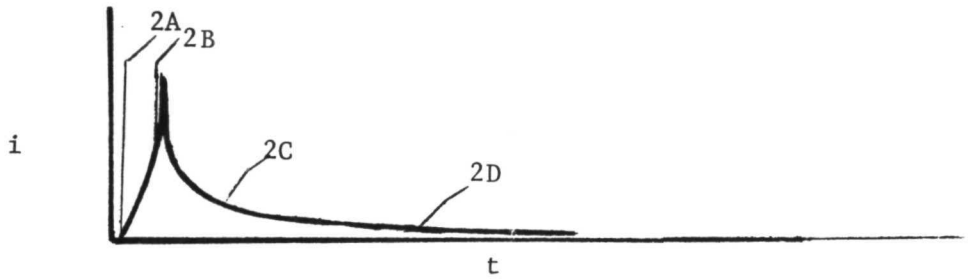

The total charge accepted, the charge represented in the mounds, and the difference for each of the four surfaces is shown below:

Micrograph	Total Charge	Mound Charge	Difference
33A	0.005 μeq	0.0007 μeq	0.0043 μeq
33B	0.010 μeq	0.0049 μeq	0.0051 μeq
33C	0.030 μeq	0.0251 μeq	0.0049 μeq
33D	0.040 μeq	0.0349 μeq	0.0051 μeq

The fairly constant value of the charge in the basal layer confirms its presence as the first oxide on the electrode surface.

Galvanostatic Oxidations

Figures 34A - 34I are micrographs (10,000X) of wire surfaces that were oxidized galvanostatically at 1.98 ma/cm^2, 0.198 ma/cm^2, and 0.0198 ma/cm^2 in 0.11 F, 1.1 F, and 11 F KOH until 8.8 mcoul of charge had been accepted. The nonuniformity of mound size suggests that progressive nucleation of sites occurs in galvanostatic oxidations. Under potentiostatic conditions, the uniform mound sizes suggested instantaneous nucleation. In Figures 34A-34E there is a trend of decreasing number of mounds with decreasing

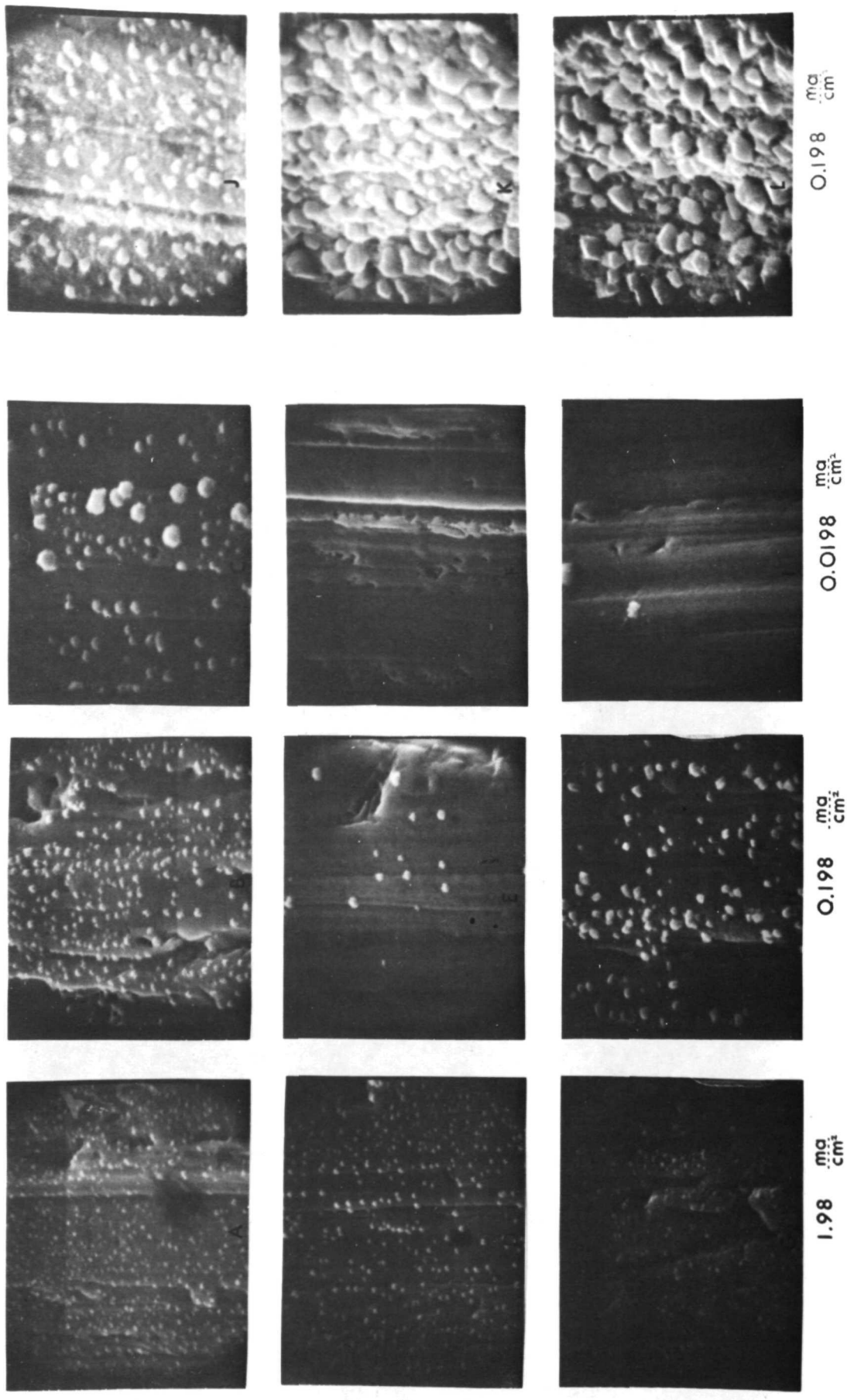
1.98 ma/cm²
0.198 ma/cm²
0.0198 ma/cm²
0.198 ma/cm²
1 F
1.1 F
0.11 F
A
B
C
D
E
F
G
H
I
J
K
L

FIGURE 34

current density. At the same time the average mound size is increasing. This trend can be understood in the light of two other oxidation trends; (1) the number of nucleated sites decreases with decreasing potential, and (2) the potential of the first plateau decreases with decreasing current density. The number of nucleated sites, and therefore the number of mounds, would indirectly be a function of current density. In some of the micrographs in Figure 34 there are no observable mounds. A possible explanation is that the electrolyte used in these experiments was unsaturated in Ag_2O. It may be that at very low current densities in unsaturated electrolyte it is difficult, if not impossible, to form the supersaturated layer required for deposition; the complex silver (I) species diffuse away from the electrode preventing saturation.

The surfaces shown in Figures 34J - 34L are of wires that were oxidized at 0.198 ma/cm^2 in 0.11 F, 1.1 F, and 11 F KOH until the potential rose to that of the Ag_2O-AgO reaction. They accepted 36, 175, and 137 mcoul of charge respectively. These values are in agreement with the data in Figure 38 that show a charge-acceptance maximum at 4-5 F KOH.

Unoxidized Silver Surfaces.--Figures 35A, E, I, D, H, and L show unoxidized surfaces of silver wire and sintered silver at three magnifications. The long scratches on the unoxidized wire surface are die marks. Some of the shorter scratches and most of the pits were caused by the coarse polishing powder in the cleanser used to prepare the wires. The much smoother surface of the microscopic particles in sintered silver appears to have been formed during the sintering process.

Oxidized Silver Surfaces.--Figures 35B and C show that on the oxidized surfaces of both the wire and the sintered silver, the Ag_2O is observed to exist as small hemispherical mounds. Using transmission microscopy, Briggs, et al. observed similarly shaped mounds when they examined the oxide occurring on a polycrystalline silver surface.[7]

Dissolution-precipitation can also explain the effect that stirring has on the size and number of mounds on the surface. Three wires were oxidized at 220μA/cm^2 for 200 seconds. In the absence of stirring, the surface density of mounds is about 50 mounds/micron^2 as shown in Figure 35B.

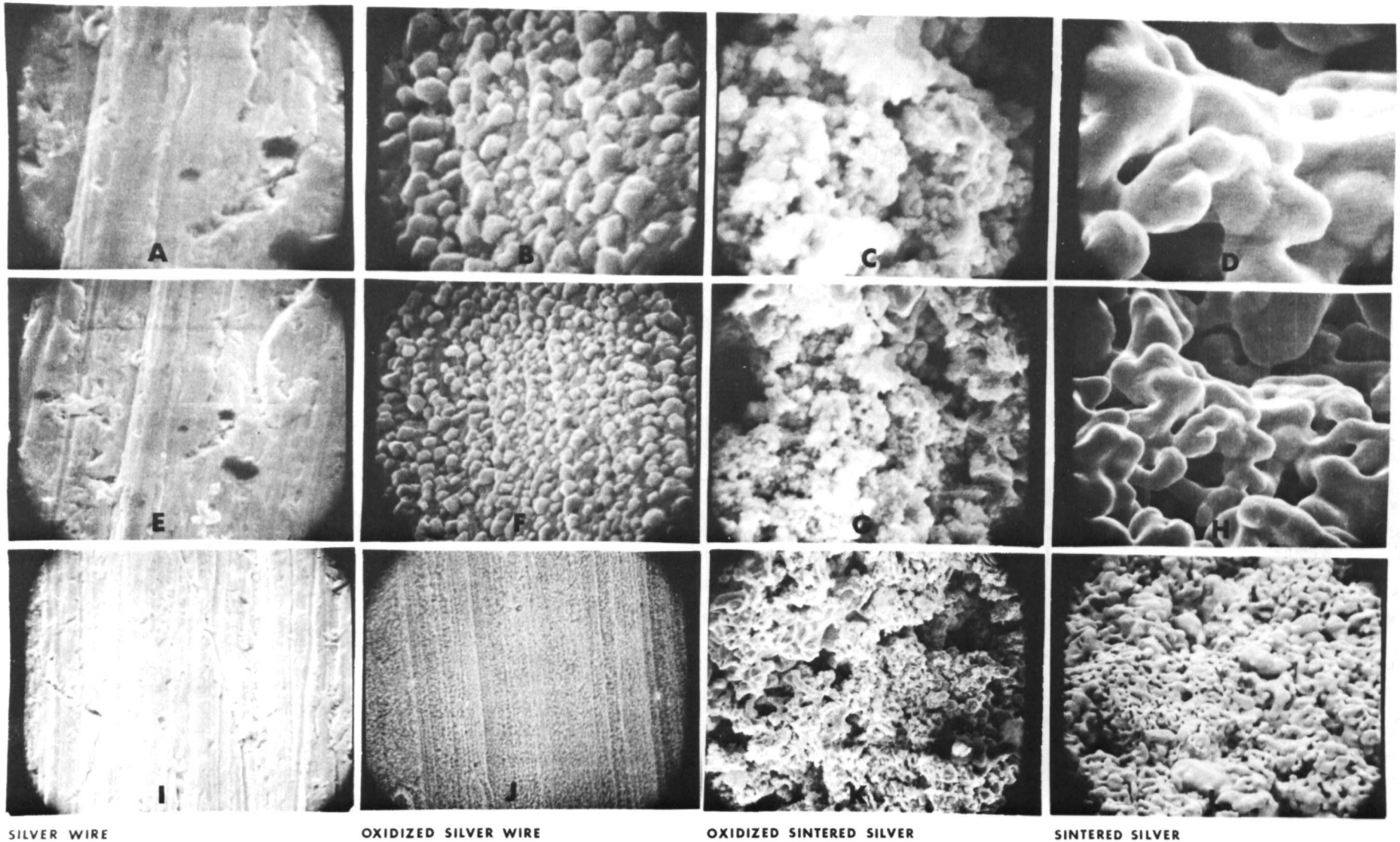
10,000
5,000
1,000
A
B
C
D
E
F
G
H
I
J
SILVER WIRE
OXIDIZED SILVER WIRE
OXIDIZED SINTERED SILVER
SINTERED SILVER

FIGURE 35

When the stirrer was operated at moderate speed (950 rpm) during oxidation the resultant mounds were smaller and had a surface density of 12 mounds/micron^2. When the electrode was reduced at 220μA/cm^2, hydrogen evolution occurred in about 40 seconds, 20% of the oxidation time of 200 seconds. With the stirrer operating at 1400 rpm, a surface slightly pitted and devoid of mounds was obtained. Reduction time for this electrode was only 10 seconds, 5% of the oxidation time. Apparently, stirring disperses the supersaturated layer of complex silver (I) species and thereby prevents the precipitation of Ag_2O.

Cycled Silver Surfaces.--Figure 36 shows uncycled and cycled wire and sintered silver surfaces; (1) in the reduced state, (2) oxidized at constant current until the potential rose to that of AgO formation, and (3) oxidized until the potential rose to that of oxygen evolution.

The effects of cycling can be observed in the Figures 36A and D. These surfaces which show extensive folding and pitting, had been oxidized and reduced (cycled) three times. The increase in surface area is striking. The silver formed by reduction of an oxide mound apparently retains the geometry of the mound. Figures 36E - H show Ag_2O mounds on cycled and uncycled surfaces. It is interesting to note that approximately 10% of the surface is left uncovered by Ag_2O mounds even though the potential had risen to the Ag_2O-AgO potential. The potential rise is apparently caused by some mechanism other than the complete covering of the surface by these Ag_2O mounds. Figures 36I - L are of cycled and uncycled surfaces oxidized to the potential of oxygen evolution. The surfaces appear to have more oxide on them, and it is still in the form of mounds. Though the electron microscope does not clearly distinguish AgO from Ag_2O, two observations can be made; (1) there is still some surface that yet remains uncovered by visible oxide growth, even though the potential of the electrode has reached that of oxygen evolution, and (2) the small pillar-like growths in Figures 36K and L were formed while the electrode was at the Ag_2O-AgO potential. Since the pillars were not in evidence in Figures 36G and H, and since AgO is formed by oxidation of existing Ag_2O[5], the pillars are probably additional Ag_2O. Additional support that these are Ag_2O comes from the observation that the pillar-like growths can be more easily explained by the Ag_2O growth mechanism

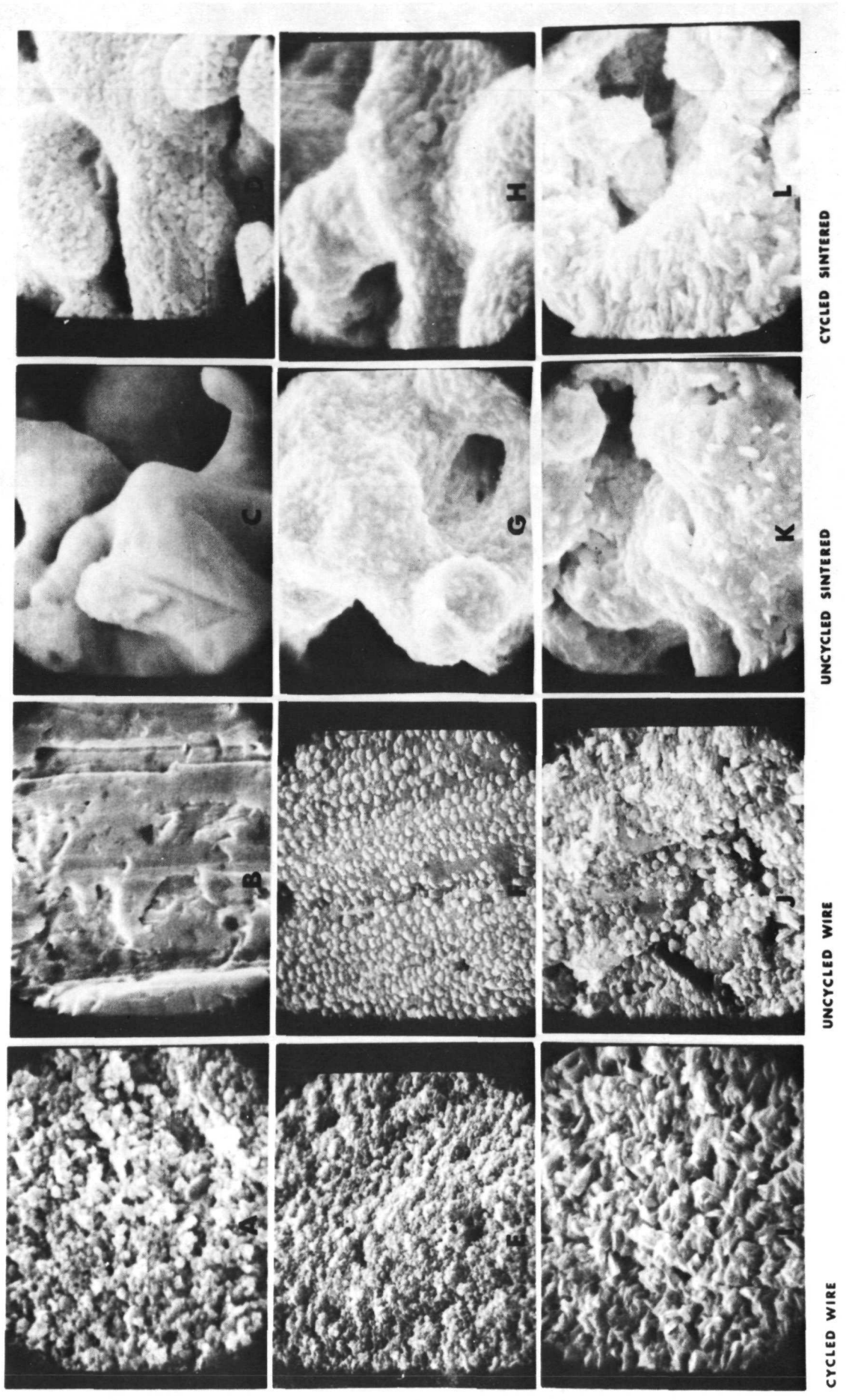
Ag
Ag_2O
AgO
CYCLED WIRE
UNCYCLED WIRE
UNCYCLED SINTERED
CYCLED SINTERED
A
B
C
D
E
F
G
H
J
K
L

FIGURE 36

(dissolution - precipitation) than by the AgO growth mechanism (direct interfacial).[5]

Electrode Phenomena

Figure 37 consists of pairs of micrographs that illustrate some electrode phenomena. Except where indicated the magnification is 10,000X.

Sintered Silver Oxidation.--Figures 37A and 37B are of different sections of a sintered silver electrode that was oxidized to the Ag_2O-AgO potential. Figure 37A is at the surface of the electrode and Figure 37B is at a point halfway through the electrode. It is evident that the electrode is less extensively oxidized in the middle than it is at the surface. This is probably caused by the iR drop in the pore between the surface and the midway point.

Dendritic Oxide Growth.--Figures 37C and 37D are of a sintered electrode that was oxidized 15 minutes past the time when oxygen evolution was first observed. Clearly apparent are some relatively large dendritic growths. Figure 37C is at 2,000X magnification and Figure 37D is at 10,000X. The dendritic growths shown here probably began as the stubs shown in the sintered silver AgO micrograph in Figure 35; and are, therefore, Ag_2O growths. The longest spike in the micrograph measures 7.5μ, or 75,000 Å. This is large compared to the average mound diameter of 5,000 Å observed in most micrographs. Falk and Salkind indicate that the growth of zinc dendrites through the cellulose separator of the silver-zinc batteries during cycling and overcharging is one of the main reasons for the short cycle life of this type of battery.[45] A SEM study of the zinc dendrites by Mansfield and Gilman shows that the lengths of these dendrites vary from 25 - 50μ.[46] Although the 7.5μ Ag_2O dendrites are only about 1/5 that length, they may still be contributing to the problem.

Surface Beneath the Oxide.--Figures 37E and 37F are of silver wire surfaces that were oxidized for different lengths of time and then the oxide was removed by dissolving it in 14.7 F NH_4OH. The surface shown in Figure 37E was oxidized for 30 seconds before dissolution and the one in Figure 37F was oxidized for 300 seconds. When 37E is compared to

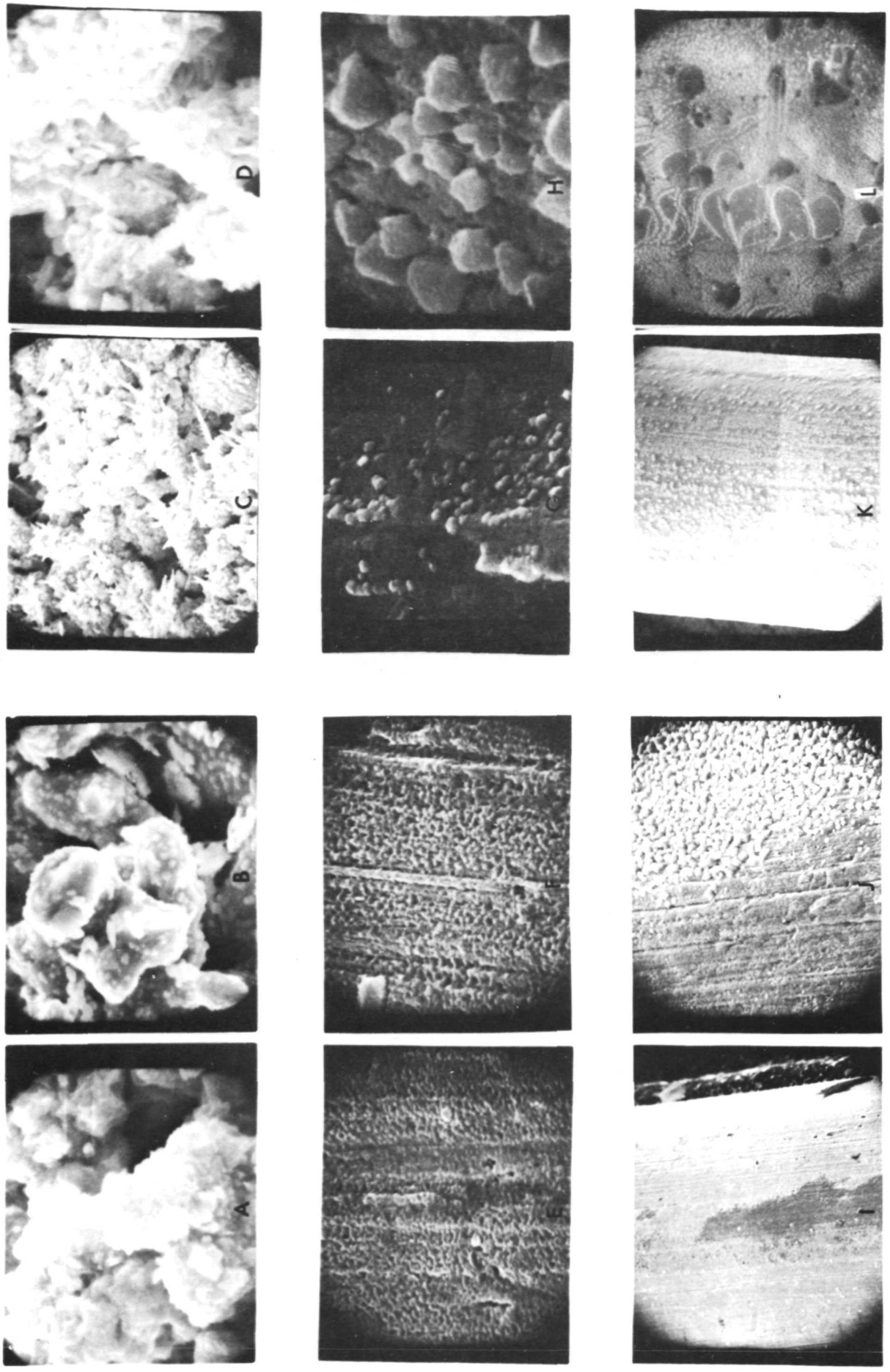

FIGURE 37

37F there is an appearance of mound growth. This is probably because an oxide mound protects the elemental silver underneath it from dissolution. The peripheral silver is not so protected and is dissolved, complexed, and then precipitated on the mound. When the oxide is dissolved in NH_3 the protected silver appears as a mound because of the etched surface surrounding it.

Basal Layer Mounds.--Figures 37G and 37H are of the three types of oxide growth observed by Briggs et al. in their transmission electron microscope study of oxidized silver surfaces.[7] Figure 37G is at 43,000X, while Figure 37H is at 20,000X. The set of smaller mounds on the surface in Figure 37G were called the primary growth. They are about 1/50 the size of the larger mounds shown in 37H. The larger mounds were called secondary growth. The small mounds on the surface of the larger mounds were called tertiary growth. The primary growth is also referred to as the compact layer or the basal layer.[7,] It has been suggested that the potential peak that occurs before the second plateau in constant current oxidations is caused by the concentration of the current into small, localized areas.[5, 47] This would occur during the course of an oxidation as the basal layer mounds grew larger, blocking off the surface and throttling the dissolution portion of the Ag_2O growth mechanism. The closing off of the silver surface by the basal layer would also be responsible for the negative slope of the current peak observed in potentiostatic oxidations.

Spotty Oxidation.--Figures 37I and 37J illustrate the microscopic differences of surfaces that appear macroscopically spotted after oxidation. The surface pictured in Figure 37I is at 50X while the surface in Figure 37J is at 5,000X. In daylight the wire appeared light grey with dark grey spots. The colors would appear to be related to the light scattering abilities of the large and small mounds and the absorbance of the oxides.

Sintered Wire Surfaces.--Figures 37K and 37L are of wire surfaces which were sintered in an attempt to obtain surfaces as smooth as those on the sintered silver particles. As the representative micrograph 37K shows, the effort met with only limited success even though a variety of sintering temperatures and times were tried. Figure 37L is at lower

magnification (200X as opposed to 10,000X) and is of a surface oxidized to AgO potential. It will be observed that the oxidation is spotty and seems to follow the sintered-unsintered pattern on the electrode. Gregor and Pitzer have observed that sintering affects surface strains, and that unsintered areas oxidize at lower potentials than do sintered.[16]

SECTION V

IONIC TRANSPORT IN SILVER OXIDE

INTRODUCTION

Studies of the ionic transport mechanism of tantalum, aluminum, silicon and several other metals during electrolytic oxidation have been published.[48,49] The growth of the oxide relative to the initial surface has been observed by imbedding immobile, inert, tracer atoms in the metal surface prior to oxidation.[48] The relative mobility of the metal and oxygen atoms has been studied by labeling either the metal or the oxygen or both.[49] The oxide film on all these metals is a uniformly thick, homogeneous layer and the thickness of this layer is linearly proportional to the oxidation voltage.[50] Similar studies have not been made for silver oxide and there is no agreement about which ion is mobile and how the ionic transport occurs. The oxide thickness is not proportional to voltage for silver oxide and the thickness of the oxide layer has been found to be non-uniform.[41,7]

A study of ionic transport in silver oxide has been undertaken to determine ionic mobility and transport mechanisms. Radioactive $^{110\ m}Ag$ has been used as the labeled atom and the experimental results have been applied to two models of oxidation of silver.

EXPERIMENTAL

A silver wire with an apparent surface area of 1.0 cm^2 was electroplated with silver to an apparent depth of 50 Å from a solution enriched in $^{110\ m}Ag$. The silver was deposited using a current of 50 μamps for 1.50 min. A uniform layer of radioactive silver was assumed because of the low current density and the small amount of silver deposited.

Approximately 0.62 cm^2 of the electrode was oxidized in 0.100 M KOH for 15 minutes at 50 μamps. The apparent depth of oxide was calculated to be 1000 Å. This oxide was immediately dissolved by immersing the electrode successively in eleven test tubes containing

3.0 ml of 0.03 M NH_3 each. Dissolution was allowed for 10 seconds in each of the first six test tubes and for 12, 15, 30, 120 and 600 seconds for test tubes 7 through 11, respectively, in order to dissolve approximately equal amounts of oxide in each fraction.

A 1.0 ml portion of each fraction was transferred to a planchet and placed in an automatic scintillation counter. The time required to register 4000 counts was determined seven times for each fraction and 21 times for background. The net counting rate was determined from these results.

The total concentration of silver in each fraction was determined by analyzing the remaining 2.0 ml portions with an atomic absorption spectrophotometer.

The specific activity of each fraction was calculated from the net counting rate, the concentration of silver in each fraction and the volume of solution in each fraction. The specific activity was plotted as a function of the depth of oxide.

RESULTS AND DISCUSSION

If it is assumed that the oxide film grows in a layer of uniform thickness then a model for oxide growth can be proposed which predicts six different mechanisms for ionic transport. The individual mechanisms can be identified by labeling the silver on the surface of the unoxidized electrode and the oxygen in the electrolyte used for the initial period of the oxidation. Two fundamental transport mechanisms are possible: (a) The silver or oxygen ions diffuse through the oxide layer to the oxide interface where growth is occuring (referred to hereafter as "direct transport") or (b) The mobile ions enter one side of the oxide layer causing all similar ions to shift one lattice position deeper ("propagational transport").[49] In propagational transport the original order of the ions is conserved. The oxidation may proceed by the transport of either silver or oxygen or both silver and oxygen. If both species are mobile, combinations of transport mechanisms are possible. The results of these six mechanisms for the oxidation of silver are shown in Table VII. The relative location of the labeled silver and the

TABLE VII

THE LOCATION OF LABELED SILVER AND OXYGEN IN THE OXIDE LAYER ACCORDING TO THE SIX COMBINATIONS OF IONIC TRANSPORT MECHANISMS

Case	Type of Transport	Location of Labeled Atoms		
		Silver-Silver Oxide Interface	Middle of Oxide	Silver Oxide-Electrolyte Interface
1	Silver - DT	Ag, O		
2	Oxygen - DT			Ag, O
3	Silver - DT and Oxygen - DT		Ag, O	
4	Silver - DT and Oxygen - PT	O	Ag	
5	Silver - PT and Oxygen - DT		O	Ag
6	Silver - PT and/or Oxygen - PT	O		Ag

DT = Direct Transport

PT = Propagational Transport

labeled oxygen after oxidation are presented for these six cases as follows:

Case 1. Silver is mobile by direct transport. Both the labeled silver and the labeled oxygen are found at the silver-silver oxide interface.

Case 2. Oxygen is mobile by direct transport. Both the labeled silver and the labeled oxygen are found at the oxide-electrolyte interface.

Case 3. Silver and oxygen are both mobile by direct transport. Both the labeled silver and the labeled oxygen are found in the middle of the oxide. The exact location of the labeled species depends upon the relative rates of mobility.

Case 4. Silver is mobile by direct transport and oxygen is mobile by propagational transport. The labeled silver is found in the middle of the oxide and the labeled oxygen is found at the silver-silver oxide interface.

Case 5. Silver is mobile by propagational transport and oxygen is mobile by direct transport. The labeled silver is found at the oxide-electrolyte interface and the labeled oxygen is found in the middle of the oxide.

Case 6. Silver is mobile by propagational transport or oxygen is mobile by propagational transport or both silver and oxygen are mobile by propagational transport. Each of these possibilities results in the labeled silver being found at the oxide-electrolyte interface and the labeled oxygen at the silver-silver oxide interface.

If only the labeled silver were located after oxidation, it would be found at the silver-silver oxide interface in only one case. In two cases it would be found in the middle of the oxide and in three cases it would be found at the oxide-electrolyte interface.

We chose to follow labeled silver first and then follow labeled oxygen if required to define the transport mechanism unambiguously. The results of the study of silver mobility are represented in Figure 39. If it is assumed that the oxide layer is dissolved uniformly across the surface of the electrode then the fraction of the silver oxide dissolved is proportional to the depth of oxide.

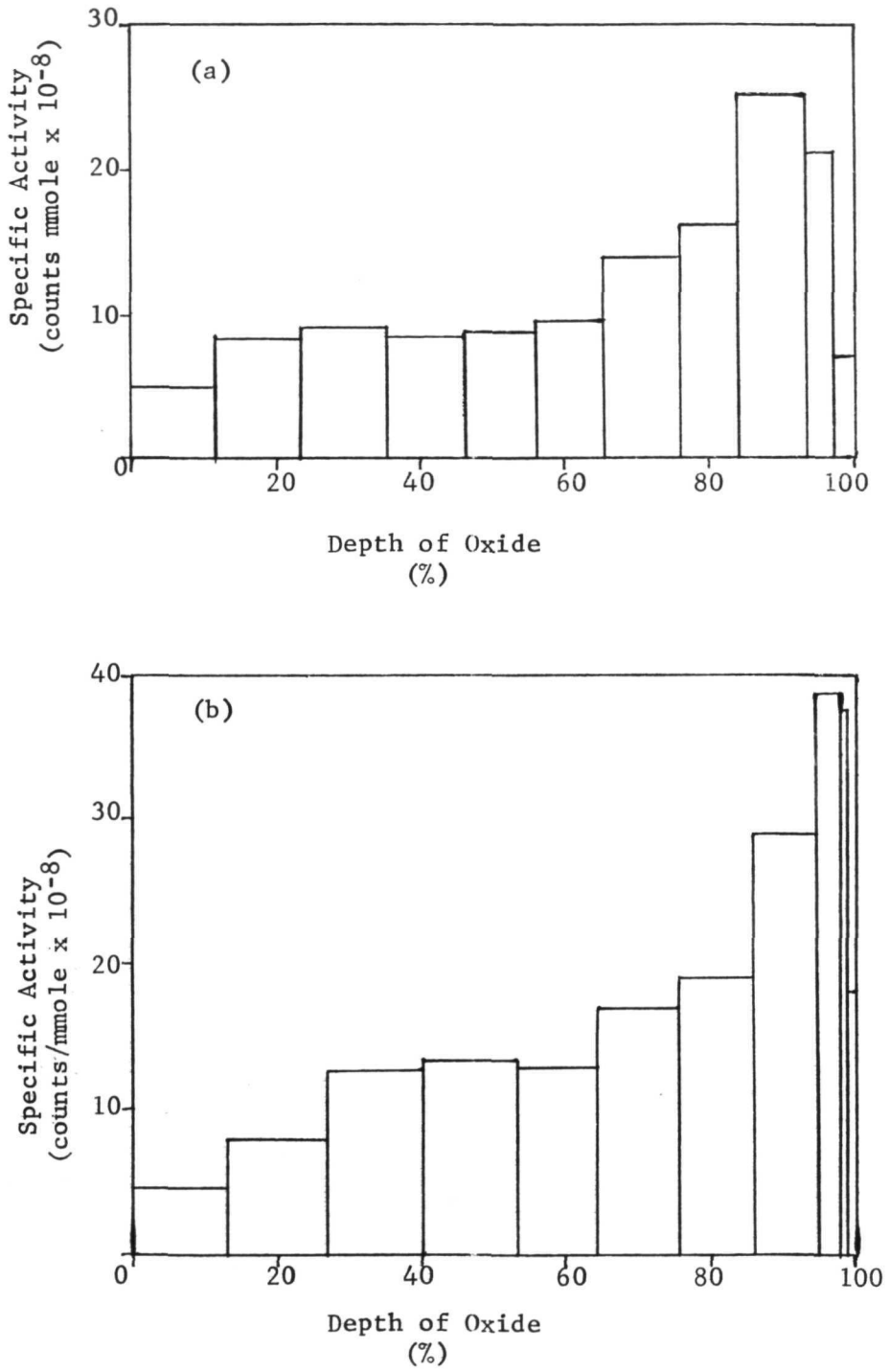

Figure 39--A plot of the specific activity of the dissolved silver as a function of depth of oxide. The silver oxide-electrolyte interface is represented at 0% and the silver-silver oxide interface is represented at 100%. The two sets of data shown in (a) and (b) were taken under similar conditions on consecutive days.

The oxide-electrolyte interface is, therefore, represented as 0% of the depth of oxide and the silver-silver oxide interface is represented as 100%.

The high specific activity in the region of 80% to 100% of the depth of oxide indicates that the labeled silver is found in greater quantity at the silver-silver oxide interface. This evidence leads to the conclusion that the silver ion is mobile by direct transport and the oxygen ion is not mobile to an appreciable degree.

The cause of the apparent decrease in specific activity at 100% is uncertain. A very low silver ion concentration in that fraction combines with a low net counting rate to produce a large uncertainty in those data points. If, however this decrease is real, several causes can be postulated: a slight mobility of silver ions by propagational transport, a slight mobility of oxygen, a slight dissolution of elemental silver after the oxide has all dissolved, a thin layer of unlabeled silver oxide present before oxidation, etc. The thickness of this unlabeled layer, if it exists, can be estimated to be about 2% of the oxide thickness or 20 Å. This represents only about 4 monolayers of oxide so whatever the origin of this apparent decrease in activity at the silver-silver oxide interface, the effect of this feature on the mechanism of ionic transport is negligibly small.

Another feature of the data represented in Figure 39 is the presence of a significant amount of activity in all the fractions of the dissolved oxide. One would not predict this result from the model previously mentioned. The basic assumption of the model is also demonstrated to be invalid by examining the oxide "layer" using an electron microscope: the oxide grows in mounds rather than in a homogeneous, uniformly thick layer.[7]

The existence of mounds of Ag_2O on the surface of the electrode can be explained by the dissolution-precipitation mechanism of oxide growth.[21] According to this model the silver metal dissolves electrolytically, complexes with hydroxide and precipitates on the growing Ag_2O surface. We will apply this model to our experiment with labeled silver, assuming that the surface of the electrode consists of mounds of Ag_2O as shown in Figure 35B.

If we oxidize an electrode which has a thin layer of radioactive silver on the surface, we can predict from the model that the dissolved silver ions at the beginning of the oxidation would have a relatively high fraction of silver that was radioactive. Some of this radioactive silver would react with hydroxide and precipitate at a nucleation site as labeled silver oxide. As oxidation continued the proportion of dissolving silver that came from the radioactive surface layer would rapidly decrease as the pits became deeper. When all the labeled surface silver had dissolved and entered the electrolyte the subsequent layers of Ag_2O which precipitated would contain a small but significant amount of labeled silver. The center of the mount of Ag_2O which resulted from this oxidation would have a high proportion of labeled silver and the rest of the mound would have a low proportion of labeled silver. The Ag_2O dissolved from the surface of the mound in the first portion of ammonia solution would have little radioactivity. Subsequent fractions of the oxide dissolved in ammonia solution would increase only slightly in radioactivity until the dissolution reached the center of the mound. These last fractions would have a relatively large amount of labeled silver. The shape of the curve of specific activity vs. the fraction of oxide dissolved would be very similar to the experimental results plotted in Figure 39. We can conclude that our experimental results lend support to the dissolution-precipitation model for the oxidation of silver.

SECTION VI

SURFACE AREA ESTIMATION

INTRODUCTION

In earlier reports of this series[41, 51] methods for surface area estimation have been presented and discussed. One method is based upon the assumption that electrolytic oxidation of smooth and rough silver electrodes occurs to the same depth if the electrodes are subjected to the same actual current density (current divided by the effective electrolytic surface area). Roughness factors (electrolytic surface area divided by geometrical surface area) of about 2 for silver foil electrodes etched with nitric acid and about 60 for sintered silver were obtained.

Another method is based upon the assumption that charge acceptance measured at constant potential is the same per unit of effective electrolytic surface area for smooth and rough electrodes. This assumption implies the same depth of oxidation for smooth and rough electrodes at the same potential. Additional data are presented in this section for the comparison of these methods.

Still another method is based upon the possible functional relationship between surface area and the height of the initial current peak under potentiostatic charging.

EXPERIMENTAL

The procedures and circuitry of the surface area estimations are discussed in earlier reports of this series.[41, 51]

The electrolyte used in the determination reported in this section was a 0.10 F KOH solution saturated with silver (I) oxide to minimize the dissolution of oxide from the electrode. All oxidations were thermostatted at $20 \pm 0.01^{\circ}C$.

For those determinations of silver by standard atomic absorption techniques the oxide film was dissolved in 0.5 F ammonium hydroxide solution.

RESULTS AND DISCUSSION

The results of the comparison of surface area estimation by constant current charging and potentiostatic charging are given in Table VIII. In the constant current method the applied currents were selected so that the times of oxidation through the first plateau were approximately the same for the sintered electrode and the standard silver-on-glass electrode. Therefore, for this particular example, the use of the standard curve (Figure 14, Ref. 51) was not necessary. The current densities are assumed equal because the oxidation times are equal and the effective electrolytic surface area, a_2, is calculated from $a_2 = a_1\ i_2/i_1$ where a_1 is the area of the standard electrode and i_2 and i_1 are the currents applied to the sintered and standard electrodes. The calculated roughness factor is 58.

In the potentiostatic method, a_2 is calculated from $a_2 = a_1\ q_2/q_1$ where q_2 and q_1 are the charge acceptances of the sintered and standard electrode. The calculated roughness factor is 81.

If one imagines an idealized porous electrode made by stacking bars of square cross section together so that only the edges touch, and the

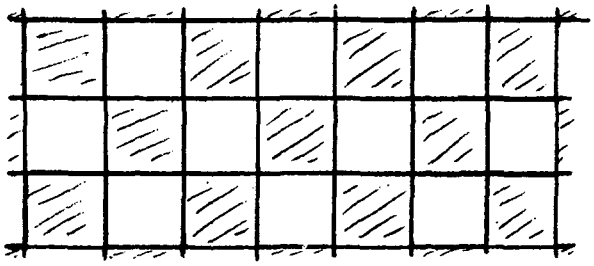

length of the bars is the thickness of the electrodes, the "roughness factor" calculated for bars 10 micron x 10 micron x 0.040 cm is 80. Almost all channels in the sintered silver electrodes shown in Figures 35, 36, and 37 are within an order of magnitude of 100 square microns, the area of a 10 micron by 10 micron idealized channel.

The values of 58 and 81 for the roughness factors of sintered silver electrodes (which are 0.040 cm thick) appear reasonable and also reflect the different ways in which different methods sense the coarseness of a surface. While a BET method may give a value that gives equal weight

TABLE VIII

COMPARISON OF SURFACE AREA ESTIMATIONS FOR SINTERED SILVER ELECTRODES USING CONSTANT CURRENT VERSUS POTENTIOSTATIC METHOD

Constant Current				
Electrode Type	Current (μamps)	Plateau Length (min)	Average Plateau Length (min)	Dev. (%)
Sintered silver electrode (.688 cm^2)	4955	9.50	9.36 = T_1	± 4
	4955	9.30		
	4955	9.25		
	4955	9.40		
Standard electrode (glass discs 2.54 cm^2)	319	9.00	9.10 = T_2	± 10
	319	9.80		
	319	9.20		
	319	8.75		
Potentiostatic				
Electrode Type	Potential (volts)	Charge Acceptance (mcoul)	Ave. Charge Acceptance (mcoul)	Dev. (%).
Sintered silver electrode (.688 cm^2)	.3560	6595	6570	± 3
	.3560	6550		
	.3560	6570		
	.3560	6575		
Standard electrode (glass discs 2.54 cm^2)	.3560	281	273	± 6
	.3560	272		
	.3560	270		
	.3560	269		
Comparison For Sintered Silver Electrode				
Constant Current			Constant Potential	
Area = 40 cm^2			Area = 61 cm^2	
Roughness Factor = 58			Roughness Factor = 81	

to all regions of the electrode both interior and near the outer extremity of the surface the methods used here may give more meaningful values for electrochemical applications because the methods are electrochemical in nature.

The lower value for the constant current method (where it is based upon the time of oxidation along the first plateau) may result from the oxidation being shifted to the potential of the second plateau before any extensive oxidation has taken place within the interior of the electrode. This is related to the iR drop increase with increasing distance into the porous channels. At a constant potential more oxidation is permitted in the interior of the electrode even though current density decreases with increasing distance into the porous channels. This is shown when the data of Table VIII are used for the following comparison of charge accepted by the standard and sintered electrodes:

	Charge Accepted Under Conditions for the Method of Surface Area Estimation	
Electrode	Constant Current	Potentiostatic
Standard	69 mcoul/cm^2	107 mcoul/cm^2
Sintered	4100 mcoul/cm^2	9500 mcoul/cm^2

That the value of the initial current peak might be proportional to the surface area was considered for potentiostatic oxidations. Initial peak values were determined for various silver surface and roughness factors calculated, based on the standard silver-on-glass electrode having a value of 1.00. These values were determined by measuring the current response with both a strip chart recorder and an oscilloscope with a persistence feature. A comparison of roughness factors with these methods of surface area estimation is as follows:

Electrode	Roughness Factors			
			Initial Current Peak	
	Constant Current	Potentio-static	Recorder	Oscilloscope
Silver on glass; vapor deposited	1.00	1.00	1.00	1.00
Electropolished foil	1.09	1.25	1.03	1.1 *
Foil etched in 6N HNO_3-10 sec.	1.3	2.1	--	1.3 *
Foil etched in 6N HNO_3-120 sec.	3.1	4.1	1.6	4.0 *
Sintered silver electrode	58	81	1.4	<2

* Wire electrodes used.

The initial current peak does correlate with imposed roughness on wire and foil electrodes. However, the initial current peak for a sintered electrode does not measure the area of the intricate pattern of convolutions of the electrode but only the apparent gross geometrical area.

The initial current peak for potentiostatic oxidations as a function of applied potential is given for silver wire electrodes in Figure 40. The linear dependence of the peak values at potentials below 0.27 v (vs. Hg/HgO) supports the conclusion that the initial current peak is due to charging of the double layer and not due to a faradaic reaction. This suggests that the initial double-layer charging of a silver electrode, at the instant the potential step is applied, occurs only on the outer surface extremity. The double-layer charging then proceeds into the convolutions or pores as the faradaic reaction starts on the outer surface extremity.

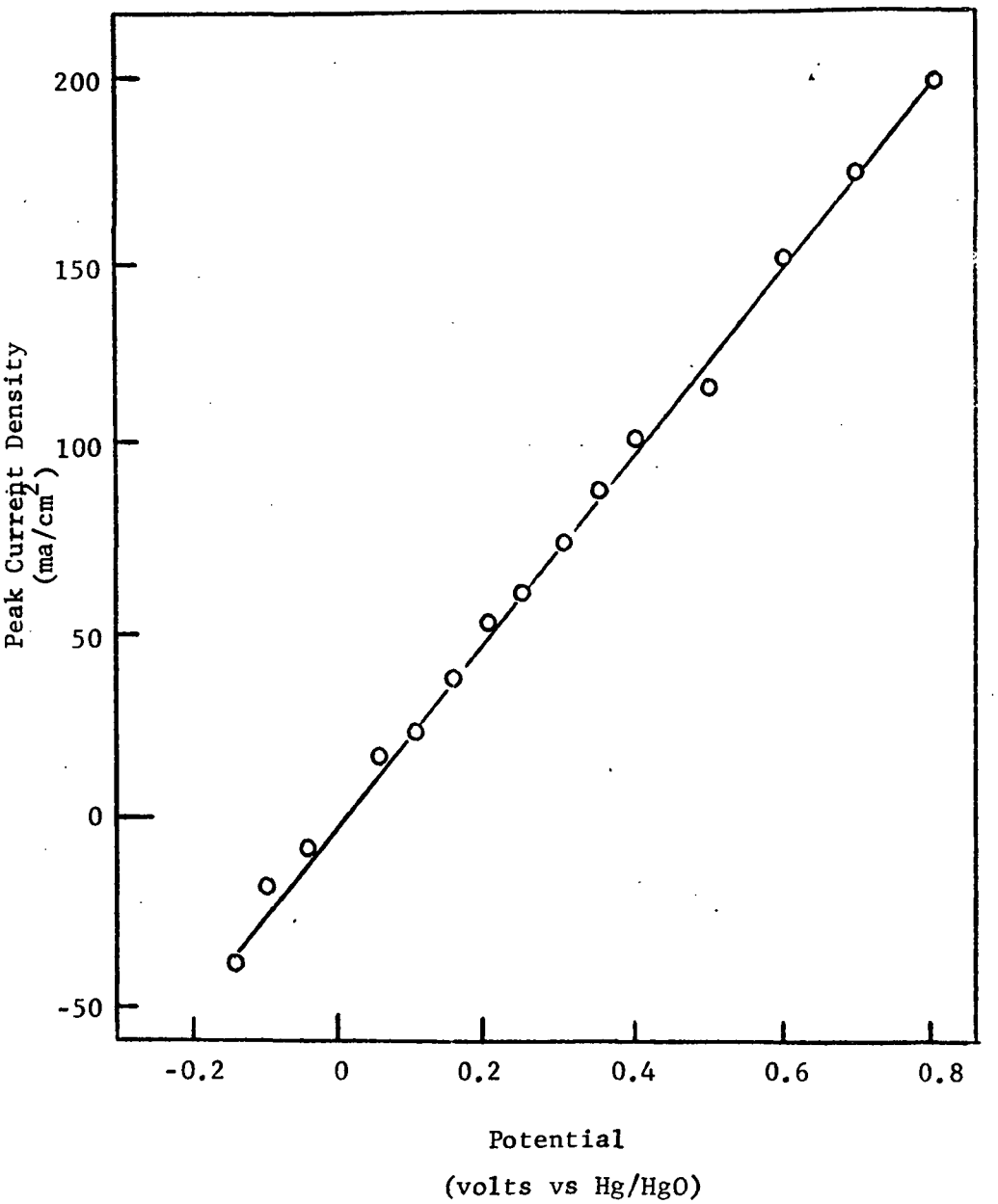

Fig. 40--Peak current as a function of applied potential under potentiostatic conditions.

In our early work on the potentiostatic method of surface area estimation it became apparent that there were some ranges of potentials where a slight change in potential caused a marked change in charge acceptance. The potential 0.356 v (vs. Hg/HgO) was selected for the determinations reported in Table VIII because this potential was in a range in which the charge acceptance was only slightly affected by variations in potential. Determinations of charge acceptance over a range of potentials were made by (1) current-time integration, (2) charge recovery on constant current reduction, and (3) analysis of silver present in the oxide layer via atomic absorption spectrophotometry. These results are given in Figure 41.

The fact that the current-time integral is higher for all oxidations indicates that the current efficiency may be less than 100% or that the oxide may be decomposing or dissolving. Even though the electrolyte is saturated with silver (I) oxide, dissolution is the preferred interpretation because dark colloidal particles gradually form in the electrolyte with continued oxidations.

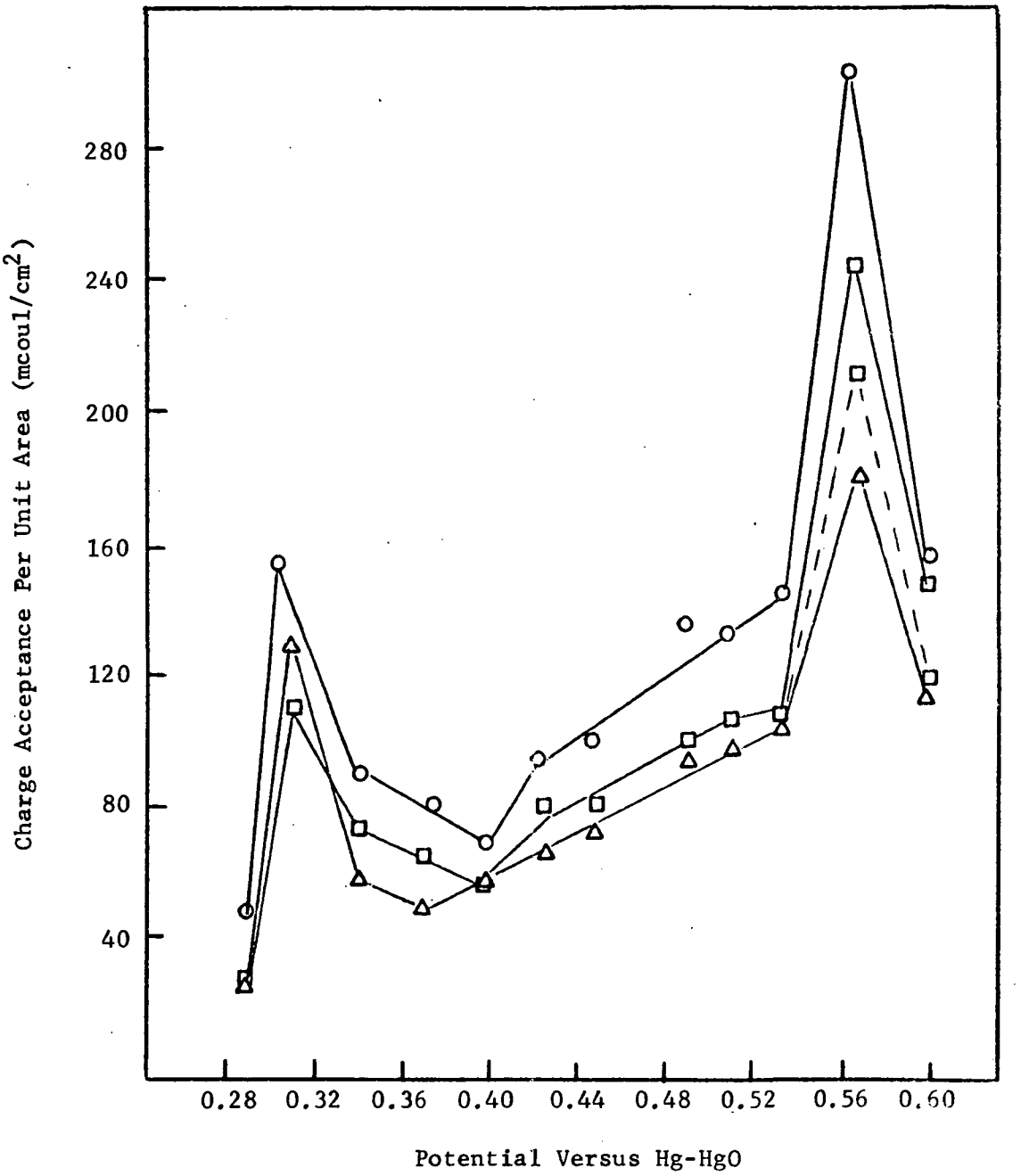

Fig. 41--Plots of charge acceptance versus applied potential as determined by (O) current-time integral, (□) constant current reduction, (Δ) atomic absorption.

SECTION VII

THE EFFECTS OF APPLIED STRESSES ON THE OXIDATION OF SILVER

INTRODUCTION

Silver foil electrodes which were oxidized while being subjected to ultrasonic vibrations showed an increase in charging capacity of 10-35% over electrodes not subjected to the vibrations.[41] In this report consideration is given to other types of applied stress on the charge acceptance of silver electrodes. Specifically a cell has been designed in which tension and torsion can be applied to a silver wire electrode while being oxidized.

EXPERIMENTAL

Figure 42 shows the apparatus used to study the effects of tension. Water at 20.0°C is pumped from a thermostatted bath through the water jacket surrounding the cell. The cell is a cylinder 10 cm long with an inside diameter of 1.7 cm. At the bottom is a rubber septum, through the center of which passes the wire electrode. The electrode is positioned by being passed through a hole in the center of a plug inserted in the top of the cell. A cylinder of platinum foil 7.2 cm long with a diameter of 1.6 cm is fitted into the cell. The end of this sleeve is positioned flush with the bottom of the cell. The level of electrolyte is maintained just at the top of this platinum counter electrode. The plug at the top of the cell contains two capillaries. One extends down to the level of the top of the platinum. This capillary is connected to an aspirator to permit the removal of excess electrolyte, thereby maintaining a reproducible electrolyte level. This level is set at the top of the counter electrode to provide uniform current distribution.[51] The other capillary extends 0.05 cm into the electrolyte and is connected by an electrolyte bridge to a calomel reference electrode.

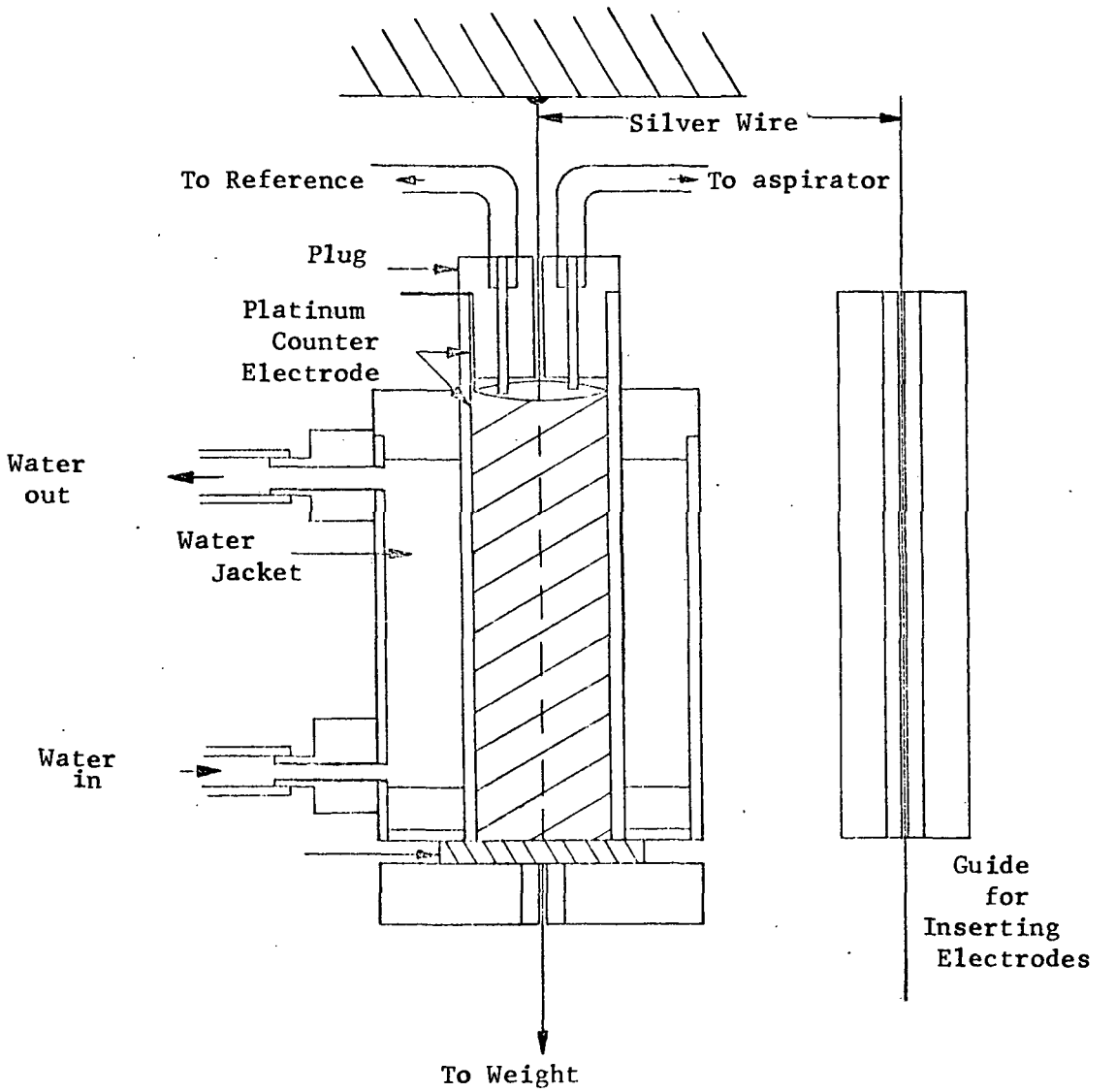

Figure 42.--The cell used for measuring the effect of tension on charge acceptance.

The silver wire electrode passing through the cell is fastened at the top to a supporting beam and at the bottom to a balance pan which contains weights. The cell is surrounded by a water jacket which is 5 cm in diameter.

The silver wire electrodes were prepared by scrubbing with abrasive cleanser and then etching in 6 F HNO_3 for 5 to 10 seconds. Inserting the wire from the bottom through the rubber septum caused contamination and passivation of a significant portion of the electrode. Insertion of the wire from the top avoids this contamination. A guide is temporarily placed in the cell to center and support the wire as it is pushed through the rubber septum. The guide is a length of glass capillary tubing encased in a plastic cylinder 1.6 cm in diameter (See Figure 42). This apparatus was modified for the study of the effect of torsion on the charge acceptance by fastening the top of the silver wire electrode to a swivel instead of to a stationary beam. This allowed the wire to be twisted any amount up to the breaking point of the wire. The wire was clamped just below the cell to limit the torsion to the part of the wire in the cell and above the cell. A two pound weight was applied to the electrode to keep it straight and centered in the cell during reaction.

A current density of 1.0 ma/cm^2 was used for all experiments.

The electrolyte used was 0.1 F KOH and was renewed just prior to beginning the cycling of a fresh electrode. The comparison of plateau lengths with and without tension (or torsion) is made from data collected from experiments with the same electrode. Therefore, the absolute surface area is not important as long as that surface area does not change as a result of dirty areas beginning to react in the course of the experiment. For this reason the initial length of the first oxidation plateau, C_1, will vary from one set of data to another. Similarly the slope of the curve of C_1 vs. run number will vary. Any effect of tension (or torsion) on charge acceptance, however, will appear as a break in the curve.

RESULTS AND DISCUSSION

Tension. - Silver wire electrodes were cycled by repeated oxidation to the end of the first plateau and reduction to the evolution of hydrogen. The wire electrode was cycled 25 times without tension and then progressively more tension was applied. Four cycles at each value of tension were run, followed by two cycles without weights. These groups are shown in Figure 43a for 2, 4, 5, 6, 7 and 7.5 pounds. The wire broke during the first oxidation cycle at 7.5 pounds. No increase or decrease is demonstrated by cycling under tension. Figure 43b is a graph of the results obtained on a different wire. Again no increase or decrease resulted from the tension. Elongation was pronounced for electrodes which had been subjected to 7 pounds of tension.

Torsion. - Wire electrodes were cycled with a constant tension to demonstrate the effect torsion has on charge acceptance. The first 15 cycles were run with no torsion and then the electrode was cycled 3 times each with 0.5, 1, 2, 3, 4.5, 6.5 and 8.5 turns. The length of C_1 for each cycle is plotted in Figure 44. Torsion was not found to have any effect on the charge acceptance during C_1 even though noticeable deformation of the wire was caused by the twisting. That is, there is no significant departure from the observed rise in charge acceptance with cycling after the torsion is applied.

When the electrode was released after being cycled at 8.5 turns it unwound only one turn. This shows that the twisting force produced a large amount of permanent deformation or shear and only a small amount of true torsion under the conditions of our experiment.

We conclude from our experiments with tension and torsion that the charge acceptance of silver wire does not increase or decrease as a result of applied tension or torsion during the first oxidation plateau of the oxidation-reduction cycle.

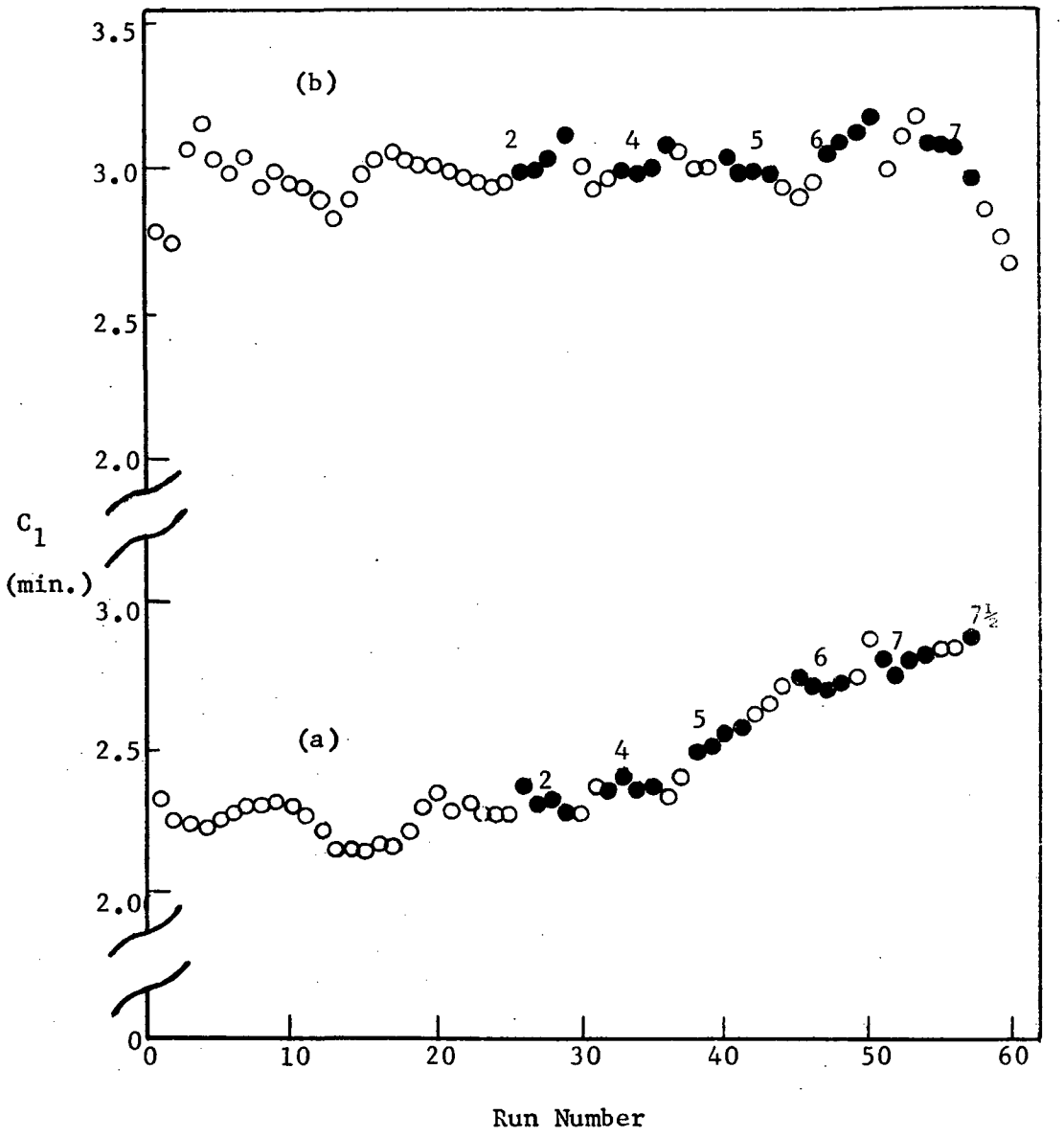

Fig. 43.-- Silver wire cycled with and without tension. Solid points indicate tension applied. Numbers above solid points represent applied weight in pounds.
Date for (a) and (b) were obtained from different electrodes.

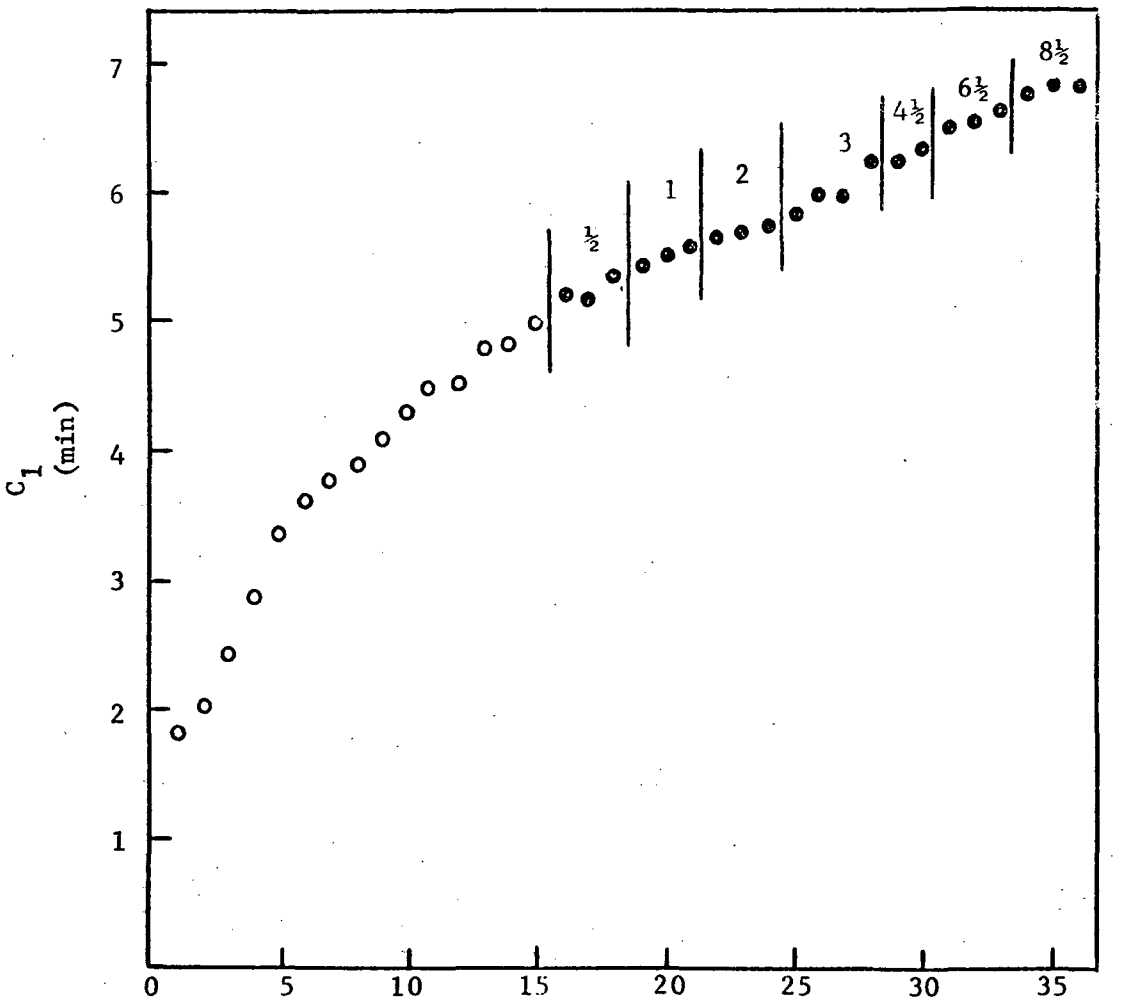

Fig. 44--Charge acceptance (time of first plateau) for silver wire cycled with and without torsion. Solid points indicate torsion applied. Numbers above solid points represent the number of turns on the wire.

SECTION VIII
A POSSIBLE SILVER III OXIDE

A recent paper by Barradas and McDonnell presented new evidence for the electrochemical formation of Ag_2O_3 on silver in aqueous KOH solutions.[52] They showed curves for the galvanostatic oxidation of silver at five temperatures from 0^o to 40^o at a current density of 0.5 ma/cm^2. The standard type of curve (Figure 45a) for galvanostatic oxidation of silver shows a second plateau at about 0.63 v (vs. Hg/HgO reference electrode). This was observed at 40^oC. However, at each of the temperatures, 0^o, 10^o, and 20^oC, a distinct second plateau at 0.85 v was observed with presaturation of the 0.1 N KOH with O_2 and Ag_2O. Later they indicated that saturation with O_2 was not "a crucial factor" but the Ag_2O addition was necessary.

We were interested in determining what bearing these results would have on our work and therefore attempted to repeat their experiment at 0^oC. The simple cell shown in Figure 21 was used. A 20 mil silver wire was placed vertically at the center of the cell with a cylindrical sheet of platinum as the counter electrode. The potential at the working electrode was measured with a Luggin capillary connected to a Hg/HgO reference electrode. The silver wire electrode used had been cycled a number of times before this study. With the cell assembly at 0^oC, O_2 bubbling through the cell and precipitated Ag_2O present, only the standard types of curves were observed as shown in Figure 45a. The silver wire was then removed and cleaned with abrasive cleaner. The oxidation of the clean wire gave a curve with an inflection at 0.40 volts and another inflection at 0.80 volts (Figure 45b). However, the charge accepted before oxygen evolution was only 31 $mcoul/cm^2$ or 9% of that in the previous oxidation. The electrode continued at oxygen evolution for about three minutes. On reduction 89 $mcoul/cm^2$ of charge was recovered, indicating that additional oxide was formed during

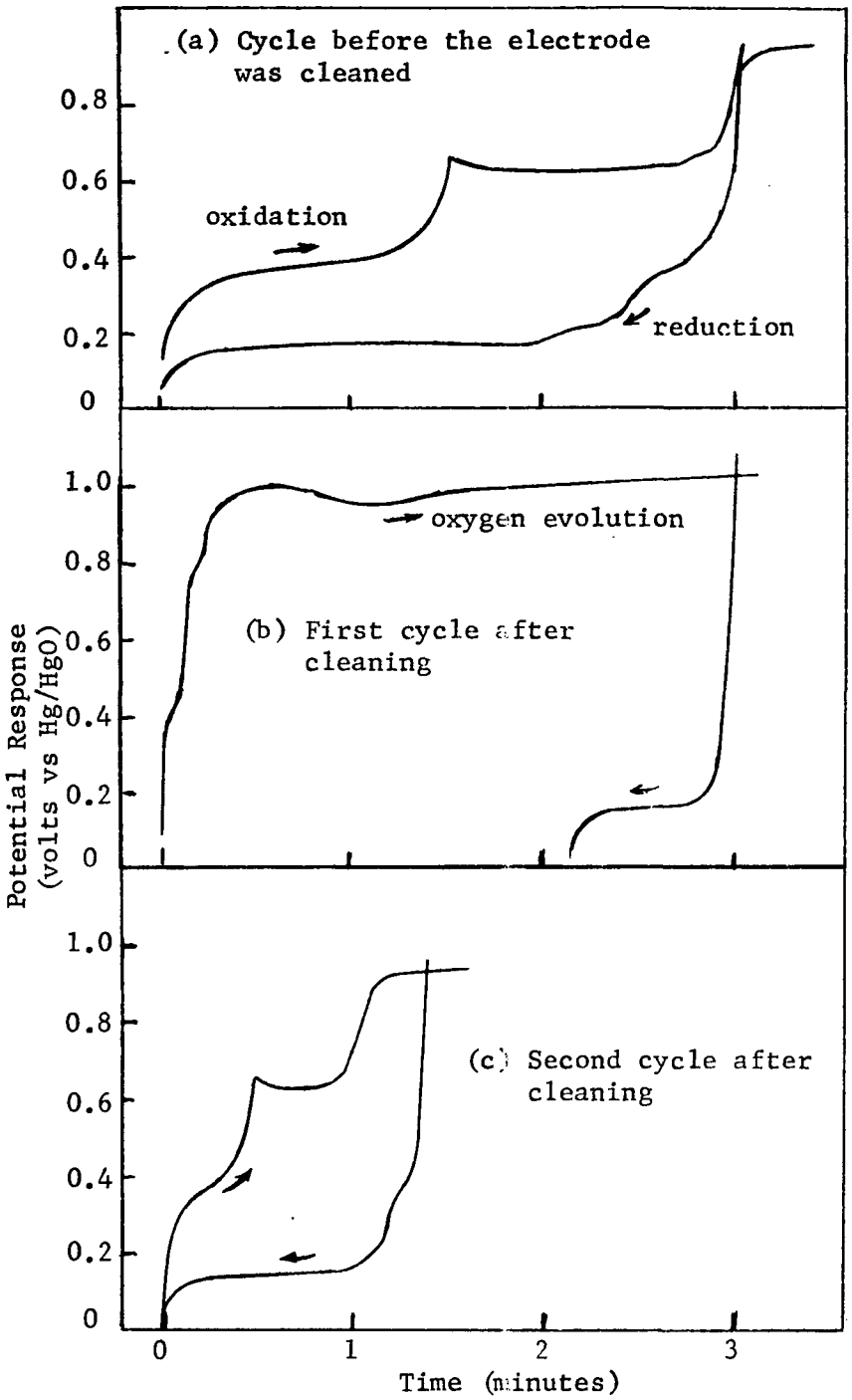

Figure 45 Galvanostatic Oxidation of a Silver Wire Electrode at $0^{o}C$.
Saturated with O_2 and Ag_2O
Electrolyte Concentration 0.10 N KOH
Current Density 1.8 ma/cm^2

oxygen evolution. The second cycle (Figure 45c) on the clean wire gave a broader inflection at 0.37 v, a rise to a peak at 0.67 v followed by a plateau at 0.63 v which is the standard behavior. With repeated cycling the charge acceptance increased and the standard potential response was observed.

Repetition of this sequence of events about five times, each time starting with the silver wire freshly cleaned, gave similar results. Only during the first oxidation after cleaning was the inflection or plateau at 0.80 to 0.85 v observed.

One possible reason for the disappearance of this plateau on the second and subsequent cycles is the increase in effective electrolytic surface area. Therefore, an effort was made to increase the current on the second cycle so as to maintain the same effective current density as on the first cycle. However, two and five fold increases in current on the second cycle did not cause an inflection or plateau at 0.85 v.

Although Barradas and McDonnell considered their observations as evidence for formation of Ag_2O_3, the absence of the oxidation at 0.85 v after the first cycle seems to require an alternative explanation or at least a reason why the Ag_2O_3 would be much less stable after the first cycle.

REFERENCES

1. B. B. Damaskin, "The Principles of Current Methods for the Study of Electrochemical Reactions", (English Translation), McGraw-Hill Book Company, New York, 1967, p. XI.

2. M. D. Wijnen and M. W. Smit, Recueil, 79, 289 (1960).

3. W. Vielstich and H. Gerischer, Z. physik. Chem. Neue Folge, 4, 10 (1955).

4. D. I. Leikis, G. L. Vidovitsch, L. L. Knotz, and B. N. Kabanov, Z. Physik. Chem., Leipzig A, 214, 334 (1960).

5. B. D. Cahan, J. B. Ockerman, R. F. Amlie, and P. Rüetschi, J. Electrochem. Soc., 107, 725 (1960).

6. C. P. Wales, J. Electrochem. Soc., 117, 680 (1968).

7. G. W. Briggs, M. Fleischmann, D. J. Lax, and H. R. Thirsk, Trans. Faraday Soc., 64, 3120 (1968).

8. N. F. Mott, Trans. Faraday Soc., 43, 429 (1947).

9. M. Fleischmann, D. J. Lax, and H. R. Thirsk, Trans. Faraday Soc., 64, 3137 (1968).

10. R. C. Alkire, E. A. Grens II, and C. W. Tobias, J. Electrochem. Soc., 116, 809 (1969).

11. S. K. Rangarajan, J. Electroanal. Chem., 22, 89 (1969).

12. D. A. Vermilyea and C. S. Tedmon, Jr., J. Electrochem. Soc., 117, 437 (1970).

13. A. H. Reed and J. McCallum, Technical Report AFAPL-TR-69-38 (1969).

14. F. A. Posey and S. S. Misra, J. Electrochem. Soc., 113, 608 (1966).

15. R. C. Alkire, E. A. Grens II, and C. W. Tobias, J. Electrochem. Soc., 116, 1328 (1969).

16. L. V. Gregor and K. S. Pizer, J. Am. Chem. Soc., 84, 2671 (1962).

17. L. V. Nikitin, Compt. Rend. Acad. Sci. U.S.S.R., 17, 167 (1937).

18. E. M. Zaretskii, Zhur. Priklad. Khim., 24, 614 (1951).

19. W. France, Chem. and Eng. News, Oct. 27, 1969.

20. J. Smit, Physica, 8-9, 587 (1952).

21. B. Miller, J. Electrochem. Soc., 117, 491 (1970).

22. M. W. Breiter, J. Electrochem. Soc., 117, 738 (1970).

23. W. M. Krebs and D. K. Roe, J. Electrochem. Soc., 114, 892 (1967).

24. G. Mamantov, D. L. Manning, and J. M. Dale, J. Electroanal. Chem., 9, 253 (1965).

25. H. E. Haring, Trans. Electrochem. Soc., 49, 417 (1926).

26. H. Göhr and E. Lange, J. Physik. Chem. Frankfurt, 17, 100 (1958).

27. N. Cabrera and N. F. Mott, Repts. Progr. in Physics, 12, 163 (1949).

28. J. J. Lingane, "Electroanalytical Chemistry," 2nd ed. Interscience, New York, 1958.

29. M. A. Genshaw, "Electrosorption," Chap. IV, E. Gileadi, ed., Plenum Press, New York (1967).

30. H. H. Uhlig, Acta Met., 4, 541 (1956).

31. A. A. Yakovleva, T. I. Borisova, and V. I. Veselovskii, Russ. J. Phys. Chem., 36, 763 (1962).

32. H. Uhlig, J. Pickett, J. MacNairn, Acta Met., 7, 111 (1959).

33. J. A. McMillan, J. Chem. Rev., 62, 65 (1962).

34. G. L. Cohen and G. Atkinson, J. Electrochem. Soc., 115, 1236 (1968).

35. G. D. Nagy, W. J. Moroz, and E. J. Casey, Proc. Ann. Power Sources Conf., 19, 80 (1965).

36. J. C. Bailar, Jr., J. Chem. Ed., 21, 523 (1944).

37. L. M. Gedansky and L. G. Hepler, Englehard Tech. Bull., 9, 117 (1969).

38. C. P. Wales and J. Burbank, J. Electrochem. Soc., 112, 13 (1965).

39. C. P. Wales and A. C. Simon, J. Electrochem. Soc., 115, 1228 (1968).

40. S. Kimoto and J. C. Russ, Am. Sci., 57, 112 (1969).

41. E. A. Butler and A. U. Blackham, "Studies of Reaction Geometry in Oxidation and Reduction of the Alkaline Silver Electrode," Final Report, J. P. L. 951911, May 15, 1968.

42. J. H. Kennedy and F. Chen., J. Electrochem. Soc., 118, 1043 (1971).

43. W. M. Krebs and D. K. Roe, J. Electrochem. Soc., 117, 557 (1970).

44. M. J. Dignam, H. M. Barrett, and G. D. Nagy, Can. J. Chem., 47, 4253 (1969).

45. S. U. Falk and A. J. Salkind, "Alkaline Storage Batteries," John Wiley and Sons, Inc., New York, 1969, p. 358.

46. F. Mansfield and S. Gilman, J. Electrochem. Soc., 117, 1521 (1970).

47. C. P. Wales, J. Electrochem. Soc., 108, 395 (1961).

48. J. A. Davies, J. P. S. Pringle, R. L. Graham, and F. Brown, J. Electrochem. Soc., 109, 999 (1962).

49. G. Amsel and D. Samuel, J. Phys. Chem. Solids, 23, 1707 (1962).

50. L. Young, Proc. Roy. Soc. London, Ser. A, 258, 496 (1960).

51. E. A. Butler and A. U. Blackham, "Studies of Reaction Geometry in Oxidation and Reduction of the Alkaline Silver Electrode", Final Report, J. P. L. 951554, April 10, 1967.

52. R. G. Barradas and D. B. McDonnell, Can. J. Chem., 48, 2453 (1970).